JOINTING IN SANDSTONES,

ARCHES NATIONAL PARK, UTAH

A DISSERTATION

SUBMITTED TO THE DEPARTMENT OF GEOLOGY

AND THE COMMITTEE ON GRADUATE STUDIES

OF STANFORD UNIVERSITY

IN PARTIAL FULFILLMENT OF THE REQUIREMENTS

FOR THE DEGREE OF

DOCTOR OF PHILOSOPHY

BY

JAMES RUSSELL DYER

AUGUST, 1983

ii

JOINTING IN SANDSTONES, ARCHES NATIONAL PARK, UTAH

James Russell Dyer, Ph.D.

Stanford University, 1983

Exceptional exposures of systematic joints are found on the flanks of the Salt Valley anticline, in Arches National Park, southeastern Utah. Pennsylvanian through Tertiary(?) sedimentary rocks crop out in the core of the breached, northwest-trending, salt-cored anticline. Since Permian time, the structural history of the area has been dominated by salt diapirism and subsequent collapse.

Systematic joints in the Moab Member of the Entrada Sandstone display a zoned character. Subparallel joints which make up a given joint zone are confined to narrow zones and have a regular interzone spacing which is on the order of the bedding thickness (27 meters). Individual fractures are confined to the Moab Member. Field relations allow determination of relative ages between sets of zoned joints. Three distinct geometric relations between younger and older joints are observed. Each interaction characterizes an area of 1 - 8 square kilometers.

Observations of the offset of sand dune cross-bedding allows determination of shear displacement along joints. In all cases, younger joints display the least shear offset. Commonly there is no observable offset on the youngest joints, only a dilational opening, indicating that zoned joints originated as extensional fractures. Stress field rotation over time leads to resolved shear stresses and shear displacements on pre-existing joints. Field evidence

suggests that zoned joints grew in response to an effective tensile minimum principal stress. High elastic strain energies near the tip of a large joint are apparently dissipated through growth of suitably sized and oriented flaws which are of subcritical size under the far-field loading. The resultant *en echelon* trend of individual joints comprises a joint zone.

Strength anisotropy due to large-scale eolian cross-bedding is rejected as a control on the orientation of zoned joints in the Moab Member. Younger joints show a systematic change in orientation as they approach older, throughgoing zones, which reflects a change in the stress field in which the younger joint set was growing. Analytic solutions for the stress field around a single joint zone subject to a combination of opening and anti-plane shear loadings are given. Changes in the principal stresses near a joint zone are functions of the orientation and ratio of the far-field stresses; and the coefficient of friction across the joint.

TABLE OF CONTENTS

Chapter Four: The Influence of Lithology on Jointing

Chapter Five: The Stress Field about a Joint Zone

LIST OF TABLES

LIST OF FIGURES

Figure   Page

CHAPTER ONE

GEOLOGY OF ARCHES NATIONAL PARK

ABSTRACT

Sedimentary rocks ranging in age from Pennsylvanian through Tertiary(?) crop out in the core of a breached, northwest-trending, salt-cored anticline. Diapiric movement of Pennsylvanian evaporites began shortly after deposition and was localized by a large northwest trending fault in sub-salt rocks. Continued diapiric movement resulted in the local thinning of Pennsylvanian(?) through Late Jurassic sediments over the salt anticline. Marine and marginal marine conditions characterize Pennsylvanian and Permian sediments. A transition to continental sedimentation occurred in the Triassic. Continental sedimentation prevailed from Triassic to Late Cretaceous time. Late Jurassic sediments are the first deposits which blanketed and covered the salt anticline. Synorogenic sediments of Late Jurassic to Early Cretaceous age indicate regional tectonic activity at this time. A marine transgression occurred in the Late Cretaceous. Continental sedimentation has prevailed since the Late Cretaceous. Rejuvenation of the salt anticline occurred after deposition of the Late Cretaceous Mancos Shale. Miocene uplift of the Colorado Plateau and downcutting of the Colorado River led to ongoing salt dissolution, salt flowage, and structural collapse. A folded and faulted sequence of Tertiary(?) fluvial and lacustrine rocks are preserved in the anticlinal core, and are the youngest rocks in the Park.

INTRODUCTION

Arches National Park, the location of this field study, contains most of the great structure known as the Salt Valley anticline. The Park comprises an area of about 114 square miles, and is located in southeastern Grand County, Utah, just north of the city of Moab. The Park boundaries are irregular. An index map showing the location of Arches in relation to other major geological structures in the region is shown in figure 1-1. The Colorado River forms the
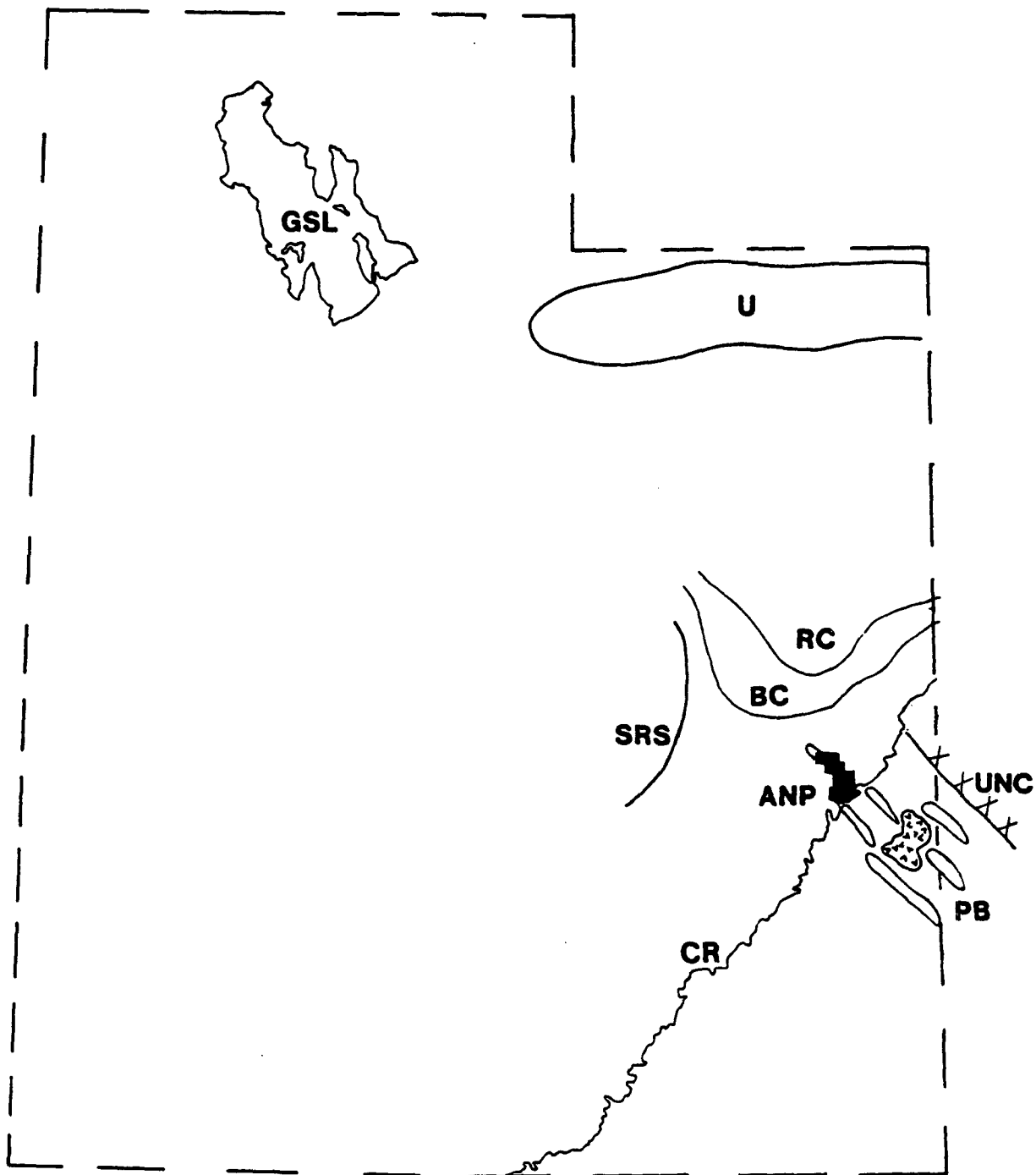
Figure 1-1

Index map of Utah. ANP = Arches National Park; PB = Paradox Basin, showing general trend of salt anticlines. Stipled pattern in center of Paradox Basin is the La Sal intrusives complex. CR = Colorado River; UNC = Uncompahgre Uplift; RC = Roan Cliffs; BC = Book Cliffs; SRS = San Rafael Swell; U = Uinta Mountains; GSL = Great Salt Lake.

southern boundary of the Park. All locations and place names used in this report are based on the U. S. Geological Survey topographic map of Arches National Park (1974, scale 1:50,000).

PREVIOUS INVESTIGATIONS

During the course of more than half a century of extensive exploration for petroleum, potash, and more recently, uranium, a good understanding of the general stratigraphic and structural characteristics of the region has evolved. The first systematic regional studies in this area were those of Gilluly and Reeside (1928), Dane (1935), and McKnight (1940). Dane's mapping included that part of the Park north of what is now called The Windows, while McKnight's work included the remainder of the Park. Subsequent detailed mapping of areas adjacent to the Park include the studies of Miller (1959) and Gard (1976). Hite (1977) studied the nature of the Paradox evaporites in Salt Valley. Geophysical data pertinent to the region was summarized by Joesting and Case (1962). Regional studies, covering most of the Paradox Basin, were presented by Elston and others (1962) and Cater (1970). Lohman (1975) has written an excellent general survey of the geology of Arches National Park. A regional study of fracture systems and tectonic elements of the Colorado Plateau was presented by Kelly and Clinton (1960).

FIELD METHODS

Geological mapping in Arches National Park was accomplished in the summer of 1977. Geology was mapped directly on U. S. Geological Survey 1:20,000 scale aerial photography and was transferred by inspection to a series of 1:24,000 scale topographic "T-Quads" which cover the area. The U. S. Geological Survey topographic map of Arches National Park (1974, scale

-3-

1:50,000) was photographically enlarged to a scale of 1:24,000 and used as the compilation base for the final geologic map (Plate 1).

STRATIGRAPHY

Sedimentary rocks ranging in age from Pennsylvanian through Tertiary (?) crop out in Arches National Park (figure 1-2). The oldest exposed rocks are evaporites, shales, limestones and sandstones of Pennsylvanian age. The rise of the ancestral Uncompahgre highland to the northeast is recorded in a series of arkoses of Pennsylvanian and Permian age. Contemporaneous diapirism of the Pennsylvanian evaporites along northwest trending salt anticlines resulted in local thinning of Pennsylvanian(?) through Jurassic clastic sediments over the rising salt. A transitional sequence of reworked arkoses unconformably overlies older rocks, and marks the westward retreat of the sea in Triassic time. An unconformity separates the transitional rocks from overlying continental deposits. Continental deposition prevailed from the Late Triassic until Late Cretaceous time and is recorded in a sequence of fluvial siltstones and sandstones and a spectacular sequence of eolian sandstones. Several unconformities in these rocks record periods of non-deposition in the area. Late Jurassic sediments are the first deposits which blanketed and covered the salt anticlines. Late Jurassic and Early Cretaceous conglomerates, together with claystones derived from volcanic ash, indicate regional tectonic activity at this time. An unconformity separates these continental deposits from a thick sequence of marine shale which records a major transgression of the sea in Late Cretaceous time. Following withdrawal of the sea in the Late Cretaceous, the area has remained above sea level. The Salt Valley anticline was breached by Late Tertiary (?) time, when fluvial and lacustrine sediments were deposited in the breached core and on the southwest flank of the anticline. The Late

AGE	NAME OF ROCK UNIT			THICKNESS (meters)
RECENT	ALLUVIUM, WINDBLOWN SAND AND SILT, AND MASS WASTING DEBRIS			0 - 20
	UNCONFORMITY			
TERTIARY (?)	FORMATION OF SALT VALLEY			35
	UNCONFORMITY			
LATE CRETACEOUS	MANCOS SHALE			1000 (?)
EARLY CRETACEOUS	DAKOTA SANDSTONE			10
	UNCONFORMITY			
	CEDAR MOUNTAIN FM.			40
LATE JURASSIC	MORRISON FORMATION	BRUSHY BASIN MEMBER		115
		SALT WASH MEMBER		70
		UNCONFORMITY		
	SAN RAFAEL GP.	SUMMERVILLE FM.		12
		ENTRADA SANDSTONE	MOAB TONGUE	27
			SLICK ROCK MBR.	85
			DEWEY BRIDGE MBR.	20
		UNCONFORMITY		
JURASSIC AND TRIASSIC (?)	GLEN CANYON GP.	NAVAJO SANDSTONE		70 - 90
LATE TRIASSIC (?)		KAYENTA FORMATION		75
LATE TRIASSIC		WINGATE SANDSTONE		60 - 90
	UNCONFORMITY			
	CHINLE FORMATION			90
	UNCONFORMITY			
MIDDLE (?) AND EARLY TRIASSIC	MOENKOPI FORMATION			0 - 90
	UNCONFORMITY			
PERMIAN	CUTLER "FORMATION"			0 - 900
PENNSYL-VANIAN	HERMOSA FORMATION	HONAKER TRAIL MEMBER		0 - 500
		PARADOX MEMBER		0 - 4000

Figure 1-2.

Generalized stratigraphic column for Arches National Park and vicinity.

Tertiary (?) sediments in the breached core were subsequently downfaulted and folded due to dissolution of underlying salt. The area is currently undergoing active erosion.

PENNSYLVANIAN ROCKS

HERMOSA FORMATION

PARADOX MEMBER OF THE HERMOSA FORMATION

The oldest rock that crops out in the area is the Paradox Member of the Hermosa Formation. This unit consists of marine evaporites, sandstone, limestone and shale. About 87% of the Paradox is halite rock, which includes some potash deposits (Hite, 1977). Paradox rocks crop out in the core of the Salt Valley anticline. Outcrops are generally poor due to erosion into a badlands topography. The rocks are so severely folded and faulted that it is not possible to determine a reliable stratigraphic sequence or to establish internal structures within the Paradox. Most Paradox rocks exposed are an insoluble caprock which overlies the Paradox salt. The Paradox has been thickened by flowage into the anticlinal core. From a synthesis of well data, Hite (1977) estimated a thickness of Paradox rocks in the core of Salt Valley of 11,800 feet (3,600 m).

HONAKER TRAIL MEMBER of the HERMOSA FORMATION

The Honaker Trail Member of the Hermosa Formation is made up primarily of fossiliferous limestones, and is also assigned a Pennsylvanian age. The best exposures of Honaker Trail rocks are on the southwest wall of Moab Canyon, north of the railroad portal. Sandy limestones and sandstones in the core of the Salt Valley anticline have been tentatively mapped as Honaker

Trail. Nowhere in the Park is the contact between Paradox and Honaker Trail rocks exposed. Elsewhere in the Paradox Basin the Paradox Member is lithologically transitional into the Honaker Trail Member (Elston and others, 1962, p. 1865).

PENNSYLVANIAN AND PERMIAN ROCKS

CUTLER FORMATION

Coarse-grained, arkosic red-beds of the Cutler Formation do not crop out within Arches National Park, but are found north and west of the Park Visitor Center in Moab Canyon. A thinned sequence is present west of the Moab Fault. Considerable dispute exists over the nomenclature of these and similar rocks. As originally proposed, the Rico Formation was a marine arkosic sequence with some limestones while the Cutler was composed entirely of non-marine arkosic red-beds. The sequence west of the Moab Fault was originally mapped by McKnight (1940) as the Rico Formation, based on the presence of occasional beds of fossiliferous limestone. Cutler, Rico and Hermosa rocks have been found to be complexly interrelated. Ohlen and McIntryre (1965) suggested the assignment of all arkosic rocks of Pennsylvanian and Permian age to a Cutler Group, but this suggestion has received only limited acceptance. Kirkland (1963) has shown that the Cutler was derived from the late Paleozoic Uncompahgre highland. The Cutler sequence is about 9000 feet thick adjacent to the present Uncompahgre Uplift, thinning to the west and southwest. Cutler deposition was locally influenced by the rise of salt anticlines, leading to thinning and pinching out over the anticlines. Cutler rocks represent a fanglomerate wedge shed off the ancestral Uncompahgre highland into marine waters of the Hermosa sea to the west and southwest. This deposition occurred during and continued after cessation of Hermosa deposition to the west.

-7-

TRIASSIC ROCKS

MOENKOPI FORMATION

The Moenkopi Formation of Middle(?) and Early Triassic age unconformably overlies the Cutler Formation. The contact is not exposed within the Park, but is exposed south of the Moab Fault on the upper slopes of Moab Canyon. McKnight (1940, p. 52) reported a maximum thickness of Moenkopi in Moab Canyon of about 450 feet (137 m). A regional study of the Moenkopi conducted by Shoemaker and Newman (1959) found that Moenkopi distribution is that of a blanket of irregular thickness with several large holes in it due to non-deposition over emergent salt anticlines. Outcrops of Moenkopi rocks are sparse within the Park boundaries, with a few isolated outcrops identified in the Salt Valley and an incomplete sequence exposed in cliff walls above the Colorado River near the Big Bend. The Moenkopi is composed primarily of chocolate-brown to reddish-brown micaceous mudstones, siltstones, sandstones, shales and arkosic conglomerates and sandstones. Bedding is regular and horizontal and ripple marks are common. Limestones are rare in the Moenkopi in this area, but both Dane (1935, p. 43) and McKnight (1940, p. 58) collected marine fossils of probable Lower Triassic age from Moenkopi limestones. The percentage of limestone in the Moenkopi increases to the west. In the San Rafael Swell, massive marine limestones were deposited to a thickness of 150 feet (46 m) during Moenkopi time (Gilluly and Reeside, 1928, p. 85). Moenkopi rocks were probably deposited in a large tidal flat or deltaic complex which bordered a Moenkopi sea to the west.

CHINLE FORMATION

The Chinle Formation of Late Triassic age unconformably overlies the Moenkopi Formation. The unconformity is exposed in the anticlinal core of Salt Valley in the NW 1/4 NW 1/4 of Sec. 14, T 24 S, R 21 E. Here the Chinle fills shallow channels cut in the Moenkopi. Incomplete sections of Chinle crop out at the base of Wingate cliffs on the south side of Salt Valley and on the north side of Salt Valley at the western Park boundary. An apparently complete, although poorly exposed, section is domed around an intrusion of Hermosa rocks in the anticlinal core. Complete sections crop out as steep slopes beneath the Wingate cliffs in Moab Canyon and along the Colorado River at the Big Bend. In Moab Canyon the Chinle is 350 feet (107 m) thick (Stewart, 1961). The base of the Chinle is characterized by an irregular thickness of strata with a mottled purple color. The Chinle is composed primarily of cherry-red siltstones. The siltstones are interbedded with lenticular sandstones and limestone-pebble conglomerates. Ripple marks are not common in the Chinle. Plants, vertebrates, freshwater pelecypods and gastropods are known from the Chinle elsewhere (Stewart and others, 1959). The fossil content, together with the nature of the rocks, indicate continental deposition. Chinle rocks probably were deposited in a deltaic environment, with streams possibly emptying into a large fresh water lake.

TRIASSIC AND JURASSIC ROCKS

GLEN CANYON GROUP

A subtle regional unconformity separates the Chinle Formation from the overlying Glen Canyon Group (Pipiringos and O'Sullivan, 1978, p. A-19). Three conformable nonmarine formations make up the Glen Canyon Group in this area. In ascending order these are the Wingate Sandstone of Late Triassic age, the Kayenta Formation of Late Triassic(?) age, and the Navajo Sandstone of Triassic(?) and Jurassic age. This group of massive cliff-forming sandstones forms the spectacular cliffs along the Colorado River and cap the southwest wall of Moab Canyon. All three formations are exposed on both the northeast and southwest walls of Salt Valley. Good exposures of the Glen Canyon Group are also found along Salt Wash between the Salt Valley and the Colorado River. Over twenty square miles (fifty one square kilometers) of essentially bare Navajo Sandstone make up the region of "Petrified Dunes" between the Windows area and the Colorado River.

WINGATE SANDSTONE

The Wingate Sandstone crops out at several localities within the Park. The Wingate consists of a series of horizontal layers of sandstone, ranging from less than 2 to nearly 80 feet in thickness (0.6-24 m). These units are separated by horizontal bedding planes that are traceable laterally for more than a mile (1.6 km) (Dane, 1935). Except on the northeast wall of the Salt Valley, the Wingate forms a nearly vertical reddish-brown cliff, streaked and stained with desert varnish. The Wingate in the northern Salt Valley is reported by Craig (1959) to be 196 feet thick (60 m). Gilluly and Reeside (1928, p. 108) reported that the

Wingate in Moab Canyon is 210 feet (74 m) thick. These thicknesses are 50-130 feet (15-40 m) less than those reported elsewhere by Dane (1935, p. 72) and McKnight (1940, p. 73). Although Dane found no systematic variation in thickness, thinning of the Wingate may be due to non-deposition across the rising salt diapirs of Salt Valley and Spanish (Moab) Valley. Such thinning was noted in the Salt anticline region of Colorado by Cater and Craig (in: Cater, 1970, p. 21). The depositional environment of the Wingate is uncertain, but the action of both wind and water in a continental environment is indicated.

KAYENTA FORMATION

The Kayenta Formation lies conformably on the Wingate Sandstone. Contact between the two formations is transitional and cannot be determined with certainty. The Kayenta typically crops out as a series of resistant benches and ledges which cap a shear cliff of Wingate Sandstone. The Kayenta rocks include lenticular, cross-bedded sandstone units, with subordinate siltstones, shales and conglomerates. Channeling and slump features are common and indicate fluvial deposition. Color of Kayenta rocks ranges from pale-orange in sandstones to dark reddish-brown and lavender in the finer grained beds. The difficulty in placing the lower contact may in part explain the widely varying thicknesses reported for the Kayenta in this area. Gilluly and Reeside (1928, p. 108) reported a thickness of 160 feet (49 m) for the Kayenta in Moab Canyon, while Dane (1935, p. 81) found that the Kayenta east of the Salt Valley ranged in thickness from 200 feet to 320 feet (67 to 98 m).

NAVAJO SANDSTONE

Extensive outcrops of Navajo Sandstone are present in the Park. The Navajo typically crops out as great rounded knolls or domes of white to pale-orange cross-bedded sandstone. In addition to the "Petrified Dunes" south of the Windows, the Navajo also crops out on the northeast and southwest flanks of the Salt Valley anticline. According to Dane (1935, p. 86) it varies in thickness in this area from 160 to 300 feet (49-91 m). The Navajo conformably overlies the Kayenta and represents a change from fluvial to eolian deposition. Thinnly bedded cherty limestones are common in the upper part of the Navajo, suggesting local lacustrine conditions in late Navajo time. A regional unconformity separates the Navajo from the overlying San Rafael Group.

JURASSIC ROCKS

SAN RAFAEL GROUP

The San Rafael Group is represented in Arches by two formations of Late Jurassic age, the Entrada Sandstone and the overlying Summerville Formation.

ENTRADA SANDSTONE

The Entrada Sandstone is about 500 feet (152 m) thick within the Park, and is divided into three members. In ascending order they are the Dewey Bridge Member, the Slick Rock Member, and the Moab Tongue or Member.

DEWEY BRIDGE MEMBER OF THE ENTRADA SANDSTONE

The Dewey Bridge Member is well exposed throughout Arches National Park. It crops out at the base of cliffs of the overlying Slick Rock Member of the Entrada. Locally erosional remnants are isolated from the cliffs as

grotesquely sculptured pillars known (in order of decreasing size) as "hoodoos", "goblins" and "stonebabies". The Dewey Bridge varies erratically in thickness, from 20 feet to over 100 feet (6 m to > 30 m). The Dewey Bridge is composed of red to orange-red and buff horizontally bedded siltstone, mudstone and sandstone. Bedding in the Dewey Bridge is commonly contorted. Large scale contortions are often traceable into the overlying Slick Rock Member, where the amplitude gradually decreases away from the contact. Exceptional exposures of the large-scale contorted bedding may be found in canyons on the south side of Courthouse Wash, on the southeast side of The Windows, and in the amphitheater southeast of Tower Arch in the Klondike Bluffs region. These rocks were originally assigned to the Carmel Formation by Dane (1935), but have been redefined and renamed the Dewey Bridge Member of the Entrada Formation by Wright and others (1962). The Dewey Bridge was probably deposited in lagoons bordering a shallow sea.

SLICK ROCK MEMBER OF THE ENTRADA SANDSTONE

The Slick Rock Member of the Entrada Sandstone crops out spectacularly in Arches National Park. Where it is capped by the overlying resistant Moab Member, it weathers into shear or rounded cliffs. In those regions where the Moab has been removed by erosion, the Slick Rock crops out as smooth erosional bowls, or, when extensively jointed, as spectacular parallel vertical fins of rock. The Slick Rock is composed of orange-buff or reddish sandstones. Petrography of this unit is discussed in more detail in Chapter 4. Planar beds 3 to 15 feet (1 to 5 m) thick are common in the lower and upper part of the Slick Rock, while the middle of the unit is commonly massive. The planar beds may show regular color banding in shades of reddish-orange alternating with gray

and nearly white. Cross-bedding is found throughout the unit. Long rows of solution pits and cavities accentuate bedding surfaces. At least two intraformational angular unconformities are present in the Slick Rock. These angular unconformities are well exposed in fins of Slick Rock near the Devil's Garden trail parking lot (SW 1/4 of NW 1/4 Sec 27, T 23 S, R 21 E, Grand County, Utah). In the northern Salt Valley the Slick Rock ranges in thickness from 226 feet (68.8 m) (O'Sullivan, 1981) to 270 feet (82 m) (Gard, 1976). In Moab Canyon, Gilluly and Reeside (1928, p. 107) measured a thickness of 315 feet (96m) of these rocks. The Slick Rock includes those sandstone beds that originally were defined as Entrada Sandstone by Dane (1935). In the San Rafael Swell these rocks are both underlain and overlain by marine rocks (Gilluly and Reeside, 1928, p. 73-79). The Slick Rock was probably deposited in and around a shallow sea. The localized nature of the intraformational angular unconformities suggests active diapiric salt movements during Slick Rock deposition.

MOAB MEMBER OF THE ENTRADA SANDSTONE

This member, sometimes referred to as the Moab Tongue, was included in the Entrada by Wright and others (1962). The Moab crops out as resistant caps above Slick Rock cliffs and as an extensive thin sheet of white to light-gray cross-bedded sandstone. Details of the petrography of the Moab are presented in Chapter 4. Everywhere within the Park the Moab Member displays a constant thickness of 88 feet (27 m), and is divisible into three sub-units, informally termed A, B and C. The upper subunit (A) and the lower subunit (C) are characterized by large scale sand-dune type cross-bedding, and are 64 feet (19.6 m) and 13 feet (4.0 m) thick, respectively. The (B) subunit is about 11

feet (3.4 m) thick and displays nearly horizontal bedding, with small-scale current ripple marks and thin clay or shale partings. The B and C sub-units are correlative with sandstones assigned to the Curtis Formation by Gard (1976, p. 20) in the northern Salt Valley. The Moab was probably deposited as sand dunes on broad marginal beaches. The absence of thinning in the Moab toward the anticlinal axis suggests that this unit originally completed covered, or almost completely covered, the entire map area.

SUMMERVILLE FORMATION

Based on lithologic similarities, Dane (1935, p. 102-105) assigned a thin red heterogeneous sequence of rocks above the Moab member to the Summerville Formation, the type locality of which lies to the west in the San Rafael Swell (Gillily and Reeside, 1928, p. 80). The Summerville Formation conformably (?) overlies the Moab Member of the Entrada Sandstone and forms a narrow red slope above the extensive white dip slope of the Moab. Within the Park the Summerville is composed of about 40 feet (12 m) of alternating beds of red to gray claystone, friable platy sandstone and thin-bedded cherty limestone. Ripple marks are commonly observed in the thin-bedded sandstones. Large concretions or knockers of chert, up to 3 meters in diameter, are common in the Summerville. Nomenclature of these rocks has been contested by O'Sullivan (1981). He assigns these beds as the Lower Beds of the Salt Wash Member of the Morrison Formation, separated from the Moab by the regional J-5 unconformity of Pipiringos and O'Sullivan (1978). These rocks were deposited in shallow, quiet water, perhaps on the lower reaches of a delta.

MORRISON FORMATION

A regional unconformity defines the base of the nonmarine Morrison Formation of Late Jurassic age. Cater and Craig (*in:* Cater, 1970, P. 39) reported that vertebrate and fresh-water invertebrate fossils of the Morrison of the Colorado Plateau indicate a late Jurassic age, although in places the uppermost part of the Morrison interfingers with the lowermost beds of the Lower Cretaceous Cedar Mountain Formation and thus may be of Early Cretaceous age. The Morrison crops out in the collapsed core of the Salt Valley anticline and along the northeastern and southwestern flanks. The Morrison is divided into two members, the Salt Wash Member and the overlying Brushy Basin Member. The total measured thickness of the Morrison in this area is 614 feet (187 m) (Craig, 1959). The Morrison is generally considered to be the oldest formation to have completely or almost completely blanketed the salt and gypsum cores of the salt anticlines throughout the Paradox Basin (Cater and Craig, *in:* Cater, 1970, p. 35).

SALT WASH MEMBER OF MORRISON FORMATION

The Salt Wash Member is about 235 feet (72 m) thick in the northern Salt Valley (Gard, 1976). It consists of alternating sandstone, mudstone and claystone beds, each less than 30 feet (9 m) thick. Sandstones are commonly silicified and coated with dark desert varnish. White to tan chert grains are common in the coarser clastics. Bedding is highly lenticular, and channeling is common. The Salt Wash is a fluvial unit, deposited in stream channels and on flood plains.

BRUSHY BASIN MEMBER OF MORRISON FORMATION

The Brushy Basin Member crops out in steep slopes with brilliant horizontal banding in hues of green, gray, red, maroon and orange-purple. These rocks are about 379 feet (116 m) thick in this area (Gard, 1976). The Brushy Basin is composed of varigated mudstone and claystone, containing lesser amounts of sandstone, conglomeratic sandstone, and limestone, all of which are commonly lensing. A distinctive red and green chert-pebble conglomerate (the "Christmas Tree" conglomerate) marks the base of the Brushy Basin Member. The dominant clay in the mudstone and claystone is montmorillonite, a swelling clay apparently derived from the hydrolysis and devitrification of volcanic ash (Cater and Craig, *in* Cater, 1970, p. 46). Pebbles of red and green chert and quartzite as well as silicified bone fragments and wood are common in the Brushy Basin. The upper beds of the Brushy Basin are glauconite-bearing and locally contain green-pebble conglomerates. Fluvial deposition initiated in Salt Wash time continued through Brushy Basin time.

CRETACEOUS ROCKS

CEDAR MOUNTAIN FORMATION

The Cedar Mountain Formation of Early Cretaceous age (Stokes, 1952; Simmons, 1957) conformably overlies the Brushy Basin Member of the Morrison Formation. Cedar Mountain rocks crop out in the collapsed core of the anticline, south of the Fiery Furnace, where they form resistant hogbacks. The Cedar Mountain in this area consists of about 135 feet (41.5 m) of alternating sandstone, claystone, and nodular limestone. The yellowish-gray sandstones are lensing, sporadically conglomeratic, and in places quartzitic. The interbedded claystones vary in color from gray to green and purple, and

-17-

weather readily. The Cedar Mountain is a fluvial deposit. The coarse clastics suggest nearby orogenic highlands.

DAKOTA SANDSTONE

The contact relation between the Cedar Mountain Formation and the overlying Dakota is unclear in Arches. Elsewhere the Dakota disconformably overlies the Cedar Mountain (Carter, 1957). The Dakota has been assigned a Late Cretaceous age. These rocks crop out in the collapsed core of the anticline, often forming a second hogback parallel to the Cedar Mountain hogback. Rocks assigned to the Dakota are only 26 feet (8 m) thick in the Park, and consist of lensing cross-stratified pebbly conglomeratic sandstone with friable carbonaceous sandstone and carbonaceous shale. Black chert pebbles are common in the pebble conglomerates. The Dakota is a terrestrial deposit that Cater and Craig (*in* Cater, 1970, p. 46) believe was deposited on a broad coastal plain in front of an advancing Cretaceous sea, which deposited the overlying Mancos Shale.

MANCOS SHALE

The Mancos Shale is of Late Cretaceous age and conformably overlies the Dakota Sandstone and is gradational into it. (Cater and Craig, *in* Cater, 1970, p. 46-47). The Mancos consists of a thick sequence of lead-gray fossiliferous marine shales. The fossil oyster *Pycnodonte newberryi* Stanton (identification by W.A. Cobban, Personal communication, 1982) is abundant in the basal 10-50 feet (3-15 m) of the Mancos. The Mancos has been downdropped into the core of the anticline. No complete section of Mancos shale is present within the Park. The nearest complete section is found between the Salt Valley and the Book Cliffs, where Fisher and others (1980) report a thickness of the Mancos of

-18-

3300 feet (1006 m). The thin-bedded Ferron Sandstone Member of the Mancos Shale is a persistent marker bed in Mancos exposures outside of the Park, but was not identified in the Salt Valley. Because the Mancos Shale is easily eroded and possesses no persistent marker beds, it was not possible to determine the internal structure of Mancos outcrops. The Mancos was deposited in a Cretaceous sea. From other areas it is known that the Mancos Shale marks the last time that marine waters covered this area. Continental deposition has prevailed since the end of Mancos time.

TERTIARY(?) ROCKS
FORMATION OF SALT VALLEY

A sequence of rocks of possible Tertiary age is preserved in the collapsed core of the Salt Valley anticline. These rocks were first discovered in the summer of 1982, and the following description is very preliminary. The best exposure noted of these rocks is in the SE 1/4 of Section 12, T 24 S, R 21 E; and the SW 1/4 of Section 7, T 24 S, R 22 E, Grand County, Utah. The sequence exposed in this area is at an elevation of about 4480 feet (1365 meters), and is folded into a gentle syncline, with the fold axis trending about east-west. The sequence is about 35 meters thick, and consists of 1-5 meters of basal conglomerate, overlain by about 25 meters of tuffs, channeled sandstones, siltstones and variegated pastel marls, which in turn are capped by 4-6 meters of tuffaceous sandstone and calcareous sandstone.

The basal conglomerate is reddish in color and is fairly well lithified, but not silicified. It crops out as a prominent ledge. The conglomerate unconformably overlies older rocks exposed in the breached core, including the Pennsylvanian Hermosa group, the Triassic Chinle Formation and the Late

Cretaceous Mancos Shale. Pronounced local channeling is noted in the conglomerate. The conglomerate contains a large fraction of angular boulders of red and tan sandstones which are as large as 40 cm in diameter, although most are less than 20 cm in diameter. Recognizable lithologies present in the conglomerate include: Late Cretaceous Mancos Shale (pycnodonte showing rounding due to transport); Late Cretaceous Dakota formation conglomerates; Late Jurassic Morrison formation (both Salt Wash and Brushy Basin conglomerates); large nodules of red chert, probably from the Late Jurassic Summerville formation; and clasts of silicified limestone containing a fresh-water gastropod fauna.

Samples of the fossiliferous limestone were examined by Dr. J. H. Hanley of the Paleontology and Stratigraphy Branch, U.S. Geological Survey, Denver, Colorado. The samples yielded assemblages of early Tertiary(Eocene) age (J.H. Hanley, personal communication, 1982). Excerpts from his report follow.

"Hand Specimen #3

The gastropod fauna exposed on the weathered surface of this irregularly silicified block, and on freshly broken surfaced includes:

Planorbidae:

Omalodiscus sp. indet.

Promenetus sp. indet.

cf. *Drepanotrema* sp. indet.

Biomphalaria? sp. indet. Form B ?

Planorbidae: indet.

Physidae:

Physa sp. indet.

Lymnaeidae:

Lymnaea sp. indet. ".

"I interpret this sample to be of Eocene age. The composition of the fauna is quite similar to that of the *Physa-Biomphalaria-Omalodiscus* association of Hanley (1976)." "Purely on the basis of generic composition, this fauna is unlike molluscan assemblages previously reported from the Jurassic through Paleocene of the Colorado and Wasatch Plateaus. The *P-B-O* association noted above is typical of the early and middle Eocene in Southwestern Wyoming and and northwestern Colorado. In those areas, this assemblage inhabits shallow, quiet-water floodplain lakes, which I term ponds to distinguish them from the main lacustrine system of the Green River proper. I cannot discount the possibility that the assemblage is of Oligocene age, but such diverse planorobid-dominated assemblages are not typical of the Oligocene of the High Plains sequence."

The Eocene age of these limestone clasts definitely dates the basal conglomerate as post-early Eocene.

Other constituent clasts within the basal conglomerate of the Tertiary(?) sequence include a suite of "exotic", hard, rounded cobbles. This cobble suite includes: red and white to reddish-purple quartzite, some showing quartz-filled fractures; and black chert, commonly laced with quartz-filled fractures. Other cobbles within this exotic suite bear characteristics suggestive of an igneous origin. Most of these "exotic" cobbles and pebbles are 2-3 cm in diameter, with the maximum diameter noted being about 7 cm. A thorough study of the petrology of cobbles of

-21-

the "exotic suite" will be the topic of future research.

Although the silicified limestones are probably from Green River-equivalent rocks, no clasts of oil shale are present in the conglomerate. Also conspicuously absent are diorite clasts, suggesting that the source area for the conglomerate does not include the La Sal mountains.

The basal conglomerate is overlain by 3-4 meters of poorly lithified pebble- and cobble-bearing marl. Large angular boulders are rare in this horizon, although rounded cobbles of the "exotic" suite float in a matrix of marl. The cobbles weather out easily to form a protective lag surface. The top of the cobble-bearing marl is a sharp horizon, overlain by about 25 meters of lenticular beds of tuff, siltstone and sandstone, interbedded with more persistent banded pastel marls. Colors of the marls range from off-white to lavender. Individual color bands are 2-4 meters thick and extend laterally for at least 50 meters.

The marls are capped by 4-6 meters of well-sorted, fine-to- medium-grained, friable, tuffaceous sandstone. The sandstone has a calcareous cement (caliche?) and contains abundant carbonized root casts.

The entire sequence has been downfaulted and gently folded. The original extent of the sequence is not now known, but Dr. Brann Johnson of Texas A & M University reports similar marls from Cache Valley and at isolated localities in Salt Valley (B. Johnson, personal communication, 1982). Additionally, isolated patches of the "exotic" cobble suite of the basal conglomerate, including silicified Eocene limestones, have been found elsewhere within Arches National Park. Extensive lag deposits of the exotic cobbles were found at an elevation of about 4900 feet (1494 meters) on the southwest flank of the anticline of the NE 1/4 of Section 7, T24S,

R21E, Grand County, Utah. Scattered lag deposits are also present in the Salt Valley at an elevation of about 4800 feet (1463 meters) in the SE 1/4 of SW 1/4 of Section 33, T 23 S, R 21 E, Grand County, Utah. Outcrops of the basal conglomerate of the formation of Salt Valley are also found in the S 1/2 of NW 1/4 of Section 4, T 24 S, R 21 E, at an elevation of about 4760 feet (1451 meters).

The nearest known outcrop of Green River rocks is in the Book Cliffs, some 50 kilometers north of the Salt Valley localities (figure 1-1). Salt Wash is an antecedent stream which crosses the Salt Valley anticline flowing south and empties into the Colorado River. The stream heads at the Book Cliffs 5 kilometers northeast of Thompson, Utah, and drains a large area northeast of the Salt Valley anticline. Salt Wash is entrenched in a 400 foot (122 meters) deep canyon from the Salt Valley to the Colorado River. Although the Eocene rocks found on the southwest flank of the anticline are completely exotic to the current drainage, it seems likely that they, as well as the Eocene cobbles in the Salt Valley, were originally transported to their current location by the ancestral Salt Wash system.

The wide area over which either outcrops or lag deposits of this unit have been found suggest that this sequence of rocks was originally fairly widespread. If an age can be determined for the sequence in Salt Valley, it will be possible to address the most recent history of the Salt Valley area. More detailed work is required before the regional implications of the Formation of Salt Valley can be addressed.

QUATERNARY(?) DEPOSITS

Mass Wasting(?) Debris

A series of isolated low mounds on the southwest flank of the Salt Valley anticline are composed of heterogeneous, chaotic breccia (figure 1-3). Most of the mounds are near-circular in shape and have a diameter of 35-100 meters. Maximum relief of the largest mound is about 20 meters. At least thirty discrete bodies are found in a northwest trending belt 300-500 meters wide that extends some 7.5 kilometers, from SE 1/4 Section 6, T 24 S, R 21 E, to SE 1/4 Section 14, T 24 S, R 21 E, Grand County, Utah. These rubble mounds are located in an area of isolated drainage. Boundaries of the drainage are the topographic highs of the Klondike Bluffs region to the north and the southwest flank of the Salt Valley anticline to the east.

The breccia mounds consist of unconsolidated rubble. There is no sorting in the rubble. Constituents range in size from boulders four meters in length to loose sand, silt and clay. Silicious clasts and boulders comprise a lag surface on the rubble mounds. Individual prismatic clasts and boulders are angular and show no evidence of extensive fluvial transport. Rounded cobbles are present, but these may be derived from disaggregated boulders of conglomerate. Many of the lithologies found in the breccia are sufficiently unique that their source beds can be determined. Recognizable lithologies found within the breccia are tabulated below, with the probable source rock noted in brackets.

A)   Chert nodules and knockers, up to 2 meters in diameter. {Summerville Formation}

Figure 1-3.

Ground view of Quaternary debris mound, southwest flank of Salt Valley anticline. Large juniper trees are ~ 1.5 meters tall. Note large boulders capping the mound and lag surface of smaller boulders. A second mound is visible in the left background. View looking south; La Sal mountains in extreme background.

B) Large, prismatic boulders of cross-bedded quartzite, commonly crusted with patches of "desert varnish". The boulders occasionally display slickensided surfaces. Boulders of up to four meters in maximum dimension are present. {Salt Wash Member of Morrison Formation}.

C) Small, irregular patches of varigated clay {Brushy Basin Member of Morrison Formation}.

D) Boulders of green-pebble conglomerate, up to one meter in diameter. Patches of small (< 2 cm), well-rounded green-tinted pebbles are common, and are probably remnants of disaggregated liths of green-pebble conglomerate. {Brushy Basin Member of Morrison Formation}.

E) Black chert-pebble conglomerate {Dakota Sandstone}

All of the breccia mounds rest upon an erosional surface of the Entrada Sandstone, commonly on the Slick Rock Member, but in places on the Dewey Bridge Member. No faults or fracture zones were recognized in the underlying Entrada Sandstone. The array of rubble mounds appears to be confined to the locus of an abrupt inflection point on the southwest anticlinal flank, with rocks to the northeast dipping to the southwest about 30 degrees, while rocks to the southwest dip 4-9 degrees southwest.

Three potential origins may be hypothesized for the rubble mounds: fluvial deposits, landslide debris and mass-wasting remnants.

A fluvial origin is considered improbable because: 1) The rubble is

-26-

absolutely unsorted; 2) individual clasts or boulders are angular and show no evidence of stream transport; and, 3) the rubble apparently includes discrete bodies of shale, which would quickly disaggregate in fluvial conditions.

A landslide could produce such a chaotic rubble, but the only possible source for landslide material would be toward the anticlinal axis. Since the rubble currently rests on an erosional surface, this would require that a slab of rock at least 250 meters thick remained perched on the steeply dipping southwest flank of the anticline while material downdip from the slab was removed by erosion. At some time, the slab may have detached and descended downslope as a catastrophic landslide. Although the current evidence cannot rule out such a scenario, a catastrophic landslide origin for the rubble is considered improbable.

A mass-wasting mechanism is considered the most probable mode of emplacement for the rubble. It is hypothesized that rubble moved slowly down the steep anticlinal flank and accumulated near the line at which the limb dip abruptly shallowed.

HOLOCENE DEPOSITS

The youngest sediments in Arches National Park include alluvium, windblown material and talus. Alluvium covers most of the floor of Salt Valley, the upper reaches of Courthouse Wash, and the drainage of Salt Wash. The alluvium was derived from erosion of the rocks that form the anticline. Alluvium and gravel bars are found along the Colorado River. Large expanses of primarily eolian material, reworked in part by water, are found south and west of The Windows and north of Delicate Arch. Talus deposits are common at the base of the steep cliffs along the Colorado River and in Moab Canyon.

-27-

STRUCTURAL GEOLOGY

REGIONAL SETTING

The Salt Valley anticline is the most northwesterly of the salt-cored anticlines of the Paradox Basin. The Paradox Basin is located in the north central portion of the Colorado Plateau, a distinct physiographic and geologic province. Rocks of the Colorado Plateau are generally flat-lying sediments which are superbly exposed in canyons which cross this arid land. Structural disruption of the flat-lying sediments is infrequent, but spectacular, as evidenced by the great monoclines such as the San Rafael Swell; the towering intrusive laccoliths of the La Sal, Abajo and Henry Mountains; and the fabulous salt anticlines of the Paradox Basin.

The Paradox Basin is a region approximately 120 miles (192 km) long and 50 miles (80 km) wide which is dominated by a series of large *en echelon* northwesterly trending anticlines. The anticlines are cored with salt and are commonly breached. The salt anticlines are localized over large, northwesterly trending faults in sub-salt rocks. A cluster of large dioritic laccoliths, the La Sal mountains, was intruded into the midst of the anticlines in the Oligocene.

STRUCTURAL GEOLOGY OF ARCHES NATIONAL PARK

FOLDS

The dominant structure in the map area is the breached, northwest-trending Salt Valley anticline. The map area also includes a portion of the collapsed Spanish Valley (Moab) anticline. Pennsylvanian-age evaporites of the Paradox Formation crop out in the core of the Salt Valley anticline. The Salt Valley anticline is about 28 km long and the valley in the breached core is

about 4 km wide. The anticline plunges gently to the northwest beneath a thick section of Mancos Shale. The anticline abruptly terminates at its southeastern end about 4 km west of Salt Wash, where it joins the east-west structure of the Cache Valley anticline.

The Salt Valley anticline is asymmetric, with limb dips on the southwest side of 12 to 30 degrees and limb dips on the northeast side of 4 to 7 degrees. The asymmetry is due in part to the infolding of Triassic(?) and younger rocks of the northeast flank into the collapsed core, as shown on cross-section B-B' (Plate II). Similar infolding and asymmetry also characterizes the subparallel Spanish Valley (Moab) salt anticline in Moab Canyon.

Several broad, shallow folds are subparallel to the Salt Valley and Spanish Valley anticlines. These include an unnamed anticline east of the Moab fault, the Courthouse syncline, and the Windows anticline. The Windows anticline lies along the southeast projection of the axis of the Salt Valley anticline, suggesting that this structure marks the original continuation of the Salt Valley anticline. A relatively tight east-west trending structure, the Windows syncline, lies north of the Windows anticline and apparently truncates it. The Windows syncline continues on to the west for about 5 km, with the fold axis trending gradually more northwesterly. North of Eye-of-the-Whale, a small doubly-plunging anticline is *en echelon* to the Windows syncline. Northwest from this area the syncline vanishes, although a continuation of the fold axis marks a sharp inflection point where rocks on the southwest flank of the Salt Valley anticline abruptly shallow in dip. This trend is truncated by the complexly faulted region near Klondike Bluffs.

-29-

FAULTS

SUB-SALT FAULTS

Baars (1966, 1979) has presented evidence that large northwest-trending faults underlie all the diapiric anticlines of the Paradox Basin. Cater (1970) documented the localization of salt anticlines in southwestern Colorado along northwest-trending faults in sub-salt rocks. The presence of a large, northwest trending fault at depth beneath the southwest flank of the Salt Valley anticline is indicated by drilling data. Subsurface geology, derived from three wells drilled on the anticlinal flanks, has been projected to cross-section A-A' (Plate II). The well data forms the primary basis for the deep structure shown on A-A'.

Shell Courthouse Wash Unit #1 is located in NE 1/4 SW 1/4 NE 1/4 of Section 12, T 24 S, R 21 E. This well is on the southwest flank of the anticline, just outside the boundary of Arches National Park. This well encountered salt at a depth of 1800 feet (elevation of 2850 feet above sea level), and penetrated a section of salt 2700 feet thick. Sub-salt rocks were encounted at a drilling depth of 4500 feet.

Pure Oil Co. NE Salt Valley Unit #1 was drilled in the SW 1/4 SE 1/4 NW 1/4 of Section 20, T 23 S, R 20 E. Salt was encountered at a depth of 848 m (2780 ft). The well was abandoned at a depth of 926 m (3036 ft) while still drilling in salt.

Union Oil Co. Devil's Garden USA #1 is located in SW 1/4 SE 1/4 of Section 5, T 23 S, R 21 E. This well penetrated the top of the salt at a depth of 2255 m (7396 ft) and was still drilling in salt when it was abandoned at a total depth of 2824 m (9262 ft) (Hite, 1977, p. 5).

Joesting and Case (1962) found that a 26-milligal gravity low over the Salt Valley anticline was compatible with a salt thickness in the anticlinal core of at least 8000 feet. From a synthesis of well data, Hite (1977) estimated a thickness of salt in the anticlinal core of 11,800 feet (3600 m). This latter figure is in accord with the data from the Devil's Garden well. The data suggest that there is at least 6000 feet of structural relief at the base of the salt between the anticlinal axis and the southwest flank, a distance of about three miles. The structural relief is not evidenced in the Mesozoic sequence on the anticlinal flanks and is inferred to be accommodated on large northwest-trending faults underlying the southwest flank of the anticline (Cross-section A-A', Plate II).

SURFACE FAULTS

Exposed faults are generally subparallel to the anticlinal axes. The faults in the thick sandstone units are generally sharp, near-planar surfaces of displacement, while faults in more heterogeneous units, such as the Kayenta, are commonly diffuse zones several meters wide. Fault morphology in thick sandstone units is of the type described by Aydin (1977) in the San Rafael Desert. These faults are characterized by localization of strain along subparallel, anastamozing deformation bands which collectively form a zone of deformation. Major displacement is accommodated by a slip surface on one side of the zone of deformation. Outcrops of sandstone near large faults are commonly laced with a complex array of deformation bands, which stand out on erosional surfaces as small resistant ribs.

Displacement on the mapped faults ranges from a few feet (~ 1m) on minor faults to over 2000 feet (> 610 m) on the Moab fault system. All major

-31-
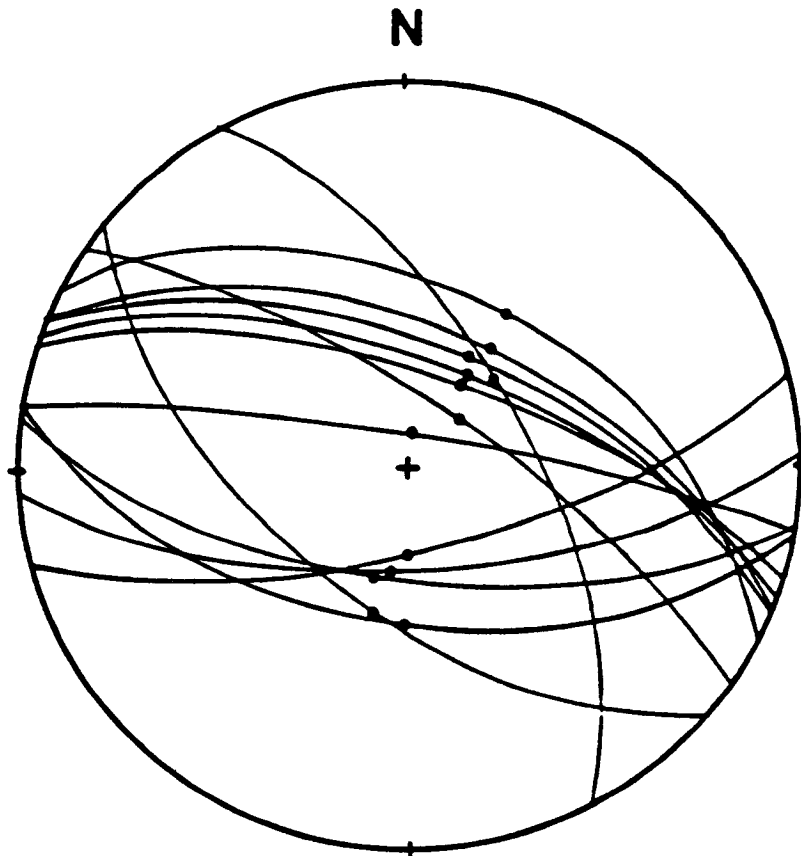
Figure 1-4.

Equal-area stereonet plot of fault planes and slip directions (black circles) for 13 faults in Arches National Park. Normal displacement was observed on each of these faults.

faults are normal faults. Slip directions were determined on more than eighty faults in the map area. Fault surfaces which show a large apparent component of strike-slip displacement are confined to the complex regions of the core of Salt Valley and the Moab fault zone, where blocks have been jostled and rotated. The fault planes and slip directions of thirteen faults located away from the complex core of Salt Valley are presented in figure 1-4. These data indicate virtually no component of strike-slip displacement on the faults.

Faults bordering the Salt Valley generally display a stairstep geometry, with cumulative downward displacement increasing toward the anticlinal core (Cross-section A-A', Plate II). Several large faults on the southwest side of Salt Valley are slightly oblique to the anticlinal trend and show pronounced "scissors" geometry, with displacement decreasing away from the anticlinal core. Similar fault geometry is also noted in several large faults south of Delicate Arch, along the northern boundary of Cache Valley.

Faults cut all rocks, but were not observed to offset alluvium in the map area. Dane (1935, p. 138) recorded the fault offset of Holocene(?) caliche layers at the east end of Cache Valley. Although some of the faulting may have originated as extensional faults over the rising anticline, the dominant movement now recorded by them is associated with collapse of the anticline. The evidence of recent faulting suggests that collapse of the salt core is still in progress.

COLLAPSE STRUCTURE

Exposed in a small body about 0.8 km north of Balanced Rock (NW 1/4 of SE 1/4 of NE 1/4 of S 23, T-24 S, R 21 E, Grand County Utah) is a jumbled mixture of chaotic breccia. Coherent blocks within the breccia may have a

maximum dimension of 20 meters. These blocks are confined to a near-circular region about 100 meters in diameter. An irregularly curved fault bounds this region to the east and south. The fault dips steeply (~70 degrees) outward from the breccia body. At the southeast contact, the breccia body is in sharp contact with extensively shattered Navajo Sandstone. Contacts to the west and north are not exposed.

Identifiable lithologies found in the breccia include: Moab member of Entrada Sandstone; Summerville Formation; Salt Wash and Brushy Basin members of the Morrison Formation; Dakota Sandstone; and Mancos Shale. The presence of Mancos Shale in the breccia, juxtaposed against Navajo Sandstone wallrock requires a minimum vertical displacement of the breccia of some 390 meters.

In geometry and character, this breccia body strongly resembles the collapse structures of Spanish Valley (Weir and others, 1961; Weir and Puffett, 1981) and the breccia pipes of Lockhart Basin (Huntoon and Richter, 1979). Similar breccia pipes are also known from the Lisbon Valley anticline, where the Rio Algom Corporation encountered a vertical breccia pipe at a depth of some 2,600 feet (790 meters) during mining operations (Mr. M. Cartwright, personal communication, 1980).

Huntoon and Richter (1979) suggest that the breccia pipes of Lockhart Basin bottom in Pennsylvanian evaporites, and formed due to upward stoping from voids resulting from solutional removal of salt. Weir and Puffett (1981) bottomed the collapse structures of Spanish Valley in Paleozoic limestone beds which overlie the evaporite sequence. The volume problems inherent in the downward displacement of at least 390 meters of section requires that the collapse pipes of the Salt Valley anticline penetrate at least to the

-34-

Pennsylvanian evaporites. Dissolution of these evaporites could create room into which the breccia bodies dropped. It is possible that sub-salt structures have localized the region of salt dissolution. Some support for this idea is gained from the position of the collapse structure, which is located slightly south of the axis of the Windows syncline. It is possible that the Windows syncline itself is a rim syncline resulting from withdrawal of underlying salt.

JOINTS AND FRACTURES

Extensive, spectacular exposures of fractured and jointed rock are present within Arches National Park. Regional fracture sets, extending over tens of square miles, are best developed in three units: the Navajo Sandstone; and the Slick Rock and Moab Members of the Entrada Sandstone.

In the area known as the "petrified dunes", a region of approximately 25 square miles ($64km^2$) located south of the windows area and west and north of the Colorado River, two sets of regional fractures are developed in the Navajo Sandstone. The northern two-thirds of this area contains a regional fracture set which trends about N 30° W. A fracture set trending about N 70° W dominates the southern third of this area. The two fracture sets interpenetrate over an area of several square miles ($\sim 5km^2$). Each of the fracture sets in the Navajo Sandstone is characterized by parallel, conjugate sets of fractures which sometimes display dip-slip displacements of up to a few meters.

The northern fracture set is subparallel to the axis of the Windows anticline, suggesting a genetic link between the extensional fracturing and faulting and growth of the Windows anticline.

The southern fracture set cuts obliquely across the axis of the Courthouse

syncline and may be related to the collapse of the northeast flank of the Spanish Valley (Moab) anticline.

Regional sets of systematic joints are exceptionally well developed in the Moab Member of the Entrada Sandstone, with about 25 square miles ($84km^2$) of spectacular outcrops on the flanks of the Salt Valley anticline. Systematic jointing in the Slick Rock Member is less extensively developed regionally, but is also spectacular.

Systematic joint sets in both of these units are characterized by subparallel sets of fractures which are perpendicular to the top and bottom bedding surfaces. Small lateral displacements have been documented along the joints in the Moab Member, but nowhere has dip-slip displacement been noted.

Although several sets of systematic joints may be present in a given area, the sets are generally sub-parallel to the axis of the Salt Valley anticline. The most prominent exception is the area known as the Fiery Furnace, where the systematic joints are almost perpendicular to the trend of the breached anticline.

A detailed description of the jointing developed in the Moab member is the topic of Chapter two, while the mechanics of jointing is the subject of Chapter three.

The timing of joint development is problematic. In places where two sets of systematic joints are developed it appears that the youngest set is related to the on-going collapse of the Salt Anticline (Dyer, 1979). This requires that the youngest systematic joint sets formed under near-surface conditions, probably with less than 200 meters of overburden. The age, and hence the geologic boundary conditions relevant during joint growth, are not known for the older

sets of zoned joints. These older joints may be associated with either the initial stage of anticlinal growth or an early stage of collapse.

AGE OF DEFORMATION

Thinning of sedimentary rocks on the flanks of salt anticlines throughout the Paradox Basin indicates that the salt cores were mobile from Pennsylvanian through Late Jurassic time. A thick sequence of Late Cretaceous and Tertiary sediments blanketed the anticline by the time of the intrusion of the La Sal laccoliths in the Oligocene.

Late Jurassic and younger rocks were folded into essentially their present form sometime after the Late Cretaceous. Two mechanisms may be hypothesized as causes of the folding: shortening of the sedimentary sequence during the Late Cretaceous-Early Tertiary Laramide orogeny; and thermal activation of salt flowage during the Oligocene La Sal intrusive event. The absence of any sediments of Early-to mid-Tertiary age in the Park precludes definite assessments of the contributions of either of these events to the post-Mancos folding.

In the eastern Paradox Basin, Cater (1970, p. 65) found that the latest phase of anticlinal growth postdated deposition of the Late Cretaceous Mesaverde Formation, the youngest rocks exposed in that region. Based on evidence of Late Cretaceous tectonism in areas adjacent to the Paradox Basin, he favored a deep-seated deformation, such as the Laramide orogeny, as the event responsible for folding (Cater, 1970, p. 65). The total absence of small-scale folds and thrust faults in the sediments in Arches tends to argue, albeit weakly, against large horizontal compressive deformation of this area.

Cater (1970) also found that collapse of the crests of the salt anticlines occurred in two stages apparently widely separated in time. The first stage of

collapse occurred shortly after the folding event, while the second stage followed uplift of the entire Colorado Plateau in the middle and late Tertiary. The core of the Salt Valley was breached and collapsed prior to the deposition of the Tertiary(?) Formation of Salt Valley. It is not known whether the subsequent deformation of these Tertiary(?) rocks is due to a distinct second stage of collapse, or whether all collapse is due to a single, long-lived event.

Hunt (1958, p. 315) was doubtful of a genetic relationship between the salt anticlines and the La Sal intrusives, although he did not detail the rationale behind this judgement. Bodell and Chapman (1982) found an average heat flow along the Salt Anticline trend of $64 m Wm^{-2}$, which is significantly higher than the average of $51 m Wm^{-2}$ observed in the adjacent San Rafael Swell and Green River Desert. Pending further investigation, it does not seem prudent to summarily dismiss thermal activation of salt as a potential contributor to the post-Cretaceous folding.

The last phase of deformation in the area is the unfolding of the northeast flank of the anticline into the collapsing core. Cater (1970, p.66) proposed that, throughout the Paradox Basin, this phase is a late, distinct episode of collapse associated with uplift of the Colorado Plateau and downcutting of the Colorado River. Following the Miocene uplift of the Colorado Plateu (Hunt, 1956, p. 77), the Colorado River entrenched itself and breached the salt cores of the salt anticlines. Dissolution of salt was apparently accompanied by flowage of salt toward the breached cores (Cater, 1970, p. 66). This phase of collapse is still active.

CHAPTER TWO

SUPERPOSITION OF ZONED JOINT SETS

ABSTRACT

Systematic joints in the Moab Member of the Entrada Sandstone in Arches National Park, Utah, U.S.A., display a zoned character. All subparallel joints which make up a given joint zone are confined to narrow zones, 0.5 - 2.0 meters wide. Adjacent zones of the same set are separated by a distance which is on the order of the bedding thickness (27 meters). Zones may extend for kilometers in lateral extent, but the individual fractures are limited to the Moab Member. Although joints may be present in overlying or underlying units, their orientation and character are distinctly different from the zoned systematic joints in the Moab Member. Field relations allow relative ages to be determined between multiple non-parallel sets of zoned joints. Three geometric relations between younger and older joints are observed: (A) younger joint zones are bounded by older zones and curve into parallelism with the older zone; (B) the younger zone is bounded by older zones and intersects the older zones at nearly a right angle; and, (C) the younger zone continues without deviation through an older, sheared and cataclasized zone. The curving of younger joint zones, seen in interactions (A) and (B), becomes more prominent in proximity to the open, through-going zone. Each characteristic interaction occurs throughout a continuous area, or domain, of 1 - 8 square kilometers. Detailed observations of the offset of sand dune cross-bedding allows shear displacement along joints to be determined. In all cases, the younger joints display the least shear offset. Commonly there is no observable offset on the youngest joints, only a dilational opening. This suggests that all the zoned joints investigated originated as extensional fractures. The systematic change in orientation of younger joint zones as they approach older zones indicates that the stress field is locally perturbed by the older zone.

INTRODUCTION

Brittle fractures in rocks are commonly classified by the shear displacement parallel to the fracture surface. *Faults* show an appreciable shear displacement, while *joints* show little or no shear displacement parallel to the fracture surface. The relationship between jointing and faulting is poorly understood. As a result, there is no adequate theory which covers the

spectrum of brittle fracture. This chapter reports observations in Arches National Park, Utah, on joints and fault-like features that originated as joints.

PREVIOUS WORK

The origin of joints is a most controversial topic in geology. Although these ubiquitous brittle fractures have been studied intensively for more than a century, there is no consensus on the nature of the unseen processes which give rise to joints. Price (1966, p. 110) may be correct in stating ". . it is unlikely in the extreme that all joints are the result of a single mechanism.", yet the simplicity and universal occurrence of joints suggest a fundamental causal mechanism. A better understanding of the origin and mechanics of jointing is necessary before tectonic and structural inferences can be drawn from joint orientation studies. Such an understanding also has considerable economic potential: the permeabilities of many reservoirs are controlled by joint systems, and joints are often pathways for mineralized fluids.

Because joints are the end result of an unobserved process, or sequence of processes, there is little direct knowledge regarding the jointing process. Field studies contribute geometric and morphological data on joints - the fracture which is the artifact of the process.

One approach to the study of joints in particular, and fractures in general, has been to seek analogs in small-scale specimens experimentally fractured in the laboratory under carefully controlled conditions. A substantial empirical data base has been developed regarding fractures produced under triaxial compression tests $(\sigma_1 > \sigma_2 = \sigma_3)$. As summarized by Stearns and Friedman (1972, p. 83), the laboratory results suggest that any triaxial stress state is characterized by three potential fracture surfaces. Two of the potential fracture surfaces are shear-fracture planes with a dihedral angle of about 60

degrees which are bisected by the axis of the greatest principal stress and whose intersection is parallel to the axis of the intermediate principal stress. The third potential fracture is an extension fracture which is normal to the axis of the least principal stress. This interpretation is based on Anderson's (1951) theory of faulting. Stearns (1968) interpreted all the fracture patterns of the Teton anticlines of Montana in terms of the three-fracture analog of laboratory fracture tests. In this interpretation, each triplet pattern is the response to a single state of stress. Burger and Hamill (1976) found that the triplet fracture pattern adequately accounted for fracturing developed on the Dry Creek Ridge anticline, Montana.

Fracture experiments conducted under true polyaxial conditions ($\sigma_1 > \sigma_2 > \sigma_3$) indicate that more than two sets of shear fractures (faults) develop under general three-dimensional strain conditions (Aydin and Reches, 1982). Aydin and Reches (1982, p. 112) used both field observations and polyaxial fracture experiments to conclude that "faulting in a three-dimensional strain field with orthorhombic symmetry requires four sets of faults to accommodate strains in all principal directions". This in turn suggests that the conjugate fault patterns of Anderson (1951) and the triplet fracture patterns of Stearns and Friedman (1972) are associated with plane-strain conditions, rather than more generalized three-dimensional strain conditions.

Other studies indicate that fracture systems consisting of one or two sets of fractures, or orthogonal fractures, are not uncommon (Engelder and Geiser, 1980; Nickelsen, 1979; Ziony, 1966; Hodgson, 1961a). Does this mean that, for some reason, only partial geometries of the triplet fracture pattern develop, or does it mean that "natural" fractures often form by a process not duplicated by triaxial compression tests? The question is crucial, and its resolution

-41-

requires detailed field investigations specifically directed at the nature of fractures in rocks.

As Nickelsen (1976) pointed out, joint patterns record a cumulative fracture history. The patterns may represent many distinct episodes of jointing, superimposed on each other. The common inability to determine relative ages of joint sets has been a major obstacle to the advancement of knowledge regarding the jointing process.

Recently, a few workers, most notably Nickelsen (1979), Engelder and Geiser (1980) and Barton (C. C. Barton, personal communication, 1981), have successfully determined relative ages of several superimposed sets of systematic joints. All of these studies indicate that a joint set is a set of sub-parallel extensional fractures which formed in response to a fairly homogeneous stress field of regional extent. Over time, the stress field rotated and later, non-parallel systematic joint sets were superimposed over the earlier joints.

This report summarizes observations on systematic joints in a single lithologic unit over an area of approximately 50 km^2 on the flanks of the Salt Valley anticline, Grand County, Utah. This area was chosen for intensive study because of the superb exposures and the simple structural style. The joints are developed in classic examples of joint zones - a sub-category of systematic joints. Due to the nature of the joint zones, relative ages of joint sets can be readily determined. Detailed observation of the offset of sand dune cross-bedding allows lateral shear displacement to be determined, and rules out a shearing origin for the joints. The youngest joints in any of the areas of detailed study show only a dilational opening.

SYSTEMATIC JOINTS AND ZONED JOINTS

A joint, in the strictest definition, is a fracture which shows only separation of the fracture surfaces perpendicular to those surfaces. Once this fracture is formed, any later shear displacement on the surface results in a reclassification of the fracture from a joint to a fault. Many of the vertical fractures examined in Arches display shear horizontal displacements ranging from millimeters to tens of centimeters. There is abundant evidence, detailed elsewhere, that all of these fractures originated as extensional joints, and that shear displacement occurred later in the history of the fracture. In this report the term joint is used to describe all fractures with an extensional origin, even though they may display small shear displacements due to later shearing.

Systematic joints, as used in this paper, refers to sets of parallel or sub-parallel fractures which maintain characteristics such as morphology, geometric orientation and spatial distribution over relatively large areas, or domains. A common assumption is that a set of systematic joints reflects a relatively homogeneous state of stress throughout the domain. As noted by Hodgson (1961a), systematic joints show the following distinct structural features:

(1) Systematic joints commonly exhibit planar or broadly curved traces or surfaces.

(2) Systematic joints most commonly occur about at right angles to the upper and lower surfaces of the rock units in which they are present, regardless of the orientation of these units.

The term, as used here, differs from Hodgson's usage in that cross-cutting criteria are not applied. No distinction is made between joints that intersect

and cross other sets, and those joints that approach or meet but do not cross other joints.

Zoned joints are a subset of systematic joints that are confined to a narrow zone, commonly with no joints of that set located between the zones. Characteristics of zoned joints include:

(1) Zones are made up of discrete, overlapping individual joints.

(2) Zones of a given set display a characteristic interzone spacing over a large region.

(3) Although a zone may be broadly curved over its length, individual joints are near-planar features.

(4) Joints within a single zone typically overlap each other laterally by a large multiple of their horizontal separation.

(5) Joints within a zone show no consistent *en echelon* pattern in either map or cross-section view.

ZONED JOINTS IN ARCHES NATIONAL PARK

Detailed examination of about 20 km^2 of outcrop of the Moab Member on the flanks of the Salt Valley Anticline, in conjunction with less rigorous traverses of the remaining 30 km^2 of outcrop, support the following findings:

(1) Zoned joints are confined to the Moab Member (figure 2-1). Individual joints do not penetrate into either the overlying Summerville Formation or the underlying Slick Rock Member. A zoned morphology is not typical of the joints in either the overlying or underlying units. All the following observations pertain only to zoned joints of the Moab Member.

-44-

Figure 2-1.

Oblique aerial view looking south of zoned joints
in Moab Member of Entrada Sandstone. Location
is near Anniversary Arch. Roads in lower left and
top center give approximate scale. Prominent
white horizon at base of Moab marks contact
with underlying Slick Rock. Note that zoned
joints are confined to Moab. Joints in Slick Rock,
visible at lower left, do not have a zoned mor-
phology and differ in strike about 30 degrees
from zones in the Moab. ABCD mark endpoints of
detailed map of figure 2-3.

(2) All joints within a given set are confined to a narrow zone 0.5 - 2 meters wide (figure 2-2). Careful examination of water-worn rock surfaces in drainages transverse to the zones revealed no joints, large or small, which might be considered a member of the zoned set. Either all jointing is confined to the zones, or all joints outside the zones were totally healed before they could record any shear displacement.

(3) The sparse vegetation present is invariably found along joint zones. This concentration of vegetation gives rise to the remarkable lineaments visible on aerial photography (figure 2-2).

(4) Joints within an individual zone show a simple relationship to each other. Joints within a zone may parallel each other for considerable distances. They may or may not link up (figure 2-3).

(5) Horizontal interzone spacing is relatively constant for a single zoned set over some distinct area. Spacing varies from 20 - 45 meters.

(6) Individual joints within the zones are simple, near-planar fractures 4 - 140 feet (1.2 - 43 meters) long in plan view (figure 2-4).

(7) The zoned nature is characteristic not only of plan view, but also in cross-section. Although a single joint may cut the entire member, often several joints overlap vertically as well as horizontally.

(8) All zoned joints are simple surfaces. In plan or section, they show no evidence of crack branching or bifurcation, except near the formation boundary (see item 10).

(9) Surface markings (plumose features or hackle marks) are exceedingly rare on joint surfaces in the Moab.

Figure 2-2.

View along a zone of systematic joints. Note the absence of regular en echelon geometry and the narrow width of the joint zone. No systematic joints are found outside of these zones.

N
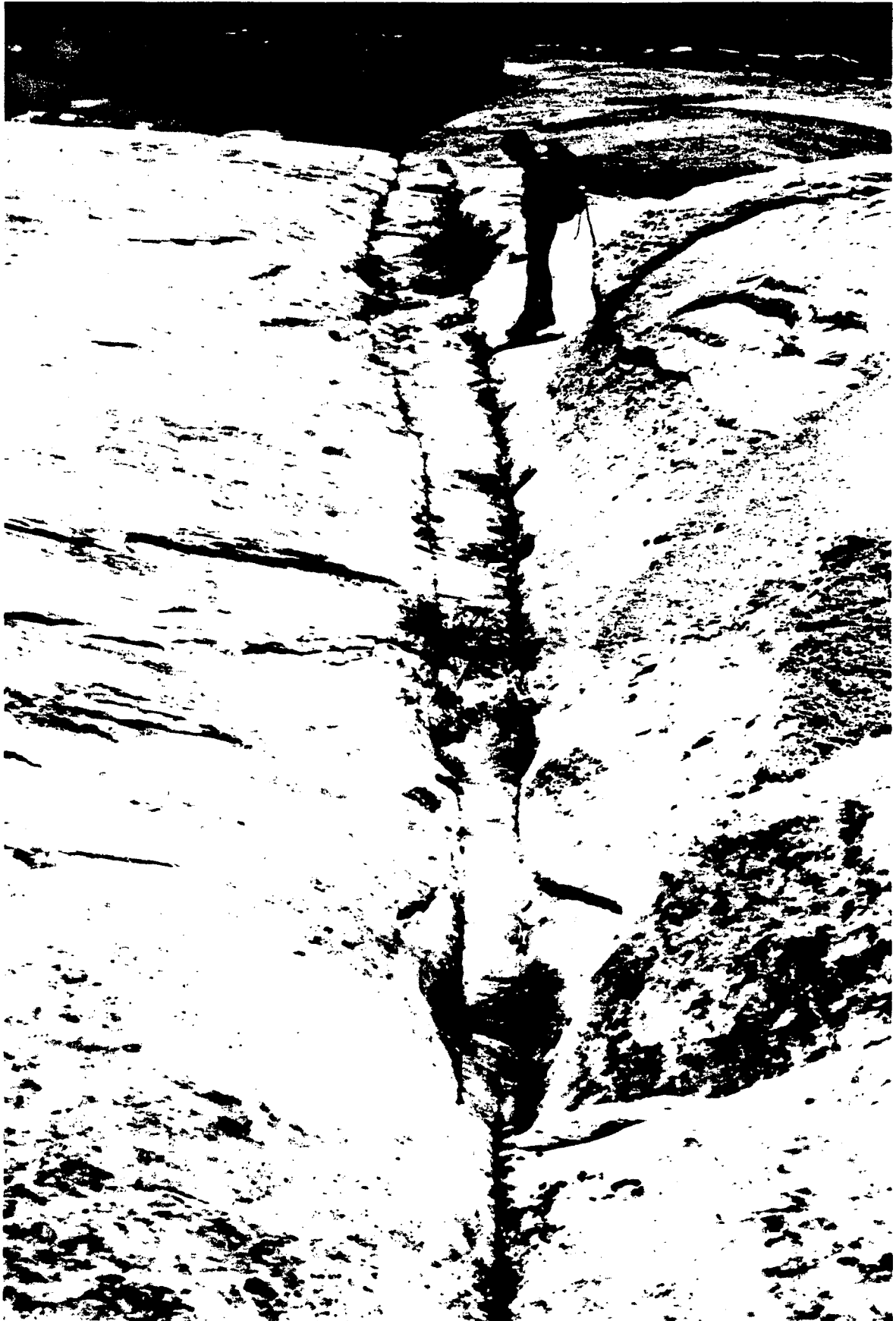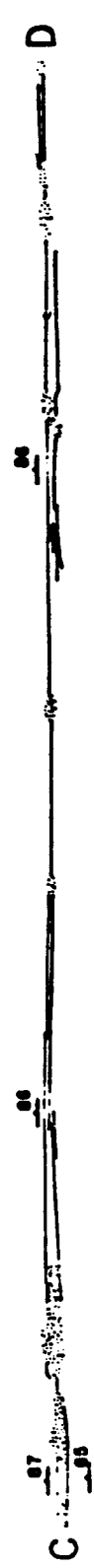
LEGEND

TRACE OF JOINT
STRIKE AND DIP OF JOINT
STRIKE AND DIP OF Jem/Js CONTACT
OBSCURED
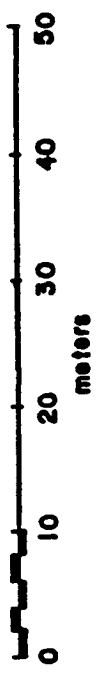
Figure 2-3.
Detailed map showing all joints in two adjacent joint zones. ABCD corresponds to locations on figure 2-1. Note that individual joints may overlap and parallel each other for tens of meters. Within a zone, two parallel joints may or may not link up. When linkage occurs, one joint will abruptly curve toward the other joint, as shown near point A. No shear displacement was noted on either of these zones, although nearby zones commonly show a few cm of left-lateral displacement. Jem = Moab Member; Js = Summerville Formation.

meters
0 10 20 30 40 50
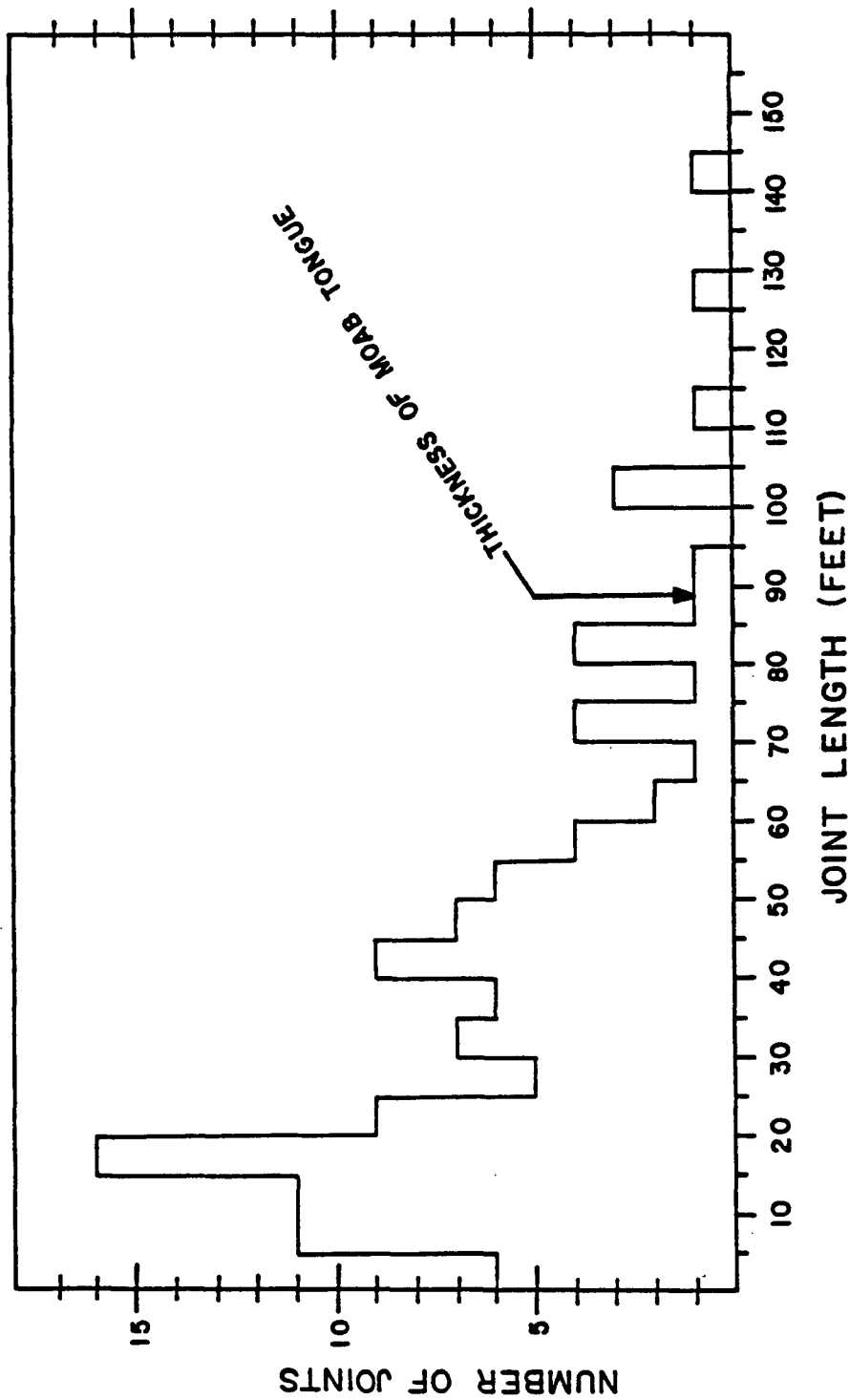
Figure 2-4

Frequency-length plot for individual joints within zones. Only measurements from joints that are totally exposed along their entire length are included. Since vegetation, while sparse, is concentrated along the joints, the measurement technique is biased against longer joints. Field observations give no reason to even suspect that the maximum length of any joint exceeds 200 feet.

(10) Single planar joint surfaces do not cut the Moab Member from upper to lower contacts. Instead, there is a small distinct zone at the upper and lower contacts, termed a "fringe zone" by Hodgson (1961b, p. 495), in which the planar fracture surface degenerates into an *en echelon* array of smaller "F-joints". The geometry of fringe zones is discussed in detail in a later section of this chapter.

(11) Cross-joints (following the terminology of Hodgson, 1961b) are commonly observed where the top 3 - 4 meters of the Moab has been removed by erosion. Cross-joints are transverse to the zoned joints, and intersect them at right angles. Cross-joints are usually curved in plan view. In section, they are commonly planar from near the base of the Moab to 3 - 5 meters below the erosional surface, where they curve to parallel large-scale cross-bedding. Cross-joints are neither zoned nor systematic in orientation.

ORIGIN OF JOINTS: SHEAR OR EXTENSION

The cross-bedded sandstones of the Moab Member provide excellent three-dimensional control for evaluating the role of shear in joint genesis. True shear offset across a joint zone was determined from the apparent offset of three non-parallel sets of cross-beds (see figure 2-11). Under optimal conditions, true displacement of the order of 1mm can be determined across joint surfaces. No dip-slip component of displacement was noted anywhere in the study area. Field relations allow the determination of relative ages of joint sets. The youngest joints generally display only opening displacement, with no detectable shear displacement. Older, bounding joints may have shear displacements of up to 18 cm, although a few cm is common. In every case in

-52-

which a determination could be made, the sense of shear observed on the older joints is compatible with an orientation of far-field principal stresses which could give rise to the later set of joints. The direction and magnitude of shear displacement observed on the older joints is variable, although it is relatively constant within a given region, or domain, of a few km^2.

Microscopic examination of thin sections from cored joints and joint terminations show:

(1) In younger joints, there is minor shattering or breaking of grains along the joint. Although it is hard to constrain shear displacement on the grain scale, the walls appear to have just pulled apart.

(2) Large joints appear to be single fractures. There is no indication that many smaller crack segments have linked together to form a larger crack.

(3) Observations of joint terminations show that the joint is primarily an intergranular fracture (figure 2-5). The fracture propagates between grains, with little attendant grain fracturing and no obvious development of microstructures such as deformation lamellae. No features which might be construed as relics of a plastic or "process" zone associated with stress concentrations near a sharp crack tip were noted.

JOINT DOMAINS

The zoned joints of the Salt Valley Anticline define several distinct domains (figure 2-6). Within each domain, two or more sets of zoned joints are present. Throughout each domain, each systematic set maintains certain characteristics, such as orientation and inter-zone spacing. The different sets also show a characteristic interaction between the sets throughout the domain.

Figure 2-5

(A) Photomicrograph of a joint tip. Grains are about
0.1 mm in diameter. Note absence of shattered
grains and diffuse, wavy nature of the joint.

(B) Joint tip, about 5 mm away from figure 2-5 A. No
grain shattering is noted. Joint is a zone of high
porosity where the walls have just pulled apart.
Joint is roughly sinusoidal, with an amplitude of
~0.2 mm and a wavelength of several mm. Note
absence of offset of corresponding highs and lows
of joint surface (small arrows).
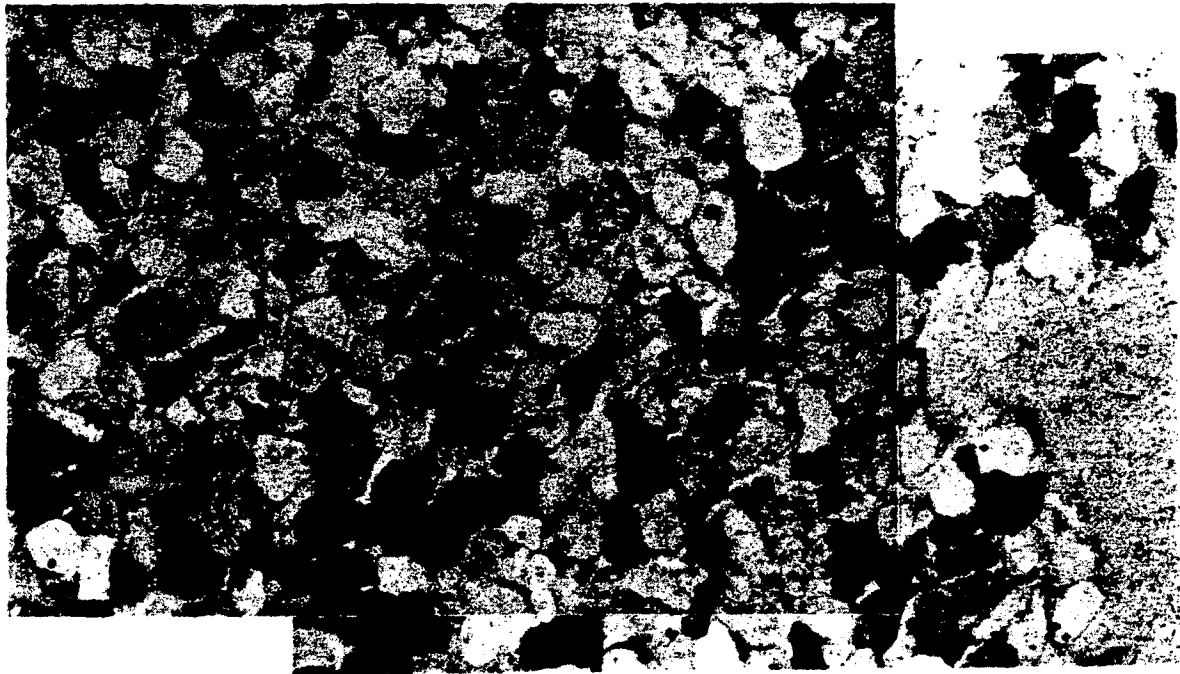
A
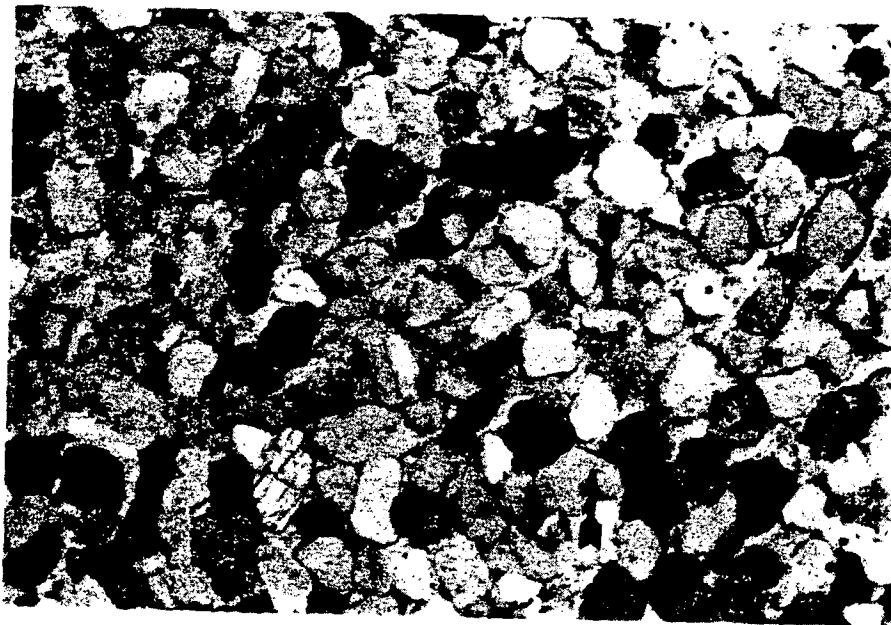
B
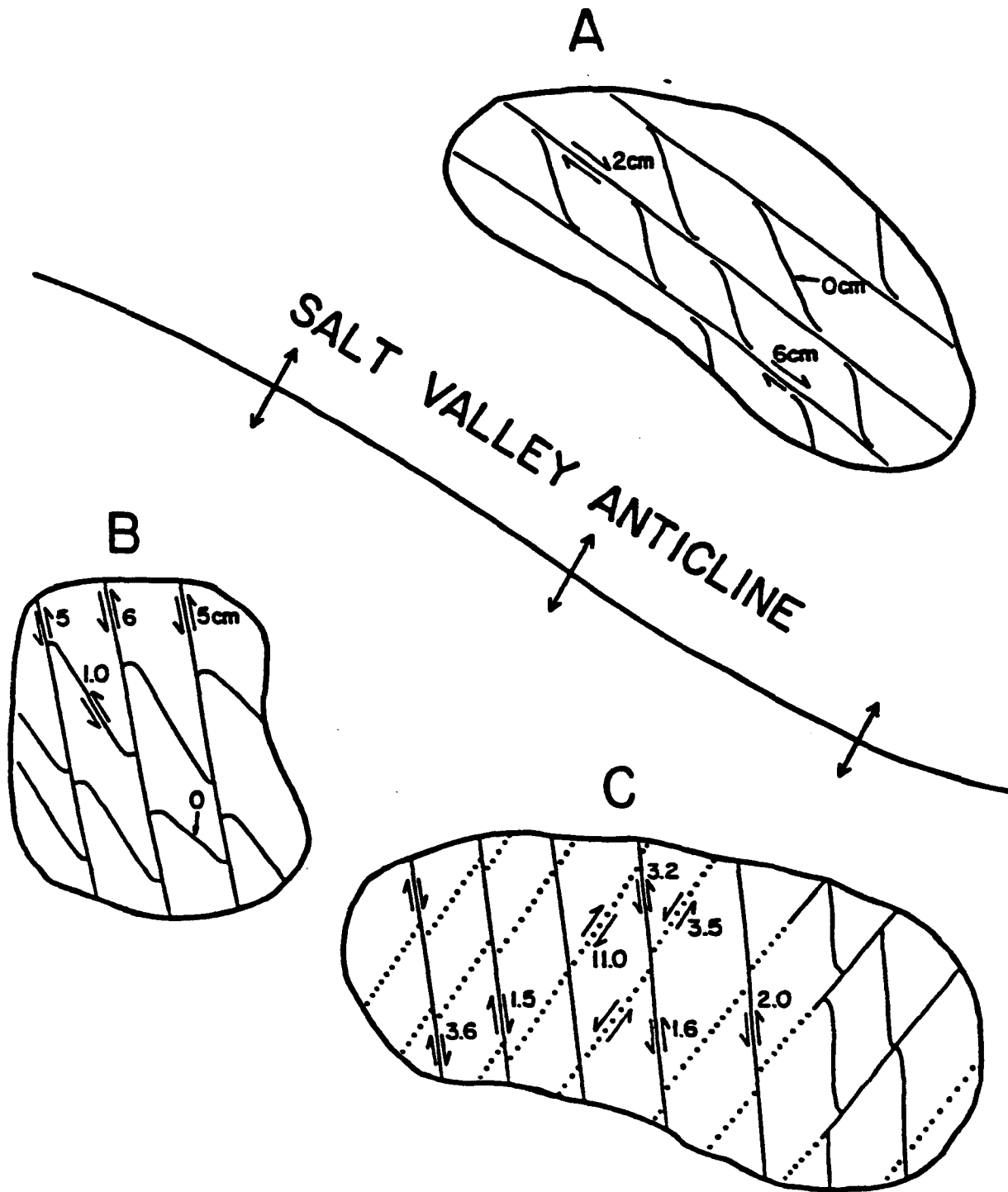
Figure 2-6

Cartoon showing relative locations and pertinent features of Domains A, B and C. Not to scale.

This characteristic interaction allows the relative ages of the different sets to be determined with certainty. The characteristics of three different domains are described in detail. All localities may be found on the U. S. Geological Survey topographic map of Arches National Park (1974; scale 1:50,000).

DATA COLLECTION AND PRESENTATION

Field Objectives

Field observations were centered around four objectives: (1) establishing the amount and sense of displacement on individual fractures; (2) determining the morphology and character of individual joints and zones of joints; (3) establishing relative age relationships between the sets of zones; and, (4) documenting the details of the change in geometry which occur when one joint zone approaches a non-parallel zone. The observations involve measurements that span six orders of magnitude, from millimeters of displacement on individual joints, to kilometers of length for a single zone of joints. Conventional maps are inadequate for presenting such a wide spectrum of data.

The Exposure Problem

Complicating the problem is the spotty distribution of definitive data points. Excellent as the exposures are, sand and vegetation, near-horizontal cross-bedding, pools of standing water, thickets of poison ivy and other natural obstructions tend to hinder observations at the majority of crucial localities. Hundreds of meters may separate points at which definitive observations on offset or geometry may be made. Nevertheless, such localities *were* found and the observations *were* made.

Field Methods

The field work was accomplished using 36 inch by 36 (91 cm by 19 cm) inch enlargements (scale ~1:5,000) of U. S. Geological Survey aerial photography for location and recording purposes. The resolution of this photography allowed identification of individual juniper trees, and ensured a pinpoint locating capability. Crucial areas showing evidence of key relationships or exceptional exposure were scrutinized in detail. Every joint zone in these areas was walked, and often crawled, along its entire length. A shovel and broom often clarified the relationships at marginal exposures. Data was recorded directly on the photographic enlargements. Exceptional exposures were documented photographically. A conservative estimate is that 50% of all the individual joint zones in the three study areas were walked out. Five localities were mapped in detail at a scale of 1:300 using plane table and alidade. Plane table mapping was found to be a generally ineffective method of documenting the large spectrum of features present. Over 160 one-inch diameter sample cores of jointed and unjointed rock were collected using a portable gasoline-powered drilling apparatus.

Presentation of Data

The cartoon of figure 2-6 provides a visual summary of the crucial observations in the three study areas. Stereonet plots are a traditional format for presentation of joint orientation data, however, stereonet plots have been purposely avoided in this report. Stereonet data does not convey the critical information regarding relative ages and interactions between zones. Photographs provide the best documentation of the key features of each area. Vertical aerial photography of each study area clearly shows the regional extent and nature of the different sets of zoned joints. Detailed observations

are summarized in the text and documented with accompanying photographs.

DOMAIN A

This domain is located on the northeast flank of the Salt Valley Anticline, and is typical of about 8 km^2 of excellent exposure. The domain includes all the outcrop area of the Moab Member within sections 15, 22, 23, 25, 26, 27, 35 and 36 (T23S, R21E). In general, the area is located to the north, east and southeast of the campground area in Arches National Park, and may easily be reached on foot from the campgrounds area.

Observations

The Moab Member dips gently to the northeast at 4-6 degrees, with the dip shallowing to the northeast. This domain is characterized by two distinct sets of zoned joints (figure 2-7). The first set (J_1^A) is oriented about N40W, subparallel to the anticlinal axis. Zones of this first set are throughgoing features, although two overlapping J_1^A zones may terminate by curving into each other. An individual zone is commonly traceable for several kilometers. Although the zones may be broadly curved over their length, each individual joint which make up the zones is a near-planar feature. J_1^A joint zones frequently display extensive weathering, resulting in vertical chasms tens of meters deep, with apparent wall separations of tens of centimeters. J_1^A zones commonly show yellow to brown banded limonitic(?) staining parallel to joint faces and extending several tens of centimeters into the unjointed rock. Where these joint zones are developed as open fissures, the walls are invariably coated with dark desert varnish. Nowhere were slickenside striations noted on J_1^A surfaces. A typical exposure of a J_1^A zone is shown in figure 2-8. Due to large wall separations and the non-planar nature of cross-bedding, it was rarely

Figure 2.7

Aerial view of part of Domain A. Enlargement is portion of frame GS-WI 26-101, U. S. Geological Survey aerial mapping photography. Jes = Slick Rock Member; Jem = Moab Member; Js = Summerville Formation. Characteristics of J_1^A and J_2^A explained in text. Note that J_2^A nowhere crosses J_1^A. Sigmoidal shape of J_2^A is apparent near annotations.

Figure 2-8

Typical exposure of a throughgoing J_1^A zone.
Subdivisions on walking stick are 10 cm
increments. Arrows indicate a sequence of thin
and thick cross-beds that can be identified on
both sides of the zone. Horizontal shear
displacement cannot exceed 10 cm.

possible to obtain definitive measurements of shear offset across the J_1^A zones. Where shear displacement could be determined, it is consistently right lateral, and ranges from two to six centimeters.

The second set of joint zones within domain A are collectively referred to as J_2^A. This set has a mean orientation of about N20W, although there is considerably more variability in the orientation of members of this set. The Dihedral angle between J_1^A and J_2^A zones ranges from 6 to 23 degrees, with a distinct maxima at 10 degrees (figure 2-14). J_2^A joints uniformly display less weathering and apparent separation than J_1^A zones. Staining or mineralization is rare. Lateral displacement of J_2^A zones ranges from zero to two centimeters, with only right lateral displacements noted.

The joints of the second set (J_2^A) do **NOT** cut, nor do they intersect, joints of the first set. Joint zones of the second set are entirely bound between two adjacent zones of J_1^A. J_2^A zones do not appear to nucleate along J_1^A zones, but rather in the central region between J_1^A zones. The traces of J_2^A zones are linear in the central part of the region between J_1^A zones, but begin to curve into parallelism with the J_1^A zones at a distance typically of $\sim$ 5 meters. The closer J_2^A comes to J_1^A, the more exaggerated the curvature, with J_2^A finally paralleling J_1^A some tens of centimeters away (figure 2-9 A,B). The local curvature of J_2^A is accomplished in two ways: not only do individual fractures become curviplanar surfaces, but the long, planar individual joints of the zone are replaced by shorter planar joints whose strike systematically deviates from the mean strike of the zone. These shorter joints show no systematic *en echelon* geometry.

Cross-joints do not cut either J_1^A or J_2^A, and usually intersect them at right angles. Cross-joints are non-planar surfaces in both map and cross-section

Figure 2-9

(A) View looking down a J_2^A zone. Geologist for scale. J_1^A trends from upper trends from upper left to lower right. Note systematic change in orientation of J_2^A as it gradually curves into parallelism with J_1^A.

(B) View looking down another J_2^A zone. Juniper tree growing in J_2^A is about 2 m tall. J_1^A trends from upper left to lower right. Note how near-planar joints in J_2^A (at arrow) systematically change orientation as J_2^A approaches J_1^A.
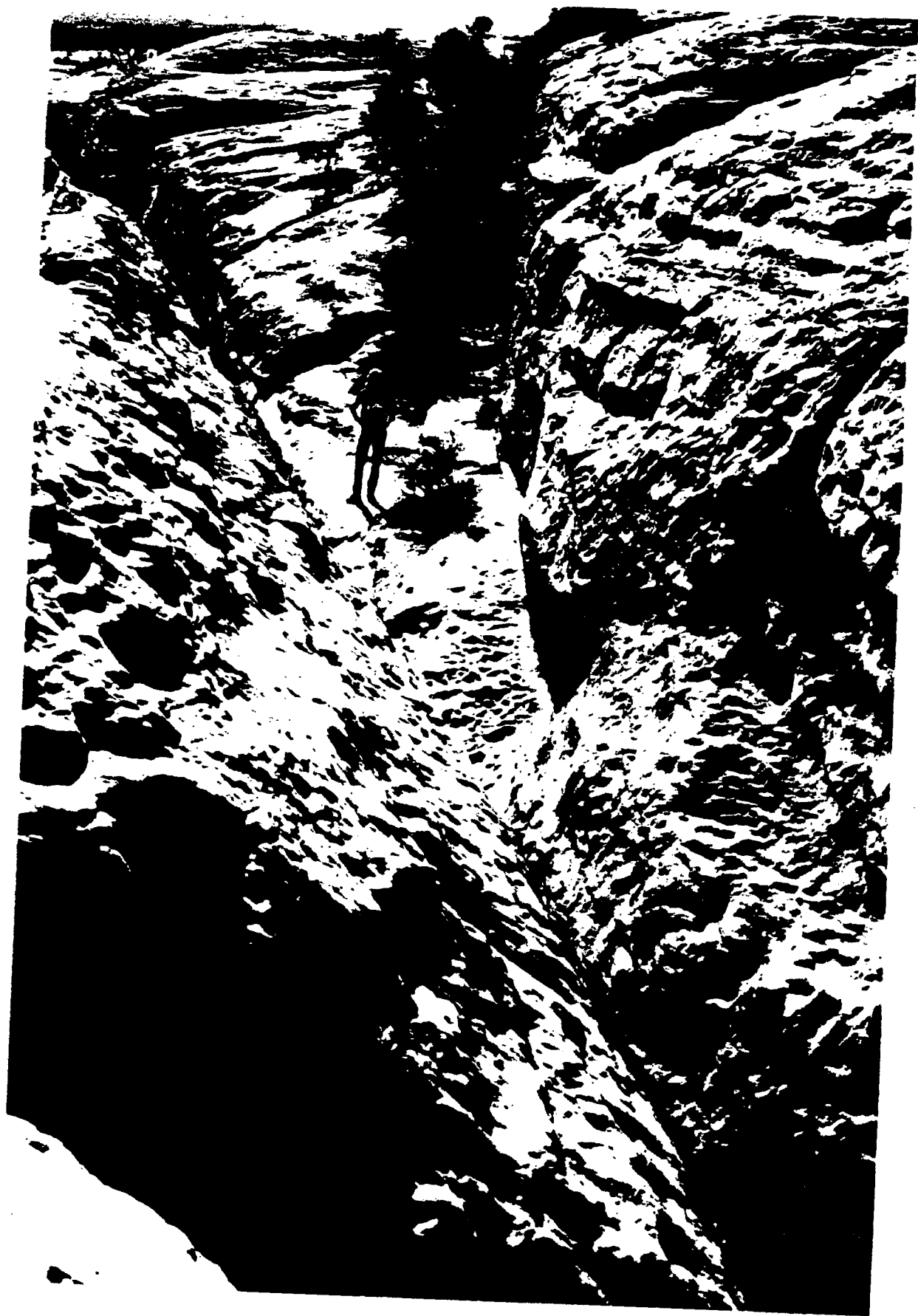
views. Staining or mineralization was not observed on any cross-joints.

Discussion

The age relationships in Domain A are unambiguous. All J_1^A zones clearly predate all J_2^A zones everywhere in the domain. These two sets of zoned joints are NOT synchronous, conjugate joints. Cross-jointing postdates both J_1^A and J_2^A. Because of their non-planar nature, cross-joints are not considered to be systematic.

The youngest sets of systematic joints, J_2^A, generally show no shear displacement, only a dilational opening. Zoned joints of J_2^A are extensional fractures. Collectively, they appear to have formed in an episode of jointing during which the causative stress field had rotated relative to that which caused J_1^A.

Although the throughgoing zones of J_1^A may display small right-lateral shear displacements, they are also inferred to have originated as extensional fractures. Support for this interpretation is mostly circumstantial: the presence of one set of sub-parallel joints argues against a shearing origin in which conjugate sets might be expected to form; while the uniform sense of shear displacement observed on J_1^A is compatible with later shear displacement due to a clockwise-rotated stress field in which the extensional joints of J_2^A were growing.

The uniform manner in which J_2^A curves into parallelism with J_1^A throughout the area indicates that the presence of the first set has a locally strong influence on the growth of the later set. In map view, the later (J_2^A) zones display a sigmoidal shape, similar to that seen in asymmetric tension gashes (Durney and Ramsey, 1973; Ramsay and Graham, 1970; Roering, 1968).

A standard explanation of such tension gashes is that they represent the localized, progressive rotation by simple shear of an originally planar crack which continued to grow during the shearing deformation, while the causative stress field remains fixed in orientation (Ramsey, 1967; p. 88-91). The resolved shear gives rise to a progressive rotation of the inner core of the tension gash, while later increments of crack growth are oriented perpendicular to the far-field direction. Such a mechanism requires material rotation in a fixed stress field. This mechanism has been used to account for the "anomalous" curvature commonly noted in *en echelon* fractures wherein the "ends of the gashes curve toward the direction from which movement occurred" (Shainin, 1950, p. 516).

Simple shear and progressive material rotation can be ruled out as the cause of the sigmoidal form of the J_2^A joint zones in Arches. Such progressive rotation would require meters to tens of meters of lateral offset along the J_1^A zones, while field observations rule out more than 10 cm of lateral offset. Estimates of the required shear displacement arrived at by examining the deflected angle of the sigmoidal form have no relation to the true lateral offset observed on the throughgoing joint set J_1^A.

An alternate hypothesis is that the throughgoing joint zone, J_1^A, locally perturbs the stress field in which a younger joint set (J_2^A) is growing. This perturbation causes rotations of the orientation of the principal stresses and also results in change of the magnitudes of the principal stresses. The perturbing effect is apparently strongest closest to the through-going joint zone. Thus, the sigmoidal form would arise not from a material rotation in a fixed stress field, but from a local rotation of the stress field due to an inhomogenity in the rock layer. A pre-existing joint zone could certainly provide such an inhomogenity.

DOMAIN B

This is a small area of $< 1 \ km^2$ located on the southwest flank of the anticline (NW 1/4 of S35, T23S R20E). This area can be reached by a combination of dirt roads and jeep trails via two different routes: either from the Burro Seep road off U. S. Highway 163 about 1.5 miles south of the Canyonlands Airport, or from the Klondike Bluffs/Tower Arch jeep trail in Arches National Park.

Observations

The Slick Rock/Moab contact in this area strikes N35W and dips 11 degrees to the southwest. An aerial view is shown in figure 2-10. The throughgoing zoned joint set (J_1^B) strikes N12E and dips 87 degrees east. Interzone spacing of the J_1^B zones is about 20 - 40 meters, although in one small area it is as small as 13 meters. J_1^B zones uniformly display left-lateral displacement of 1-6 cm (figure 2-11). J_1^B zones cut and offset small E-W trending paired conjugate cataclastic normal fault bands which dip to the north and south. Later generations of joint zones in this region are collectively designated J_2^B. The strike of J_2^B varies considerably, from N10E to N39W, giving J_1^B / J_2^B dihedral angles of 2-51 degrees (figure 2-14). As was the case in domain A, J_2^B joints or zones do not cut across J_1^B zones, but are bound by J_1^B. The J_2^B zones consistently curve abruptly *toward* the throughgoing J_1^B zones, with J_2^B intersecting and terminating in a J_1^B zone at almost a right angle (figures 2-12, 2-13). The change in strike of J_2^B occurs very abruptly, typically about 1-2 meters from the J_1^B zone. Lateral offset on J_2^B varies from less than 1 mm to about 1.2 cm, with all observed offset being left-lateral. J_2^B joints with more westerly strikes show the least offset.

Figure 2-10.

Aerial view of Domain B. Enlargement is a portion of frame GS-WI 8-144, U. S. Geological Survey aerial mapping photography. Jes = Slick Rock Member; Jem = Moab Member. J_1^B and J_2^B explained in text. Circle marks location of figure 2-12. Note jointing in underlying Slick Rock.

Figure 2-11

View down J_1^B zone. Cross-bedding is offset 5 cm
left-lateral along J_1^B (arrows). Pocket knife is 13
cm long. Small joint originating in puddle
terminates in upper left corner of picture.

Figure 2-12.

Intersection of J_1^B and J_2^B. Location given in figure 2-10. J_1^B trends from top center to lower left. Note abrupt curvature of J_2^B at feet of geologist.

Figure 2-13.

View down a J_2^B zone. J_1^B trends from lower left

to center right. Brunton compass in center right

for scale. Note that J_2^B intersects J_1^B at nearly a

right angle, and is terminated by J_1^B.

Joints in the underlying Slick Rock Member strike N13W, while joints in thin sandstones of the overlying Summerville Formation range in strike from N10W to N45W. No lateral offset was detected on joints in either the Slick Rock or Summerville.

Discussion

As in Domain A, there is no question about the relative ages of the two sets of zones. The throughgoing set, J_1^B, predates J_2^B. The younger joint set has been superimposed over the older set. J_2^B zones with more westerly strikes show little or no shear offset and are presumably the youngest joints. As in domain A, the observed lateral offset on the throughgoing joint zones rules out the possibility that the local change in orientation observed on J_2^B is due to a progressive rotation by simple shear.

The observations are compatible with two episodes of extensional jointing. The first episode occurred in a stress field whose orientation was relatively stable, and resulted in the throughgoing, parallel zoned joints of J_1^B. The joints of J_2^B record joint growth in a stress field which rotated progressively over time about 45 degrees counterclockwise. During this second episode of jointing, all J_1^B joints and the oldest J_2^B joints were subject to resolved shear stresses. These resolved shear stresses gave rise to the shear displacements noted on J_1^B and the more easterly striking J_2^B zones.

The similarity in orientation of the younger J_2^B joints in the Moab and the joints in the Slick Rock and Summerville suggests that they all formed essentially contemporaneously in the same regional stress system. The underlying Slick Rock shows no signs of a jointing episode correlative with J_1^B. If jointing in the Slick Rock did not in fact develop until the later J_2^B set formed in the Moab Member, then this is a strong argument against the hypothesis of

-79-

Hodgson (1961a, 1965) that joints propagate successively upwards through the sedimentary sequence. Ziony (1966) and Stearns and Friedman (1972) have also presented data that are incompatible with the upward propagation of joints.

DIHEDRAL ANGLE BETWEEN JOINT SETS, DOMAINS A AND B

Observations

The horizontal angle between all older and younger zoned joint sets in Domains A and B was measured on U.S.G.S. vertical aerial photography and is plotted in figure 2-14. The horizontal angle is the angle, measured on the vertical photography, between the linear, throughgoing older joint zone (J_1) and the linear portion of the younger, truncated joint zone (J_2). In Domain B, some joint zones assigned to J_2 are truncated at one or both ends by other J_2 joint zones. Data from these situations is not included in the histogram of figure 2-14B, which tabulates only the J_1^B / J_2^B dihedral angle for J_2^B zones that are clearly truncated at both ends by J_1^B zones.

The data was field checked by measuring the strike and dip of selected adjacent older and younger joint zones in both Domains A and B. The dihedral angle between the older and younger joint zones was then determined using an equal-angle stereonet. In all cases examined, the true dihedral angle is within a few degrees of the horizontal angle determined from vertical photography. Figure 2-14, then, is an accurate representation of the true dihedral angle between the younger and older joint zones of Domains A and B.

As seen in figure 2-14A, the zoned joints of Domain A show a distinct maxima in the dihedral angle between J_1^A and J_2^A at about 11 degrees. The range of dihedral angles is rather tight, with only one observation below six

Figure 2-14

Histogram of dihedral angles between joint sets. (A) dihedral angle between J_1^A and J_2^A. (B) dihedral angle between J_1^B and J_2^B.

degrees and one above 22 degrees.

Conversely, the data from Domain B (figure 2-14B) show no distinct maxima in the dihedral angle, but rather a fairly even distribution from a dihedral angle of three degrees up to an angle of 51 degrees.

Discussion

Reches (1976) has argued that areal sets of joints should be defined in terms of the dihedral angle between joint sets, rather than directional trends. Nur (1981) suggested that the dihedral angles between tensile lineament sets arise due to rotation of the principal stress orientations and are controlled by the ratio of the tensile strength of virgin rock to that of preexisting fractures, which may be partially healed. Nur proposed that there is a minimum dihedral angle between tensile fracture sets, which leads to a discretization in both the number of fracture sets and in their dihedral angels.

The dihedral angle data from Domain A are at least partially consistent with the ideas of both Nur (1981) and Reches (1976). There is a clear discretization of the dihedral angle, with a significant minimum dihedral angle of about nine degrees. Using the relations proposed by Nur (1981, eq. 15), this suggests that the ratio of the tensile strength of the fracture to that of the unfractured rock was about 0.98 in Domain A at the time of the J_2^A jointing episode. This in turn suggests the the J_1^A joints were almost totally healed at the time of the J_2^A jointing. Such a conclusion does not appear to be warranted by the field observations. Although joint walls in J_1^A zones are often mineralized, the joints are everywhere open fractures, with no evidence that the fracture was ever closed and healed.

The dihedral angle data from Domain B are inconsistent with the proposals of both Reches (1976) and Nur (1981). There is no clear discretization of the

dihedral angle, nor is there a statistically significant average dihedral angle between J_1^B and J_2^B.

DOMAIN C

This domain characterizes the Moab outcrops in an area of about 3 km^2 on the southwest flank of the anticline. The area includes the Moab outcrops in sections 1 and 12, T24S/R20E, and section 7, T24S/R21E. Access to the area is gained by a combination of dirt and jeep roads from Dalton Well, approximately 2.8 miles north of the Seven Mile Canyon turnoff to Dead Horse Point State Park. A dirt road leads directly to the site of Shell Oil Co.'s Courthouse Wash Unit No. 1, located in the SW 1/4 of NE 1/4 of Section 12, T24S/R20E.

Observations

The upper surface of the Moab Member in this area strikes about N50W and dips 13 degrees SW in the northern part of the area, changing to N14W, dip 6 degrees W in the southern part of the area. Figures 2-15 and 2-16 show vertical and oblique aerial views, respectively, of this area. Figure 2-17 is a detailed map of a small area of Domain C.

Two types of fractures are recognizable in this area. Field relations suggest that one fracture type (J_1^C and J_2^C) delineates older joint sets that have subsequently been the locus of significant shear deformation. This fracture type is characterized by thin, resistant ribs of comminuted quartz. Thin sections (figure 2-18 A,B) reveal that the grain size in these ribs has been significantly reduced. There is a localized shattering of grains.

These resistant ribs are present either as single linear features (figure 2-19), or as anastomozing zones of deformation (figure 2-20). The single ribs and zones display overlapping, *en echelon* geometry and a periodic interzone

-83-

Figure 2-16.

Aerial view of Domain C. Enlargement is a portion of frame GS-WI 8-182, U. S. Geological Survey aerial mapping photography. Jes = Slick Rock Member; Jem = Moab Member. J_g^c and J_g^c explained in text. J_f^c not visible on aerial photography. Rectangle marks location of detailed map of figure 2-17.

Figure 2-16.

Oblique aerial photography looking south-southwest at Domain C. Rectangle denotes area of figure 2-17. Arrow shows location of figure 2-22 and shows joint-like morphology locally developed on $J\xi$.

Figure 2-17.

Detailed Map of portion of Domain C showing relationship between J_1^C, J_2^C and J_3^C. Location shown in figures 2-14 and 2-15. J_1^C are cataclastic bands striking N 70 E. Cataclastic bands and zones of J_2^C strike N 30 E. Zoned joints of J_3^C strike N-S. J_1^C is offset by J_2^C, while J_3^C offsets both J_1^C and J_2^C.

N

EXPLANATION

JOINT

CATACLASTIC BAND OR ZONE

STRIKE AND DIP OF JOINT OR CATACLASTIC BAND

VERTICAL JOINT OR CATACLASTIC BAND

STRIKE OF SAND-GRAIN "FABRIC"

LATERAL OFFSET OF CROSSBEDDING; OFFSET IN CM.

J_3^C LATERAL OFFSET OF A BY B OR A AND B BY C. OFFSET IN CM.

J_1^C

J_2^C
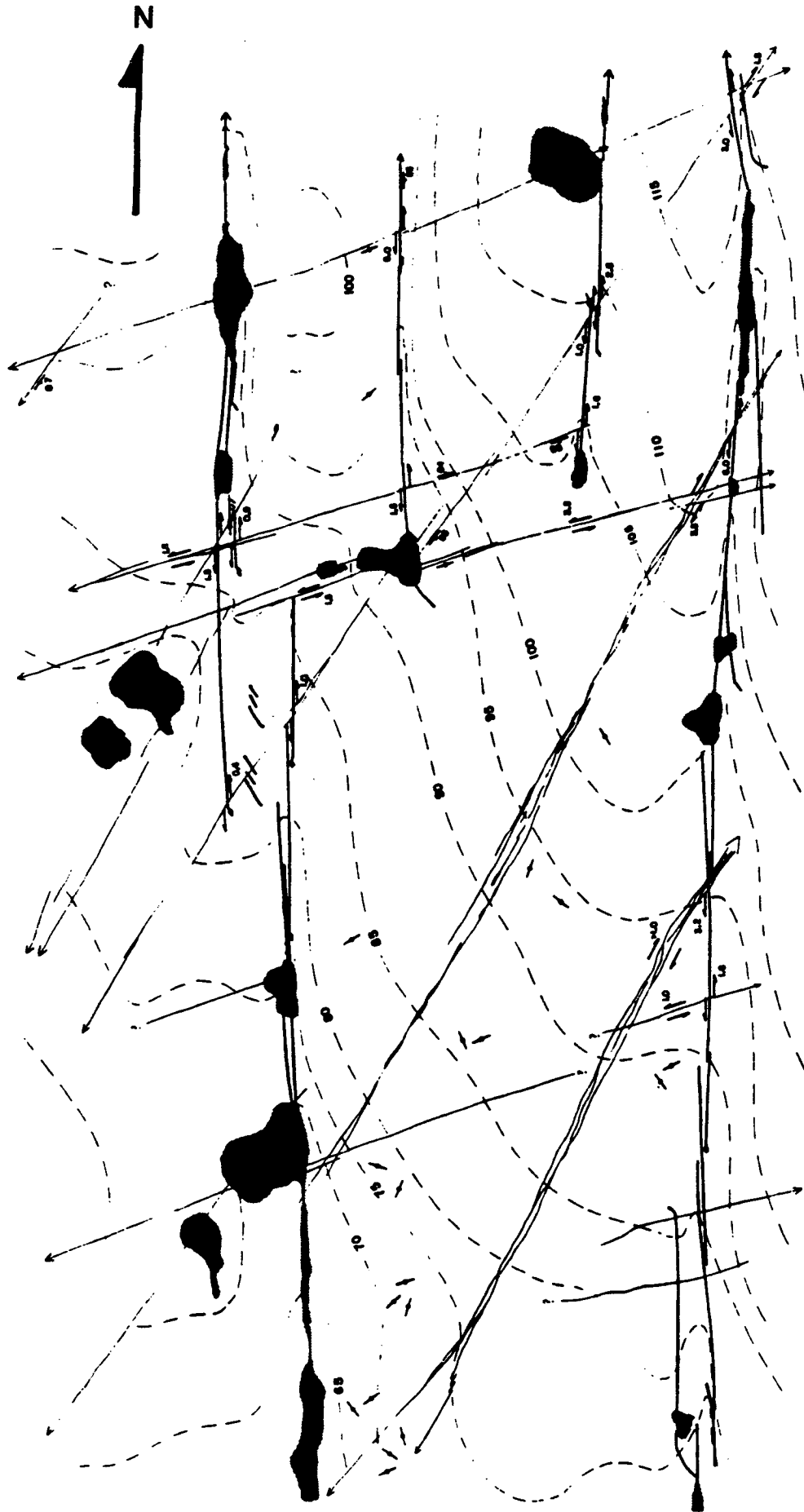
TOPOGRAPHY ON ARBITRARY DATUM. CONTOUR INTERVAL 5 FEET

OBSCURED BY SAND OR VEGETATION

20   40   60   80   100 FEET

5   10   20   30   40 METERS

Figure 2-18.

(A) Photomicrograph of a J_2^C cataclastic band. In the field this feature shows $\sim$ 10 cm left lateral displacement. Note grain size reduction of quartz in sub-parallel bands. Scale bar is 1 mm long.

(B) Photomicrograph of a J_2^C cataclastic band, same location as 2-18 A. Note anastomozing shear surfaces. Grain fracturing occurs at grain-to-grain contacts. Scale bar is 1 mm long.
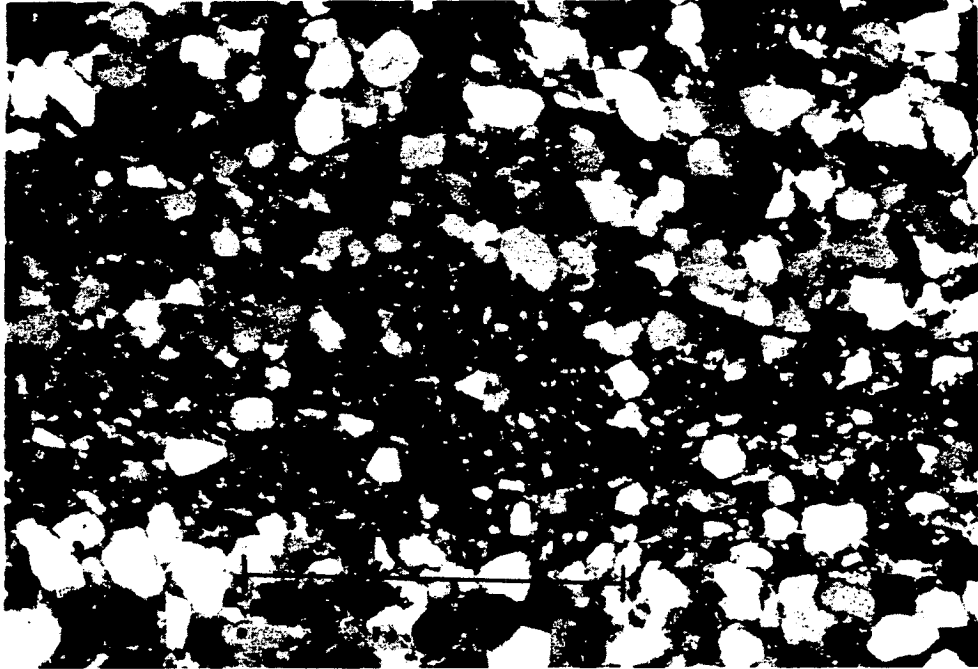
A
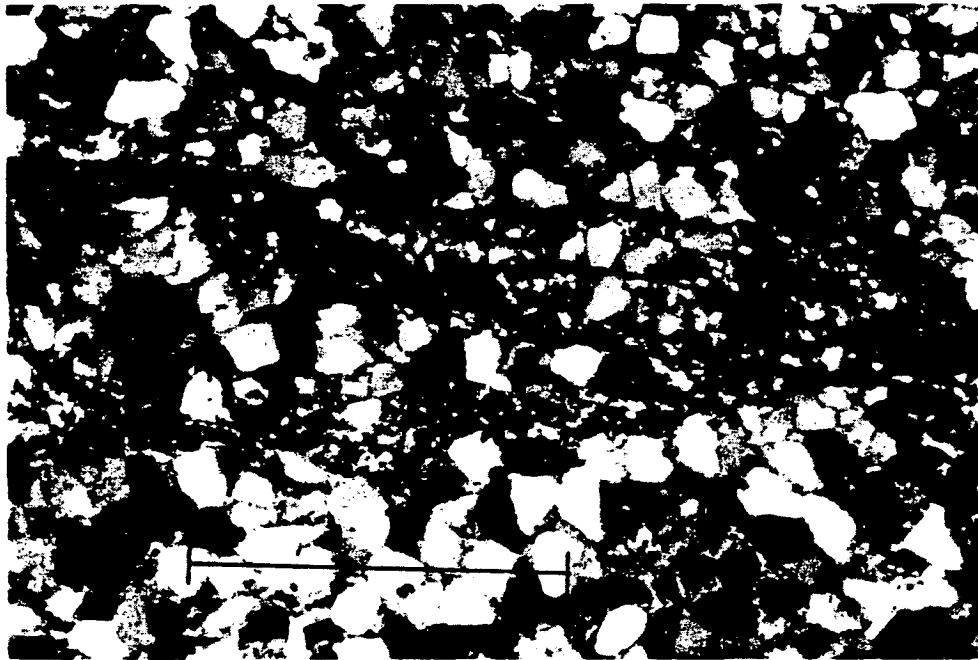
B

spacing which is typical of that of joint zones (figure 2-21). They are uniformly perpendicular to the upper and lower bedding planes of the Moab.

Generally, any single *en echelon* segment of J_1^c or J_2^c will be characterized by a linear band or an anastomozing morphology, although the morphology may change from segment to segment (figure 2-17). A few *en echelon* segments have a mixed morphology (figure 2-20), with one or more near-planar fractures co-located with an anastomozing zone. In no case could conclusive evidence be found to establish whether one fracture type predates the other.

The internal geometry of the anastomozing zones is complex. Aside from the localization of all fractures into a relatively narrow diffuse zone, generally less than three meters wide, there is no consistent geometry observed within the zones. Individual (?) fractures appear to interweave and produce no consistent cross-cutting relationships. Along a given fracture trend, estimates of the cumulative shear displacement across all fractures within an anastomozing zone are of the same order of magnitude as the shear displacement noted where a single band morphology is developed. There is no clear correlation between the fracture morphology which develops and the shear displacement accommodated across the fracture(s).

Since these resistant ribs are not open fractures in sandstone, vegetation does not grow along these zones. For this reason, the resistant ribs and zones are not easily visible on aerial photography. They are easily traced on the outcrop, and the individual fracture zones can be walked out for almost a kilometer.

When these resistant bands or zones are traced toward the east or northeast, (downsection, toward the anticlinal core), they often abruptly change character, turning into zones of weathered joints. These joints show

Figure 2-19

Cataclastic band of J_2^C, showing about 7 cm left-
lateral displacement. Scale is 17 cm long. Note
complex, anastomozing pattern of resistant ribs
between overlapping en echelon segments.
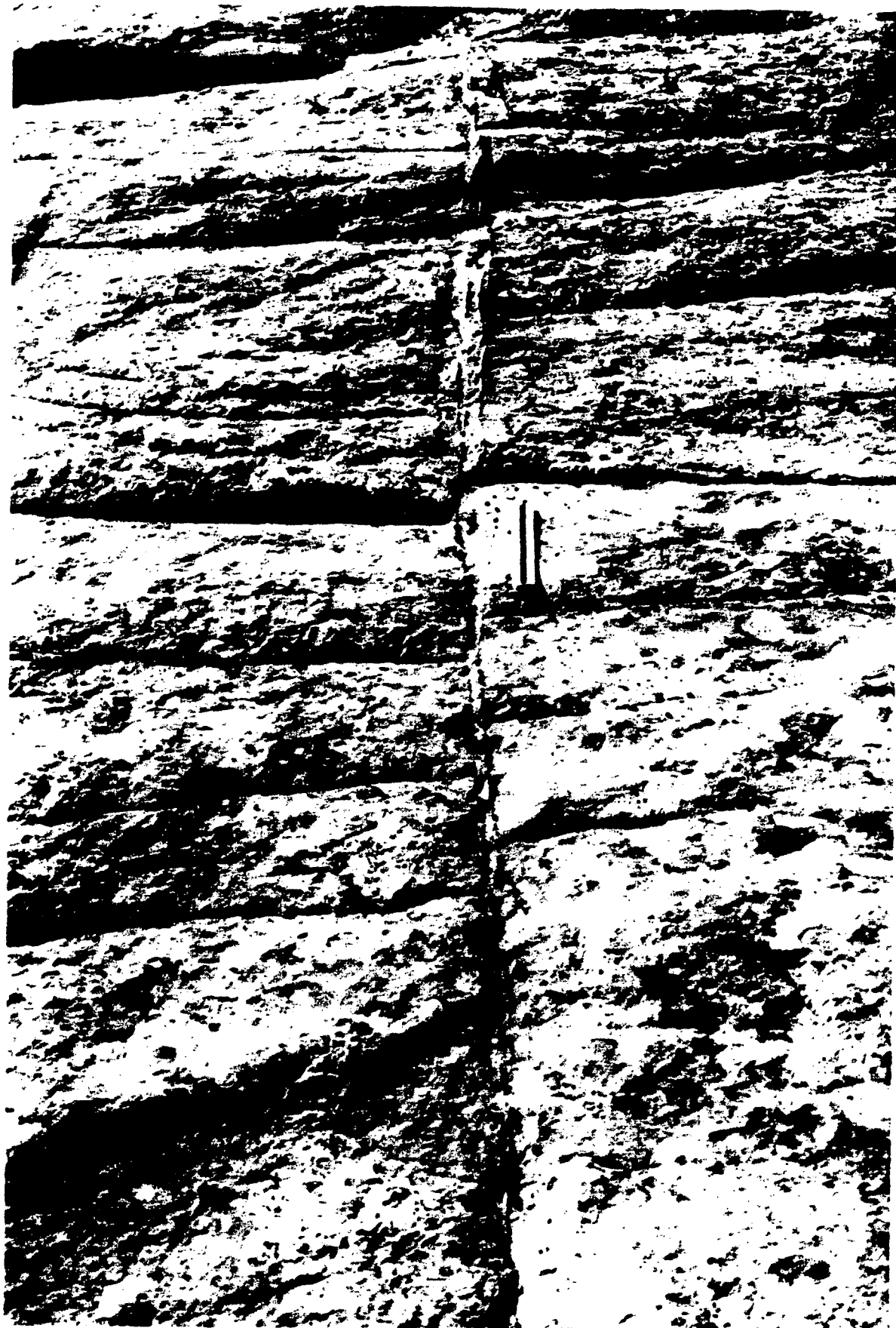
Figure 2-20.

J_2^C developed as diffuse, anastomozing resistant bands. Note continuation of feature into background. Brunton compass near center for scale.

Figure 2-21.

Aerial view of part of domain C. Open arrows indicate trace of adjacent J_2^C zones. Throughgoing zones running top to bottom are J_3^C. Average interzone spacing of J_2^C is $\sim$ 30 m.

exactly the same trend and characteristic spacings as the sheared bands. For the most part, the joints weather into deep fissures, easily visible on air photos. Small patches of slickensided material are rarely found on these joint surfaces, and confirm that movement has been subhorizontal and parallel to the upper and lower bedding surfaces. Where J_1^C or J_2^C are developed in a joint-like morphology, they are the bounding features - no other sets of joints cross them (see figure 2-16).

A map of one of these abrupt transitions from cataclastic band to "open" joint is shown in figure 2-22. The two features have exactly the same strike and dip. The joint-like segment is characterized by numerous small fractures that are preferentially developed on one side of the larger feature. The density of these small fractures decreases away from the main joint, suggesting that they nucleate on the main fracture. No joints, large or small, were found which crossed the joint-like segment of this feature. This is in sharp contrast to the observations in figure 2-17, where joints of J_3^C continue without deviation across the cataclastic bands and zones of J_1^C and J_2^C.

Two spatial sets of cataclastic features were identified in Domain C: J_1^C, striking N70E, and J_2^C, striking N35E. J_2^C is well-developed throughout the area, while J_1^C is best developed in the southern part of the area. Both sets display measurable shear offset, with the lateral offset on J_1^C ranging from less than 1 mm to 6.0 cm, with both left and right lateral displacements noted. In general, J_1^C fractures in the northern part of the area display right-lateral displacement, while those in the southern part of the area show left-lateral displacements. J_1^C was not observed to offset J_2^C, although J_2^C commonly offsets J_1^C. In addition, numerous cases were noted where the senses of displacement noted on J_1^C and J_2^C are incompatible with that expected from a synchronous

Figure 2-22

Map showing abrupt transition of J_8^c from cataclastic band to morphology of a zoned joint. Location shown on figure 2-15. Open arrow corresponds with open arrow in figure 2-15. Note that no joints cross J_8^c where it shows a joint-like morphology. Where developed as a cataclastic band, it resembles figure 2-18. No J_8^f fractures were identified in this area.

EXPLANATION

— Joint

--- Cataclastic Band

J_2^C SHOWS ZONED JOINT MORPHOLOGY

J_2^C IS A CATACLASTIC BAND

Obscured by sand or vegetation

ARROW ON END OF FRACTURE INDICATES THAT FRACTURE CONTINUES OFF MAP.

J_3^C

J_2^C

N

meters

0   10   20   30
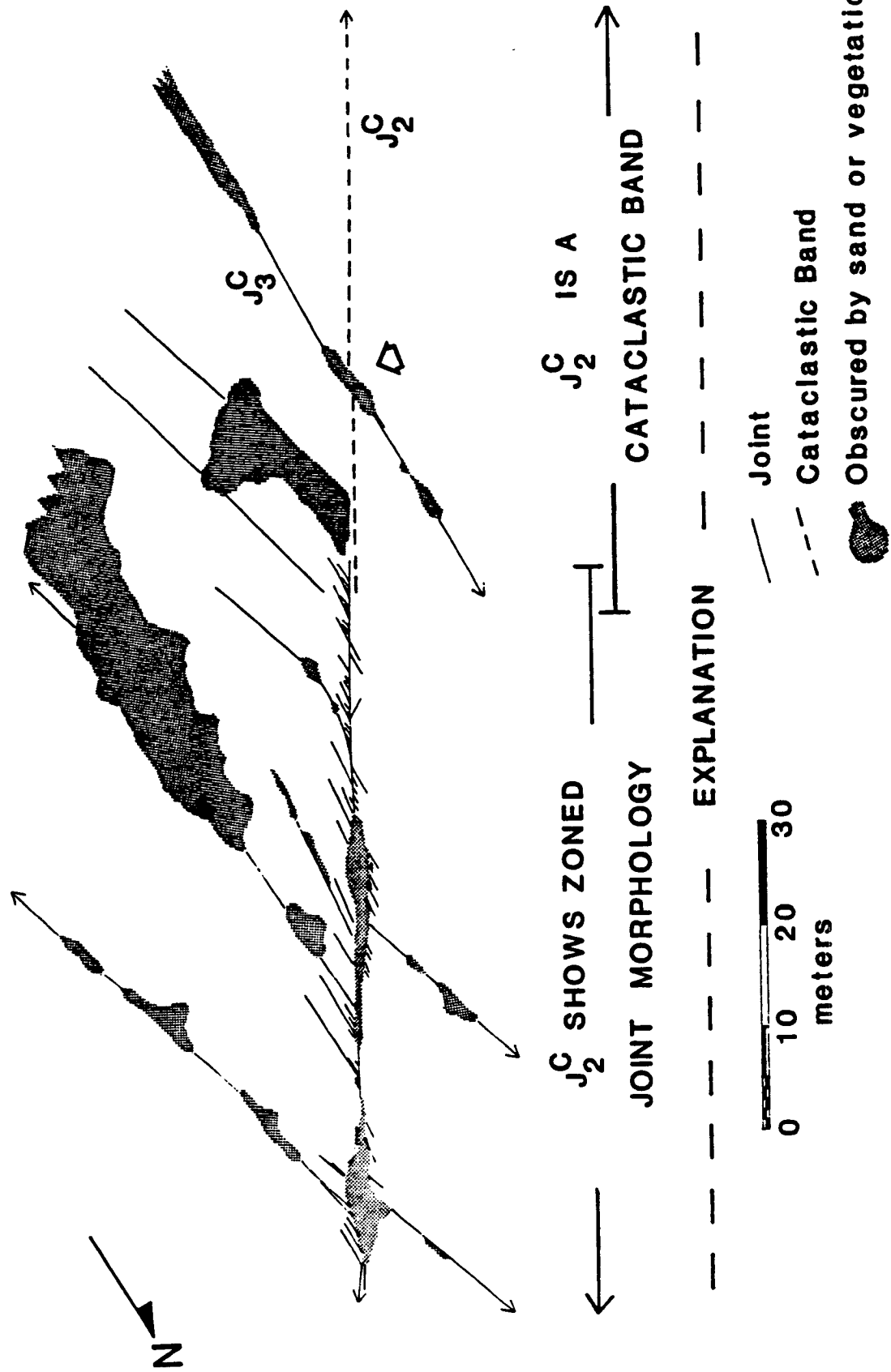
"conjugate" set of fractures.

Lateral displacement of J_2^C varies from 0.5 cm to 11.0 cm, with both left and right lateral senses of displacement noted. In general, displacements in the northern part of the area are right lateral, while both left and right lateral displacements are noted in the southern part of the area. Where J_2^C intersects and offsets J_1^C, the same amount of offset is noted in cross-bedding across J_2^C as the amount and sense of offset of the J_1^C fracture plane surface. This observation insures that the apparent displacement of J_1^C is in fact a true displacement.

The open joint set which is throughgoing in much of this area is J_3^C. These joints have an approximately north- south strike (trending slightly east in the northern portion of the area), and dip about 85 degrees E. Interzone spacing is typically 27-38 meters. These joints display a variable offset, ranging from 0.1 cm to 18.0 cm, with both right and left lateral senses of displacement noted in the region. In general, right lateral displacements on J_3^C are found in the southwestern part of domain C, while left lateral displacements are found in the northern and eastern part of the domain. In the extreme southeastern part of the area the pattern is complex, with both left and right lateral displacements noted on J_3^C. When these joints intersect the resistant bands/zones of either J_1^C or J_2^C, they cut and cross the other fracture without the slightest hint of a change in orientation (figure 2-23). The youngest systematic joints are *en echelon* joints locally found in regions of overlap between two J_3^C zones. (figure 2-17). No shear displacement was noted on any of these small *en echelon* joints.

Locally, a thin band of resistant quartz can be identified along the J_3^C fractures (figure 2-23). This material was sampled, and in thin section is found

-102-

Figure 2-23

Relationship between J_3^C and J_2^C. J_3^C trends top to bottom. J_2^C indicated by open arrows. J_2^C strand indicted shows ~ 1cm right-lateral displacement of cross-bedding. J_2^C is in turn cut and displaced ~ 3.5 cm left lateral by J_3^C. Note that orientation of J_3^C is in no way affected by J_2^C. Small arrow shows small patch of incipient cataclasite locally developed on J_3^C. Scale is in centimeters.

to be comminuted quartz. The degree of grain crushing is highly variable along a single joint, ranging from incipient cataclasis to a texture very similar to the cataclastic bands of J_1^C and J_2^C (figures 2-24 A,B,C,D).

Toward the anticlinal axis, where J_1^C and J_2^C have the form of open joint sets, they are the throughgoing features. J_3^C zones are bounded by J_1^C or J_2^C and display the characteristic sigmoidal geometries observed in domains A or B. Exposures are relatively poor due to extensive erosion and vegetation, but in a small area (about 16,000 m^2) that was mapped in detail, only the type B interaction was noted, with J_3^C curving into J_2^C at nearly a right angle. In some other areas, vegetation trends suggest that J_3^C curves into parallelism with J_2^C (type A interaction), but this could not be confirmed.

Discussion

In contrast to Domains A and B, the cumulative fracture pattern of Domain C is exceedingly complex. There is little doubt that J_3^C originated as a set of parallel extensional joints. Resolved shear stresses in a later, rotated, stress field led to shear displacement on the existing joints. Segments of J_3^C have undergone incipient cataclasis, although the fracturing of grains is usually not as severe as in the cataclastic bands of J_1^C and J_2^C. Variations in the amount and sense of displacement observed on J_3^C indicate a complex behavior of the post-J_3^C stress field in Domain C.

The cataclastic features of Domain C are unique to this area. Although similar resistant cataclastic ribs are found elsewhere in the Park, they are invariably associated with normal faulting, and themselves often show normal or dip-slip displacement. There are no faults known within two miles of Domain C.

Figure 2-24.

This series of microphotographs was prepared from cores taken along a 20 meter interval of a single $J\S$ zone in the southeastern part of Domain C. This zone uniformly shows 5 cm of left-lateral displacement.

(A) Calcite filled joint. Wall separation is ~ 1 mm. Calcite in center has been sheared. A few small fragments of quartz are floating in the calcite, but virtually all of the joint filling is calcite. Note lack of microfractures in quartz grains in the joint wall.

(B) Calcite filled $J\S$ joint showing incipient cataclasis. Average grain size of quartz is ~ 0.1 mm. Note that top of a topographic high has been beveled off (open arrow). A planar surface of discontinuity has developed (dark band). Small fragments of quartz are relatively abundant in the sheared calcite. Note microfracturing of quartz grains at grain-to-grain contacts in joint walls. Microfracturing is totally absent 2 mm away from joint walls.

A
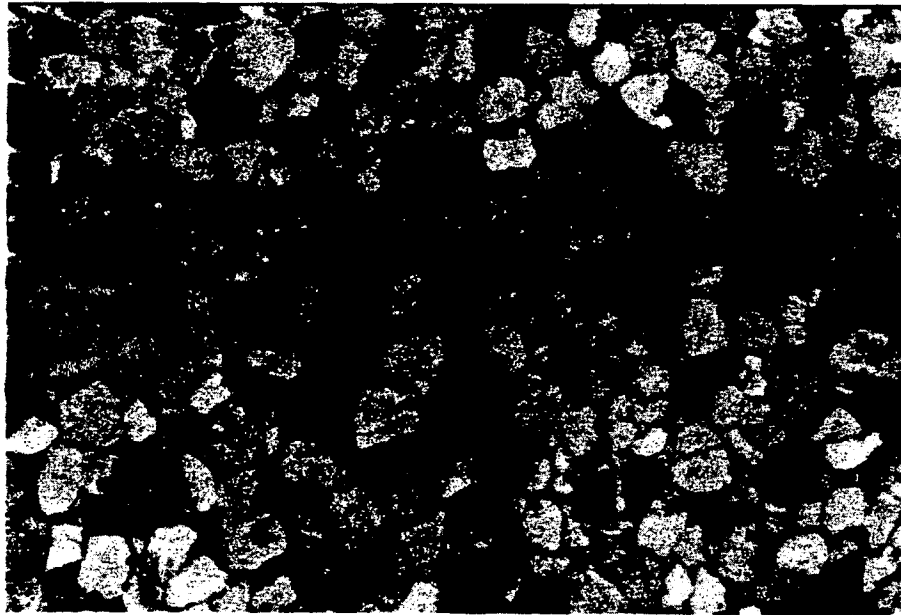
B

Figure 2-24, continued.

(C) Photomicrograph of J_S^C showing pervasive microfracturing of quartz grains in joint walls. Note abundance of small quartz fragments in the planar "shear zone" (open arrows). Average size of intact quartz grains is ~ 0.1 mm.

(D) Photomicrograph from same core as figure 2-24 C. Location is 2 cm away from 2-24 C. Note pervasive microfracturing of quartz grains and development of anastomozing slip lines. Quartz and calcite grains in a topographic low show minor fracturing (open arrow). Same scale as 2-24 C. Microfracturing is totally absent 8 mm away from the joint. Compare with figure 2-18.
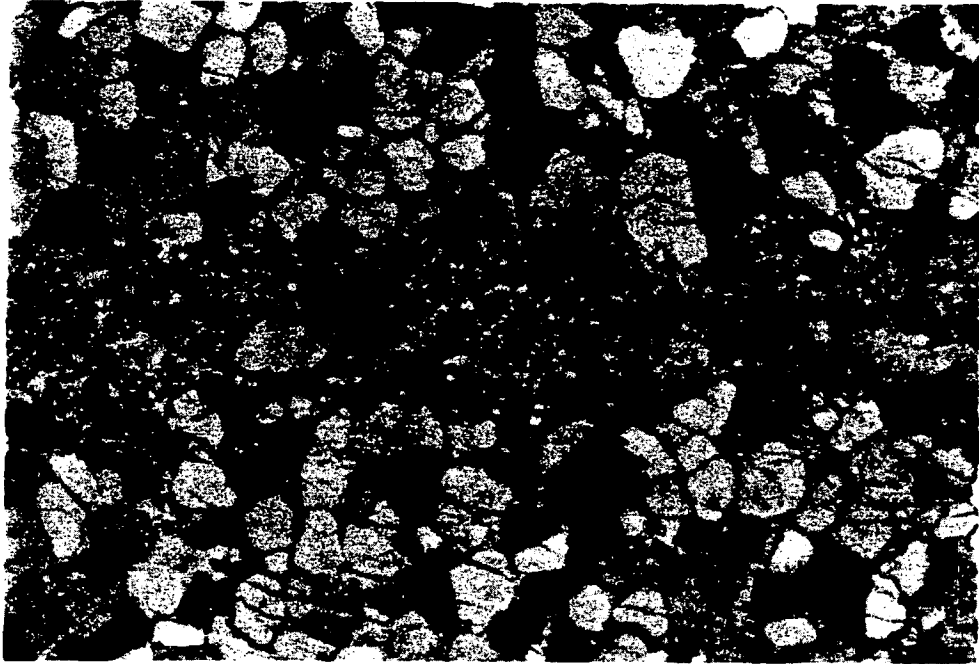
C
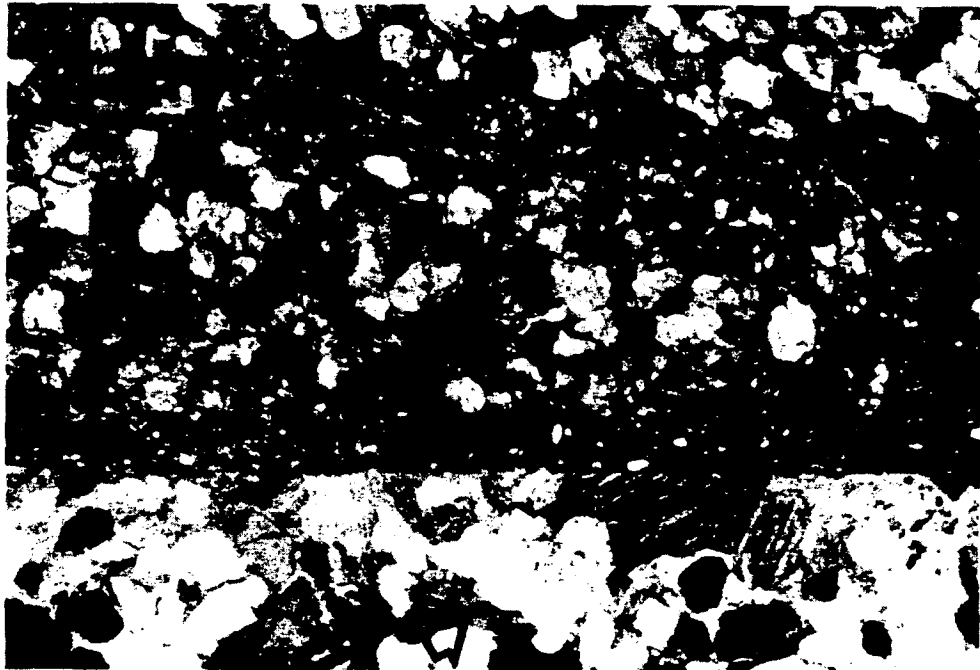
D

Morphologically, the cataclastic features of J_1^C and J_2^C bear a striking resemblance to the small faults (deformation bands and zones of deformation) studied by Aydin (1977) in the San Rafael Desert and at localities in Arches. Several lines of evidence, however, suggest that at least the linear cataclastic features of J_1^C and J_2^C resulted from the concentration of shear strain along existing zones of joints.

(1) *Geometry:*

All of the cataclastic bands and zones are near-vertical, *en echelon* features. These features are commonly traceable for hundreds of meters.

(2) *Characteristic Spacing:*

The cataclastic zones and bands show a strong characteristic spacing that is similar to that noted for all zoned joints in the Moab Member.

(3) *Abrupt Change in Character:*

The ability to walk out a cataclastic feature into a weathered rift which shows all the characteristics of a throughgoing zoned joint suggests a genetic link between the features (figure 2-22).

(4) *Incipient Cataclastic Texture on Joints:*

The presence of proto-cataclastic textures on J_2^C joints is convincing evidence that existing joints can be the locus of cataclastic deformation.

All field evidence indicates that J_1^C initially formed as an extensional joint set, probably with a zoned morphology, and was later subjected to lateral displacement. This lateral shear resulted in the breaking and comminution of quartz grains along the J_1^C fracture planes. These fractures then became the locus of strain for later deformation, resulting in the complex anastomozing pattern of quartz ribs which now commonly characterize the features. In all

-110-

cases noted, it appears that J_1^C was formed as a joint set and subsequently sheared and locked before the formation of J_2^C. A similar history is proposed for J_2^C. The cataclastic portions of both J_1^C and J_2^C were then locked during the formation of J_3^C, and later while cataclasis was being localized on the zoned joints of J_3^C, and possibly on the joint-like segments of J_1^C and J_2^C.

THREE-DIMENSIONAL GEOMETRY OF JOINTS

In detail, the zoned joints of the Moab Member are not simple planar fractures which extend from the top to the bottom of the member. In the top and bottom one to two meters of the Moab Member, the simple planar fracture surface degenerates into a series of short (1-4 meter) *en echelon* fractures. The geometry of these *en echelon* fractures appears to be identical to those of features termed "F-joints" by Hodgson (1961b, p.494), which he observed to occur in a "fringe zone" near the top and bottom of individual beds.

Observations

A systematic investigation was made of these *en echelon* fractures at the top and base of the Moab Member in Domains A, B and C. Poor exposures due to extensive weathering and limited access preclude any definitive statements regarding the *en echelon* geometry at the base of the Moab. Extensive exposures of the gently sloping Moab/Summerville contact allowed investigation of the upper fringe zones associated with more than 400 throughgoing joint zones. Observations were made only along throughgoing joint zones (J_1^A in Domain A, J_1^B in Domain B and J_3^C in Domain C).

The fringe zones were investigated to determine the character of the *en echelon* geometry (consistently left-stepping, right stepping or mixed), the rotation in strike of the *en echelon* segments from the throughgoing joint zone,

and the three-dimensional geometry of the fringe zones.

The gentle relief and resistant nature of the upper Moab surface ruled out any definite observations regarding the three dimensional geometrical relationships between the main joint and the fringe zone. A crucial, unanswered question is whether the *en echelon* fractures are consistently developed on one side or another of the main joint trace, or whether they straddle the underlying joint trace. Also unknown is the exact manner in which the planar joint surface breaks down into *en echelon* F-joints.

The only observations that could consistently be made at the upper Moab surface were the nature of the *en echelon* geometry of the F-joints, and their rotation in strike from the throughgoing joint zone.

TABLE 2-1

Area	Geometry Developed			
	Right Stepping	Left Stepping	No F-joints Developed	Obscured
Domain A (J_1^A)	104	1	21	187
Domain B (J_1^B)	4	0	4	13
Domain C (J_5^C)	6	11	9	44
Total Observations = 403				

Discussion

In the relatively simple areas of Domains A and B, the strike of the F-joints is consistently 5 to 35 degrees westward (counter-clockwise) of the strike of the throughgoing joint zones. Both of these Domains are characterized by

right-stepping geometries of the F-joints (Table 2-1). The *en echelon* geometry of the F-joints in Domains A and B is apparently independent of the orientation of the younger zoned joint sets: J_2^A strikes eastward (clockwise) of J_1^A, while J_2^B strikes westward (counter-clockwise) of J_1^B. This suggests that the F-joints develop as a consequence of fracture propagation during the initial (J_1) jointing episode, and not during a later (J_2) episode.

The F-joints of J_3^C in Domain C display both left and right *en echelon* geometries, with about two-thirds of the observations being left-stepping (Table 2-1). The reason for this complexity is not readily apparent, but may be related to the relatively complicated strain history of this area.

SUMMARY OF OBSERVATIONS

The field observations support the following statements about the joints in Arches:

(1) Joints in the Moab Member display a zoned character.

(2) A length scale, on the order of the Moab thickness, characterizes not only interzone spacing, but also the length of individual joints.

(3) The development of zoned joints is dependent on lithology.

(4) Relative ages of zoned joint sets can be determined in Arches.

(5) Detailed observations of joint zone geometries do not support a synchronous, conjugate origin for the jointing.

(6) Jointing is an extensional process. The fracturing accommodates an extensional strain in the rock.

(7) More than one episode of jointing has occurred, with later sets confined between older sets.

-113-

(8) The pre-existence of a zoned joint set has caused a later, non-parallel, zone to assume a non-planar geometry. This deviation from a planar surface is systematic in a given region, and the magnitude of the deviation is a function of proximity to the through-going zone.

(9) Localization of shear deformation and cataclasis may occur along pre-existing joints.

CONCLUSIONS

The relationship between fracture spacing and bed thickness has previously received considerable attention (Ladeira and Price, 1981; Sowers, 1973; Hobbs, 1967; Lachenbruch, 1961). However, the observation that bed thickness also provides a length scale for individual fractures seems to be new. The actual three-dimensional geometry of individual joints in the Moab Member is still unknown, although the observations indicate that the geometry is somewhere between a thin square and a penny-shaped crack.

The ability to separate relative ages of zoned joints leads to the conclusion that the joints represent a cumulative, superimposed fracture pattern of extensional fractures. As shown on figure 2-25 A, the oldest, throughgoing joint zones formed perpendicular to a regional extension. Over time, movement of salt at depth led to rotation of the stress field (figure 2-25 B). Younger joints growing in the rotated stress field formed normal to the new extension direction, while resolved shear stresses on the older zones led to shear displacement on these older zones.

The characteristic interactions noted between younger and older joint zones in Domains A and B, while spectacularly developed in Arches, are not unique to Arches. The mode B type of interaction, where the younger joint hooks into the older joint, has long been recognized as an effective criteria for

Figure 2-25.

(A) Throughgoing zoned joint set forms perpendicular to regional least principal stress (arrows).

(B) Over time, rotation of stress field leads to resolved shear stresses on the throughgoing set of zoned joints, which in turn causes shear displacement on the oldest set. Younger zoned joints growing in this rotated stress field nucleate in the region between the throughgoing zones, perpendicular to the new direction of σ_3 (heavy arrows). Compare with figures 2-7 and 2-10.
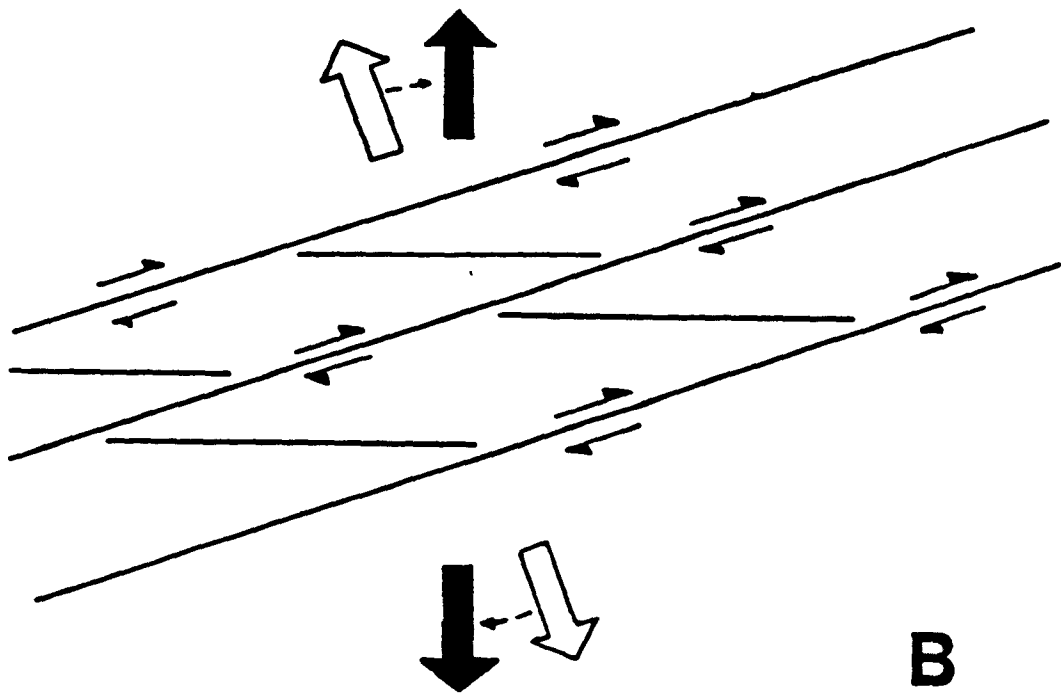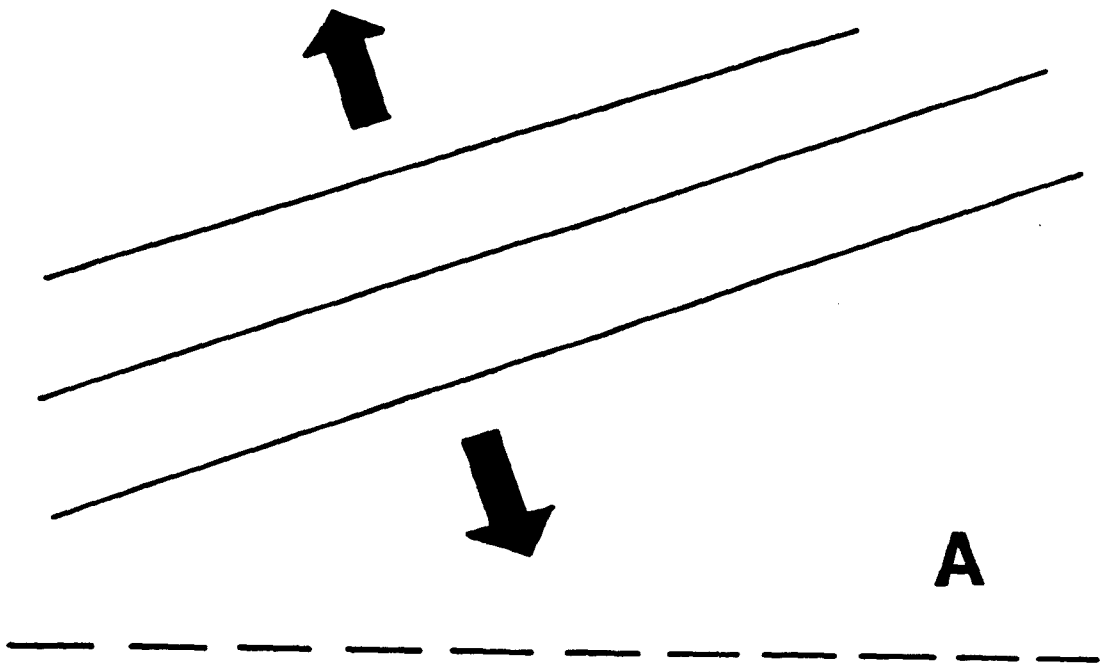
relative age determination. Wheeler and Holland (1981, p. 397) used this criteria to sort out jointing episodes in the eastern Plateau province of West Virginia. The type A interaction, where one joint set curves into parallelism with a second set of joints, was noted by Ziony (1966, p. 41) in his study of systematic joints on the Monument Upwarp. R. L. Wheeler (personal communication, 1982) reports that he has observed this type of interaction in many exposures in the central Appalachians. The advantage of the Arches observations is that there is no doubt as to relative ages, and therefore we can begin to interpret these characteristic interactions from a mechanistic basis (see Chapter 5).

The observation that fault-like features can form along joints raises serious questions regarding the somewhat arbitrary division of brittle fractures into faults and joints. What are the real differences between faults and joints, and how are they related? Is it possible that every fault arises from shear strain concentrated on a pre-existing "joint"? These questions are currently unanswerable, but their resolution will greatly enhance our understanding of processes at work in the earth.

CHAPTER THREE

ORIGIN OF ZONED JOINTS

ABSTRACT

A shear or shear-extension mechanism is rejected for the zoned joints in Arches National Park. The joint systems are a cumulative fracture pattern due to the superposition over time of several sets of extensional joints. Although each set of joints formed as extensional fractures, rotation of the stress field over time leads to resolved shear stresses and shear displacements on pre-existing joints. Joint growth probably occurred at quasi-static rates. Several characteristics of zoned joints indicate that they grew in response to an effective tensile minimum principal stress ($|\sigma_3 - P| < 0$), and are true tensile joints. These characteristics include: (1) size (~ 20 m) and aspect ratio (10^4 - 10^5) of individual joints; and, (2) the zoned nature of the joints. Examination of thin sections from cores adjacent to zoned joints reveal no concentration of microfractures that might be indicative of a plastic or process zone associated with the propagating crack tip. Permeability measurements on several suites of cores taken transverse to the zoned joints show no systematic change as a function of distance from the joint, also suggesting the absence of a process zone of microfracturing. High elastic strain energies near the tip of a large tensile joint are apparently dissipated through growth of suitably sized and oriented flaws which are of subcritical size under the far-field loading. These joints in turn grow and encourage the growth of still more flaws near their tips. The resultant en echelon trend of individual joints comprises the zoned joint observed in the field.

INTRODUCTION

Criteria for brittle fracture in rocks can be broadly subdivided into two general groups: those which predict or require shearing failure; and those in which shear failure plays no role. Examples of the first group include the Coulomb failure criteria and numerous variants on this theme (e.g. McClintock and Walsh, 1962; Brace, 1960; Anderson, 1951). Under compressive triaxial loading, this type of failure is characterized by synchronous shearing along

critically oriented, conjugate surfaces. Muehlberger (1961) extended the theory to account for shear-extension joints. We may discount shearing mechanisms for the origin of the joints in the Moab member because of two basic observations: (1) the youngest joints display no observable shear displacement; and, (2) the joint sets are not synchronous, conjugate sets, but superimposed sets of parallel fractures, with distinct age relationships observed between the different sets. The zoned joints of Arches are superimposed single sets of extensional brittle fractures.

Most mechanisms proposed for extensional brittle failure are based on the Griffith theories of brittle fracture (Griffith; 1921, 1924). According to these theories, brittle fracture occurs due to the growth of small cracks or flaws. Incremental crack growth occurs to satisfy energy-balance equilibrium. The criteria for determining whether crack growth will occur is a function of the crack geometry and orientation with respect to the far-field principal stresses; the magnitude of the far-field and crack stresses; and some rock property (either tensile strength or some measure of fracture energy). Very rapid (dynamic) crack growth typically occurs at velocities which are a large percentage of the velocity of sound in the material. Dynamic crack growth is characterized by bifurcations and branchings of the fracture surface. Bifurcations and branchings are not found on zoned joints in the Moab Member (see figure 2-2). This suggests that joint propagation rates for the zoned joints in the Moab Member were probably quasi-static, and that a mechanical examination of these joints is amenable to a static analysis.

GROWTH OF EXTENSION FRACTURES

Extension fractures form normal to the least compressive principal stress (σ_3). Following the pioneering work of Secor (1965, 1969), who showed that "high" fluid pressure could lead to effective tensile stresses and tensile fracture at any depth, geologists have been less reluctant to consider tensile stresses as a cause of brittle fracture.

STRESSES AROUND AN ELLIPTICAL CRACK

The stress distribution around a single flaw in an infinite, homogeneous, isotropic elastic body can be determined by specifying the shape of the flaw, the pressure internal to the flaw, and the far-field loading. Numerous workers have shown both theoretically (Bergvist and Guex, 1979; Erdogan and Sih, 1963) and experimentally (Erdogan and Sih, 1963; Bombolakis, 1973; Anderson, 1978) that growth of a single crack will be such that it tends to orient itself parallel and perpendicular to the applied principal stresses. Hence, we will confine our investigation to a crack oriented parallel and normal to σ_1^{∞} and σ_3^{∞}, respectively. For simplicity we will limit ourselves to a two-dimensional analysis.

Consider a fluid-filled elliptic hole with aspect ratio of $\frac{a}{b}$ which is embedded in an infinite, two-dimensional, homogeneous, isotropic elastic body and subject to a uniform internal fluid pressure (P). If the crack is oriented in relation to the far-field stresses as in figure 3-1, the stress, σ_t, at the crack tip ($x = a$) may be found using a slight generalization of the treatment of Jaeger and Cook (1979, p. 268). We find that:

$$\sigma_t = \left[-\sigma_1^{\infty} + \left[1 + \frac{2a}{b} \right] \left(\sigma_3^{\infty} - P \right) + 2P \right].$$

(3-1)

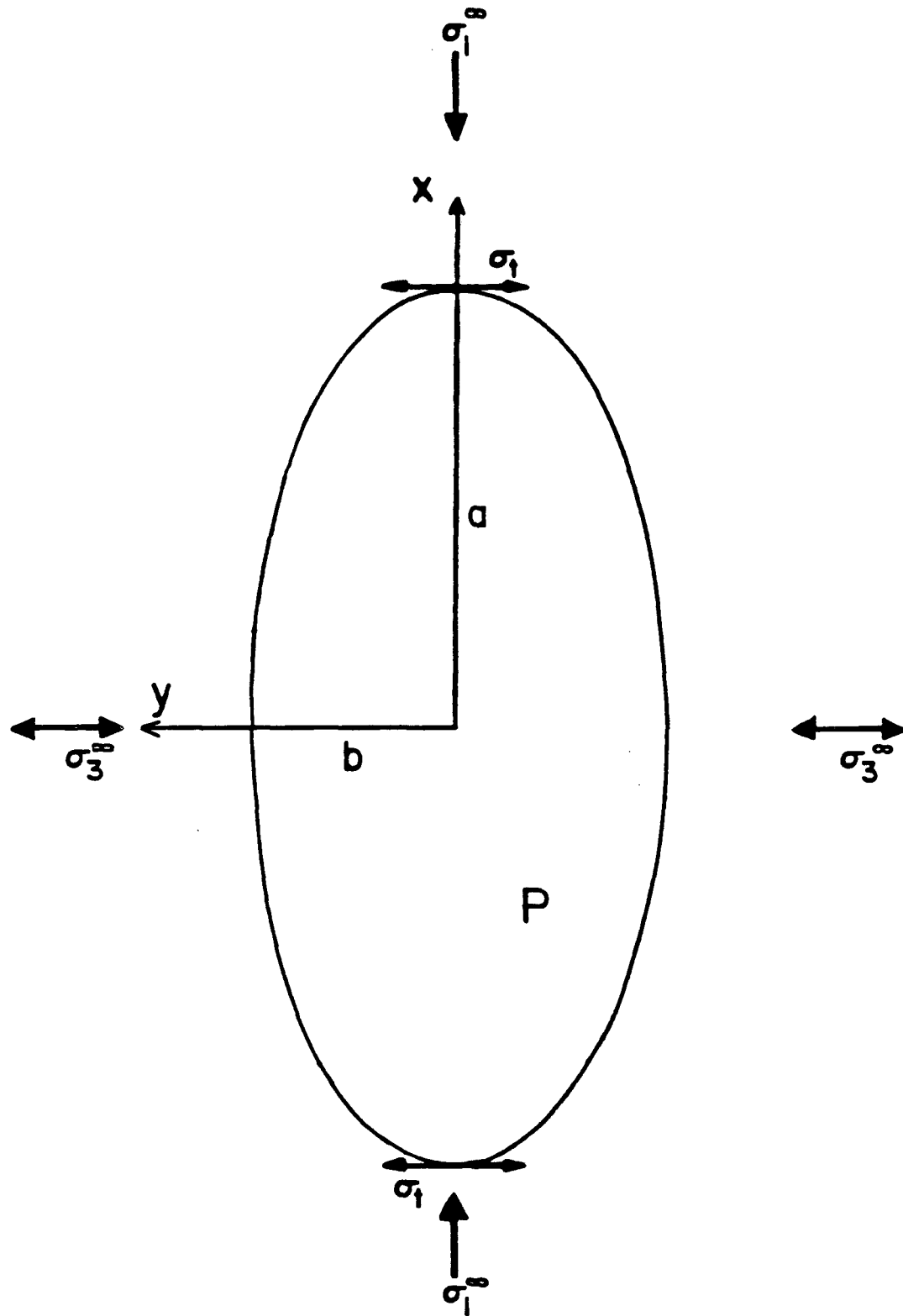**Figure 3-1.**

Fluid-filled ellipse of aspect ratio $\frac{a}{b}$, subject to far-field stresses σ_1^∞ and σ_3^∞, and internal fluid pressure P. σ_t is the crack tip stress at $x = a$.

where σ_1^∞ and σ_3^∞ are the maximum and minimum principal far-field stresses and P is the fluid pressure in the crack. We use the sign convention that positive values of stress are compressive. For $\frac{a}{b} \gg 1$, equation 3-1 becomes

$$\sigma_t = -\left[\sigma_1^\infty - \frac{2a}{b}\left(\sigma_3^\infty - P\right)\right] + 2P. \qquad (3\text{-}2)$$

It is tempting to use equation 3-2 as the basis for a propagation criteria for extensional fractures. A possible propagation criterion based on equation 3-2 might specify: in order for extension of the crack tip to occur, σ_t must equal the effective tensile strength of the material. Note that a negative (tensile) value of $(\sigma_3^\infty - P)$ does not guarantee a tensile value of σ_t. If $(\sigma_3^\infty - P) \approx \frac{-b}{a}$, then it is still possible for σ_t to be compressive. However, examination of equation 3-1 or 3-2 reveals that for large crack aspect ratios $(\frac{a}{b} \gg 1)$ the geometric amplification of the $(\sigma_3^\infty - P)$ term will far outweigh the contribution of σ_1^∞. The zoned joints of Arches have large aspect ratios $(\frac{a}{b} \approx 10^4)$, suggesting that geometric amplification of stress is an important factor contributing to growth of these joints. If $(\sigma_3^\infty - P) < 0$ (more accurately if $\left|\sigma_3^\infty - P\right| < \frac{-b}{a}$) then crack dilation will occur and tensile stresses will exist at the crack tip. This situation could arise from any combination of internal fluid pressure in the crack (Secor, 1965) or tectonic remote tensile stresses. The greater the aspect ratio of the crack, the greater is the enhanced tension felt at the crack tip. In the limit of a flat elliptical crack with an aspect ratio of ∞, there is a stress singularity at the crack tip. Details of the stress field near the crack tip are highly dependent on the exact crack geometry. Mavko and Nur (1978) have shown that a stress singularity need not exist for sharp, tapered,

-122-

non-elliptical cracks subject to tensile loading normal to the crack. High tensile stresses exist in the vicinity of the crack tips, but they are everywhere finite.

STRESSES AROUND A FLAT CRACK

Figure 3-2 shows a fluid-filled flat elliptical crack (with aspect ratio of ∞ in the unstressed state) under uniform loading normal to the crack. This corresponds to the Mode I loading of linear elastic fracture mechanics. If $\left|\sigma_3^- - P\right| < 0$, then the elastic stresses and displacements around the crack tip due to the combined effects of the internal pressure and the far-field stress may be duplicated by subjecting a crack with no internal pressure to a remote stress normal to the crack of $\sigma_3^\bullet$, where $\sigma_3^\bullet = \sigma_3^- - P$. Crack dilation and propagation can only occur if $\sigma_3^\bullet < 0$.

For $0 < r \ll c$, the approximate stress field components are given by Lawn and Wilshaw (1975, p. 53) as:

$$\begin{bmatrix} \sigma_{xx} \\[2ex] \sigma_{yy} \\[2ex] \sigma_{xy} \end{bmatrix} = \sigma_3^\bullet \sqrt{\frac{c}{2r}} \begin{bmatrix} \cos(\frac{\theta}{2}) \left[1 - \sin(\frac{\theta}{2})\sin(\frac{3\theta}{2})\right] \\[2ex] \cos(\frac{\theta}{2}) \left[1 + \sin(\frac{\theta}{2})\sin(\frac{3\theta}{2})\right] \\[2ex] \sin(\frac{\theta}{2})\cos(\frac{\theta}{2})\cos(\frac{3\theta}{2}) \end{bmatrix}. \tag{3-3}$$

The orientation and magnitude of the local principal stresses, σ_1 and σ_3 are found from the familiar Mohr circle construction. At the point (r, θ), we have:

$$\sigma_m = \frac{\sigma_{xx} + \sigma_{yy}}{2} ; \tag{3-4}$$

$$\tan 2\Phi = \frac{\sigma_{xy}}{\sigma_{xx} - \sigma_m}; \tag{3-5}$$
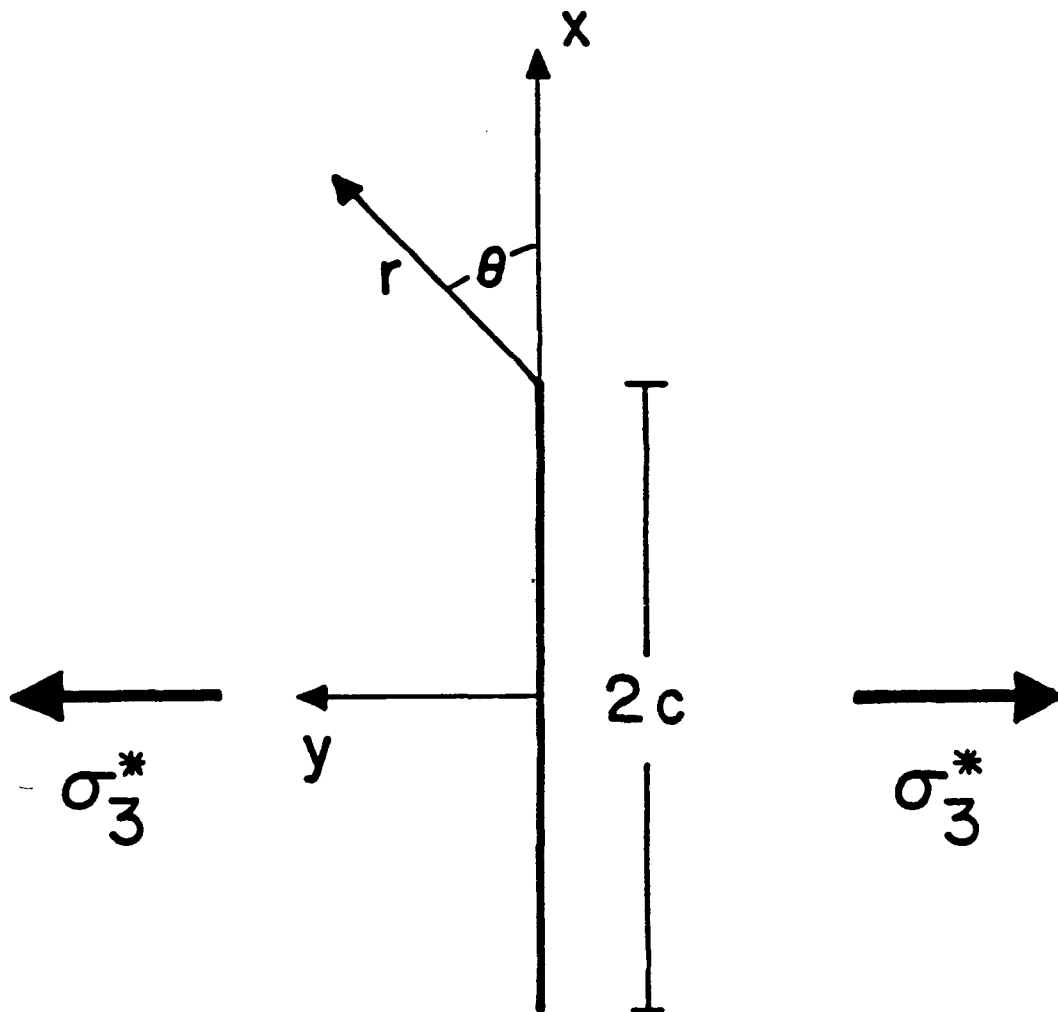
Figure 3-2.

Coordinate systems and loading for a crack of height 2c subject to Mode I (opening mode) loading.

where Φ is the angle between the x-axis and σ_1. The magnitudes of the principal stresses are given by:

$$\sigma_1 = \sigma_m + \left| \frac{\sigma_{zz} - \sigma_m}{\cos(2\Phi)} \right|; \tag{3-6}$$

$$\sigma_3 = \sigma_m - \left| \frac{\sigma_{zz} - \sigma_m}{\cos(2\Phi)} \right|. \tag{3-7}$$

If the magnitude of σ_3 is plotted in the vicinity of the crack tip, we find a region of increased tensile stress, as in figure 3-3. Note that the size of this region of enhanced tensile stress is a function of the half-length of the crack, c. As c increases, the size of the region of enhanced tension also increases.

Griffith's original theory of brittle failure (1921) was based on the concept of energy balance. He found that the critical tensile stress required for brittle crack growth is a function of crack length and material properties; namely Young's modulus (E) and the free surface energy per unit area (γ). For a narrow, elliptical crack of length 2c oriented normal to remote, uniform tensile stress field, under plane strain conditions, as in figure 3-2, crack growth will occur when (Lawn and Wilshaw,1975; p. 8):

$$\sigma_{crit} = \left[\frac{2E\gamma}{\pi c \left[1 - \nu^2 \right]} \right]^{1/2} \tag{3-8}$$

The failure criterion is commonly expressed in terms of the strength of the stress singularity at the crack tip, the stress intensity factor. For the plane-strain Mode I loading shown in figure 3-2,

$$K_I = \sigma_3^* \sqrt{\pi c}. \tag{3-9}$$
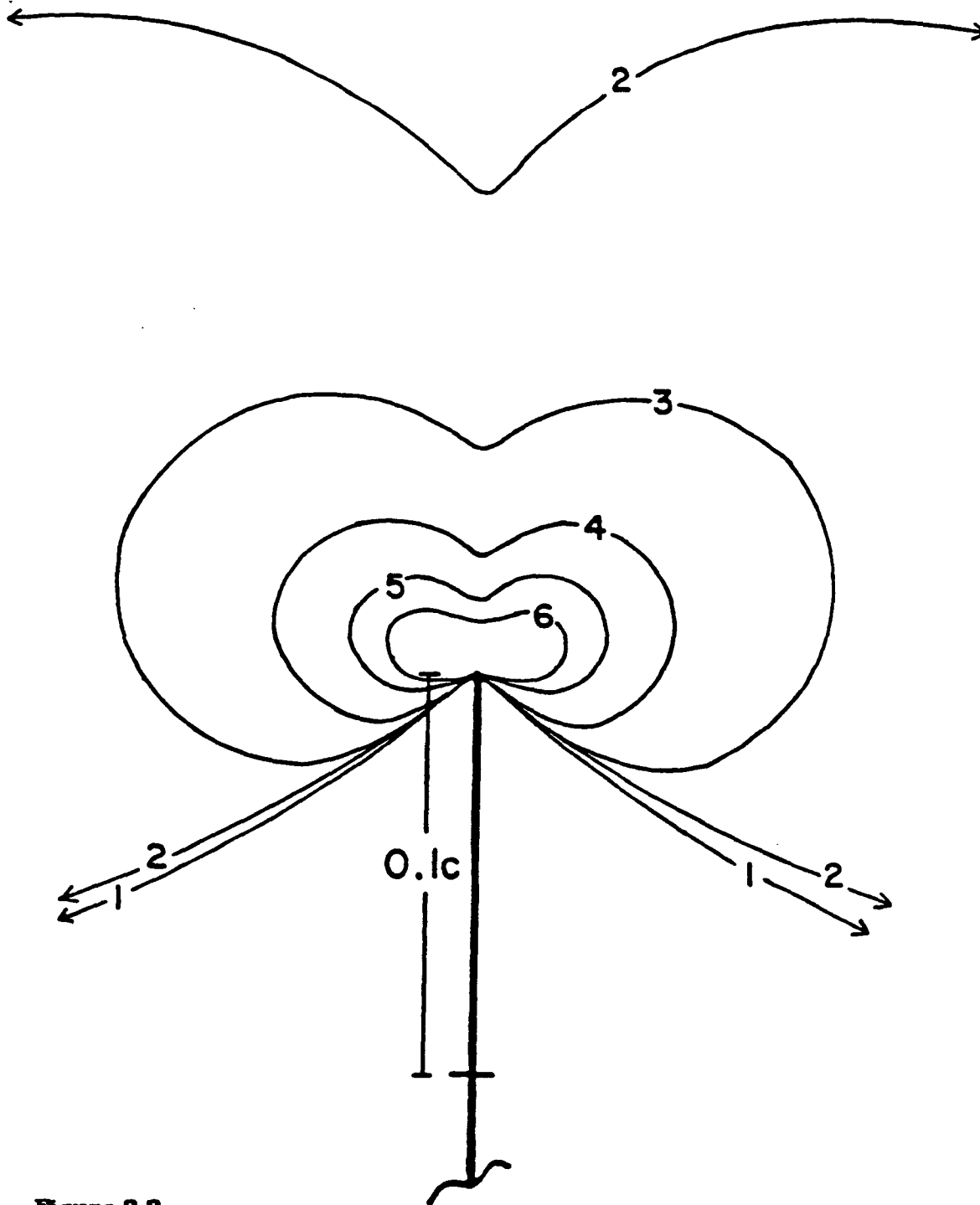
Figure 3-3.

Plot of normalized magnitude of least principal stress $(\frac{\sigma_3}{\sigma_3^*})$ near tip of flat elliptical crack for loading shown in figure 3-2. Note scale. σ_3 increases without bound near the crack tip (r=0). Note lobate form of the stress contours. A relative minimum for σ_3 exists along the X-axis. Addition of a compressive loading, σ_1, along the x-axis does not change the form of the stress contours within the region $(\frac{\sigma_3}{\sigma_3^*}) \gg (\frac{\sigma_1}{\sigma_3^*})$.

-126-

There is a critical K_I at which brittle failure will occur. This is denoted by Kf and is a property of the material. Crack growth will occur when

$$Kf = \sigma_3^\bullet \sqrt{\pi c}.$$

(3-10)

From the above equation it follows that we may calculate the critical crack half-length, c_0, of a crack that will just begin growing with the application of a driving stress of $\sigma_0 = \sigma_3^- - P$.

$$c_0 = \frac{1}{\pi} \left\{ \frac{Kf}{\sigma_0} \right\}^2.$$

(3-11)

This means that under a given loading, there is a threshold size for crack growth. Suitably oriented large cracks will preferentially grow, while smaller cracks will not. There is no difficulty in producing large, extensional cracks (joints) if $\sigma_3^\bullet = \left| \sigma_3^- - P \right| < 0$. In fact, it is not obvious from equation (3-11) why there should not be just one enormous joint. If large cracks grow easier, and if the larger a crack grows the easier it is for it to grow, we might expect catastrophic growth of a single joint. This is assuredly not what is observed in the field, where joint sets consist of many discrete, sub-parallel joints. Growth of a set of parallel cracks was addressed by Segall (1981), who found that the force that drives crack propagation varies as a function of: (1) change in crack length; (2) change in remote displacements; (3) elastic interaction with nearby cracks; and, (4) stress relaxation due to decrease in the systems effective modulus. The single crack with uniform load is inadequate to explain sets but this more complex theory does allow their stable growth.

ORIGIN OF JOINT ZONES

The origin of zones of joints appears problematic. It is highly improbable that all critically sized flaws in the Moab member just happened to be confined to these distinct zones. An alternate hypothesis is that the propagation of a joint zone somehow selectively encourages joint growth in proximity to the propagating zone front. This hypothesis is similar to that proposed by Delaney and Pollard (1981, p. 37) to explain local joint sets developed sub-parallel to dike sets at Ship Rock, New Mexico.

We have seen in figure 3-3 that a region of enhanced stress exists near the crack tip. Although an exact description of the stress field near the crack tip requires an exact specification of the crack geometry, it is reasonable to expect stresses near the crack tip with a magnitude of at least $5\sigma_0$. This value is chosen arbitrarily, but is felt to be reasonable. The critical half-length, c_1, of a crack which would grow under this enhanced loading is then

$$c_1 = \frac{1}{\pi}\left[\frac{Kf}{5\sigma_0}\right]^2 = \frac{1}{25}c_0 \tag{3-12}$$

In this manner, growth of sub-critical sized cracks (much smaller than c_0) can be locally induced by the enhanced loading near a large crack tip. This mechanism is especially attractive for the formation of joint zones in porous rocks, where there will be a wide distribution in the size of flaws or protocracks consisting of linked pore spaces. In an ideal body containing a number of parallel cracks of different sizes oriented normal to the far-field tension, we expect the extensional strain to be accomodated by preferential growth and dilation of the largest cracks. Growth of large cracks will be accompanied by a region of enhanced tension at the crack tip. Within this region, we might expect the enhanced tensile loading to cause growth of small cracks whose

-128-

growth is not energetically feasible under the remote loading, but which are of sufficient length to grow in the enhanced stress field.

Thus, the relief of extensional strain by brittle fracture arises from two competing mechanisms. If we consider only a single fracture in an elastic body, the larger this single fracture becomes, the easier it is for this fracture to grow. The situation becomes considerably more complicated when several cracks are considered. Competing against the unlimited growth of a single fracture will be the tendency for smaller cracks to grow in the region of enhanced tension ahead of the tip of the large crack. As the large crack and its region of enhanced tension grows, the probability increases that a suitably sized flaw (of "subcritical" size under the far field loading) will lie in the enhanced region and begin to grow. In this manner, strain may be accommodated by a self-propagating zone of fractures. Because of the symmetry of the stress field at the crack tip, we would not expect any regular en echelon geometry to develop.

Although this approach is intuitively appealing, the detailed mechanics of zoned joint growth will be complex. If the flaws grow large enough, they will interact with the large crack. The enhanced loading in the region of the larger crack is certainly not uniform, leading to complications in the detailed behaviour of the small cracks. The final geometry may be highly dependent on the rate of growth of the large and small cracks - it is possible that the large crack would pass by the small crack before it had time to grow to an appreciable size.

Finally, it must be noted that the controlling length scale, c_o, is itself unknown. As discussed in chapter 2, the shape of an individual joint in the Moab Member must be somewhere between a thin square and a penny-shaped

crack, but the details of the three-dimensional geometry of the crack front are unknown. Additionally, any crack front lies at the end of a long zone of joints. Is the effective mechanical "length" of the crack the length of a single crack ($\approx$27 meters), or is it the length of the entire zone (several km)? The characteristic spacing between joint zones in the Moab Member suggests that the controlling length scale, c_0, must be on the order of the half-thickness of the Moab Member.

DEFORMATION AT THE CRACK TIP

According to the elastic stress field solutions (equation 3-3) a stress singularity exists at the tip of a mathematically flat crack subjected to Mode I loading. Real materials cannot support a large tensile stress, and tend to exhibit a yield stess. Metals, especially, deform plastically above this yield stress. A great deal of work in materials science has been devoted to investigating the shape and character of the plastic zone associated with a crack tip. A concise summary of this work may be found in Broek (1978, Chapter 4). It is by no means clear that such a plastic zone develops in rocks. If we hypothesize that the permeability of the rock is related to the density of microfractures in the rock, then permeability measurements should reveal something about the microfracture density.

Eighteen 2.5cm diameter vertical cores were recovered along four sample lines normal to a J_c^3 joint zone. The cores were trimmed and hand lapped into right-circular cylinders about 4cm long. The cores were vacuum dried for several days. Permeability was determined using a capillary tube air permeameter. The air supply was compressed air at $\sim$ 100psi. Because of the limited range of air injection pressure available, it was not possible to

-130-
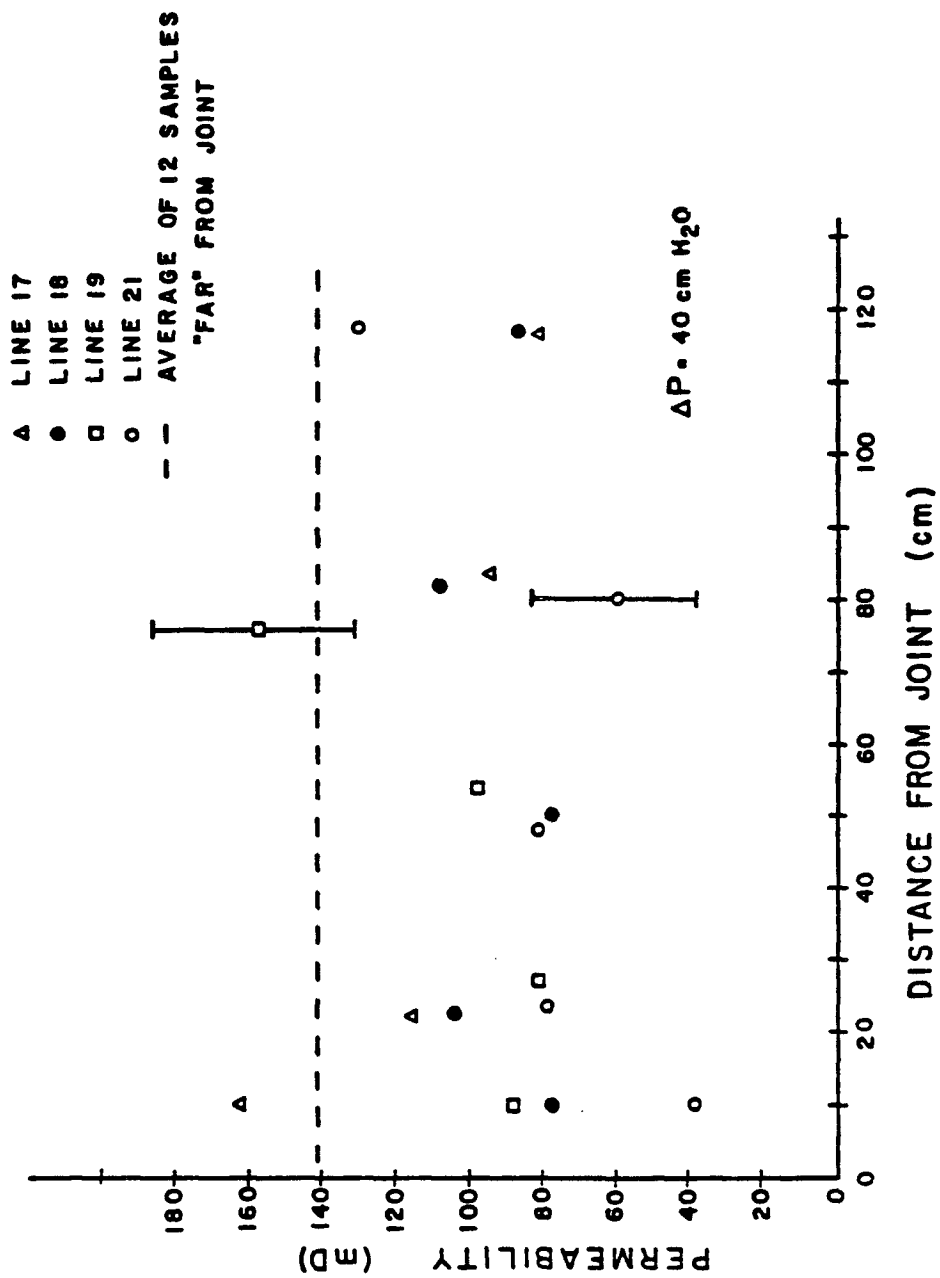
Figure 3-4.

Plot of measured air permeability vs. distance from J_3^C joint. Injection pressure for all samples is 40 cm H_2O above atmospheric pressure. Error bars are considered typical for all measurements.

determine a Klinkenberg correction for the permeability.

Figure 3-4 shows the calculated permeabilities at a constant injection pressure of 40 cm of H_2O above atmospheric pressure. Error bars are shown for samples 19D and 21D.

As evident in figure 3-4, there is no systematic relationship between the measured permeabilities and distance from the joint. Sample line 17 shows an apparent exponential decrease in permeability as a function of distance from the joint. Sample line 21 suggests a quasi-linear increase in permeability as a function of distance from the joint. Sample lines 18 and 19 show near-constant permeabilities of about 90 millidarcies.

Within the range of experimental error, there is no systematic change in permeability as a function of distance from the joint zone. This suggests either that there is no appreciable microfracturing associated with the joint zone, or that all such microfractures have been healed, possibly by secondary cementation. Thin sections were examined under the petrographic microscope, using polarized light and cathodoluminescence. No secondary cement, grain fracturing, or other grain-scale features that might be attributable to microfracturing were noted.

In lieu of a crack tip plastic zone, it is proposed that high elastic strain energies near the tip of a large joint are dissipated through growth of suitably sized and oriented flaws which are of subcritical size under the far-field loading. These joints in turn grow and encourage the growth of still more flaws near their tips. The resultant en echelon trend of individual joints comprises the zoned joint observed in the field.

CONCLUSIONS

The joint systems of the Moab Member are a cumulative fracture pattern caused by the superposition over time of several sets of extensional joints. The size (≈ 20 meters) and aspect ratio ($10^4 - 10^5$) of individual joints is a compelling argument against a compressive origin for these extensional fractures. All observations are compatible with a conventional linear elastic fracture mechanics interpretation for crack growth. This in turn requires that for each episode of jointing, $\sigma_3^{\bullet} = \left|\sigma_3^{\bullet} - P\right|$ must have been less than zero. Lack of crack branchings and bifurcations indicates that the joints grew at quasi-static rates. No evidence was found of a plastic zone associated with a crack tip. High elastic strain energies near a crack tip are apparently dissipated by induced growth of smaller flaws, leading to the zoned geometry noted in Arches.

CHAPTER FOUR

THE INFLUENCE OF LITHOLOGY ON JOINTING

ABSTRACT

Lithology contrasts between the Moab and Slick Rock Members strongly influence both the susceptibility of these units to jointing and the jointing style which ultimately develops. The Moab is characterized by large, pristine, interconnected pores and an absence of intergranular cement. Diagenetic clays (primarily kaolinite) clog pores and entwine grains in the Slick Rock Member. In a homogeneous stress field, fracture mechanics considerations suggest that the Moab would be more susceptible to tensile fracture due to the large, interconnected pores and the absence of grain-to-grain bonds. This is in agreement with the field evidence. Strength anisotropy due to large-scale eolian cross-bedding is rejected as a control on the orientation of zoned joints in the Moab Member. Tentative results suggest that ultrasonic laboratory measurements of compressional- and shear-wave velocities do not reflect the susceptibility of a lithology to jointing.

INTRODUCTION

The extent to which lithology affects the jointing process is poorly

understood. Past investigators have been divided on the issue.

Hodgson (1961a), in his regional study of jointing on the Colorado Plateau,

found that jointing patterns as a whole extended through the entire exposed

rock sequence. Although bedding strongly influences the orientation and

spacing of systematic joints, he noted no influence due to contrasting

lithologies. He concluded that joints form very early in the history of a

sediment and inherit their pattern from upward propagation of pre-existing

joint patterns from underlying rocks.

Spencer-Jones (1963) studied joint patterns in the massive sandstones of the Paleozoic Grampians Group rocks of Western Victoria, Australia, and found that joint orientation is independent of lithology.

Conversely, Harris and others (1960), in their study of structural control on fracturing, found that the susceptibility of any stratum to fracturing is dominantly controlled by the thickness and lithologic character of the stratum, while the trend and density of fractures is controlled by the structure.

Parker (1942) examined regional systematic jointing in Paleozoic sediments of New York and Pennsylvania. Based on the characteristics of fractures, he distinguished three sets of regional joints. In alternating beds of sandstone and shale, he noted preferential development of the dominant joint set was controlled by lithology (Parker, 1942, p. 395-397). An extension of this study by Engelder and Geiser (1980, p. 6323) noted that "joints in siltstones and sandstones have a regular spacing, whereas joints in shales tend to be less regularly spaced. In vertical sections, joints often terminate at lithologic boundaries. Some beds contain as many as three joint sets, whereas beds either below or above may contain only nonsystematic joints."

Nickelsen (1979), in his detailed study of structures associated with the Alleghany orogeny, noted that extension jointing in coals preceded extension jointing in interbedded sandstones and ironstones.

Nelson and Stearns (1975), in their study of regional fractures in the Lake Powell area, noted changes of strike of these regional fractures from formation to formation. They concluded that strength anisotropy due to large-scale primary sedimentary structures controlled the orientation of subsequent regional fractures.

Stearns and Friedman (1972) enumerated known factors that affect fracturing in rock. These include: (1) rock type; (2) temperature; (3) effective confining pressure; and, (4) strain rate.

The field study of jointing in Arches National Park clearly indicates that lithology has a strong influence not only on the susceptibility of a unit to jointing, but also on the style of jointing which develops in that unit. This may be clearly seen in figure 2-1. Evenly spaced, throughgoing zoned joints (J_1^β) are developed only in the Moab Member. Joints in the underlying Slick Rock Member do not show a zoned morphology and are uniformly closer spaced, even though the Slick Rock is about three time thicker than the Moab. In chapter two, evidence was presented which suggests that, in Domain B, the joints in the Slick Rock postdate the J_1^β jointing episode in the Moab. It is doubtful that the Moab and Slick Rock have experienced significantly different thermal or strain histories. The burial history for the two units is identical, although pore pressures in the two units may have varied considerably. It appears that the dominant control on joint development in Domain B is lithology.

In this chapter we will examine the qualitative differences in lithology between the Slick Rock and Moab Members. Quantitative properties are examined by velocity measurements. The role of strength anisotropy due to preferred directions of cross-bedding as a control on orientation of zoned joint sets in the Moab Member is examined and rejected. Lithologic differences between the Moab and Slick Rock are interpreted in a fracture mechanics context to better define the role of lithology in the jointing process.

LITHOLOGIC COMPARISONS

MOAB MEMBER

The Moab Member is a well-sorted quartzose eolian sandstone (figure 4-1 A). The dominant constituent is sub-angular to rounded quartz grains ($\geq$ 95%), with minor amounts of feldspar and lithic fragments present. The average grain size is ~ 0.1 mm. In general, there is no cementation in the Moab. The rock is held together solely by pressure-solution intergrowths at grain contacts (figure 4-1 B,C). There are no overgrowth of either quartz or calcite on the quartz grains. Pore spaces are large, open, and interconnected (figure 4-1 A,B). The absence of secondary quartz intergrowths indicates that the quartz dissolved during pressure solution, presumably during diagenesis, has been entirely flushed from the system. Calcite cement is noted near the top of the unit and occasionally within the unit. Porosity of the Moab is about 19% and the dry density is about 2.10 g / cm^3 (Table 1).

SLICK ROCK MEMBER

The Slick Rock Member conformably underlies the Moab Member and is everywhere separated from the Moab by a thin shale horizon or shaly partings. The Slick Rock is considerably more heterogeneous than the Moab, consisting of interbedded reddish-brown to orange silty sandstones and thin (< 3 meters) grey- to white cross-bedded sandstones. The silty sandstones comprise the majority of the unit and are the subject of the following observations.

Throughout Arches, this lithology is a fine-grained to very fine-grained dirty sandstone, with an average grain size of about 0.03 mm (figure 4-1 D). Grains are sub-angular to sub-rounded. Bimodal sorting is reported for these

Figure 4-1.

(A) SEM photograph of Moab Member. Scale bar is 1mm long.

(B) Moab Member. Scale bar is 0.1mm. Note pressure solution sutures and absence of overgrowths on quartz grains. The Moab has no intergranular cement.

(C) Moab Member. Scale bar is 0.01mm. Close up of pressure solution suture.

(D) Slick Rock Member. Scale bar is 0.1mm. Quartz grains are entwined in a clay cement.

(E) Detail of Slick Rock Member. Scale bar is 0.1mm. Note absence of pore space. Compare with (B).

(F) Authigenic kaolinite filling pore in Slick Rock (left side of picture). Scale bar is 0.01mm.

MOAB

SLICKROCK

A

B

C

D

E
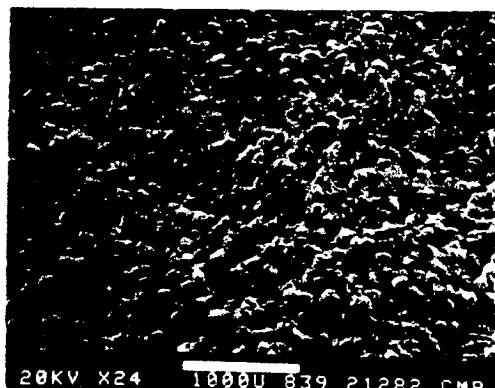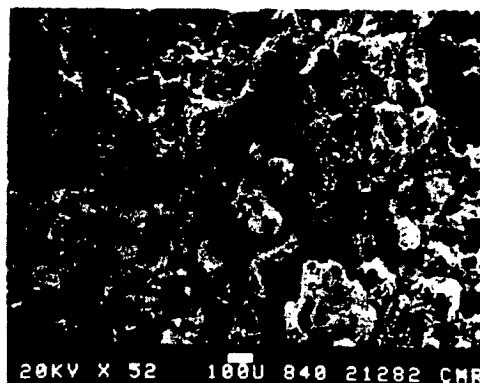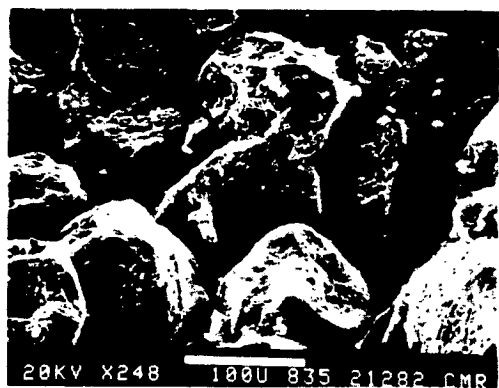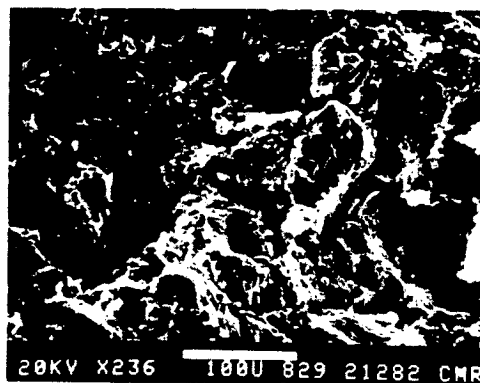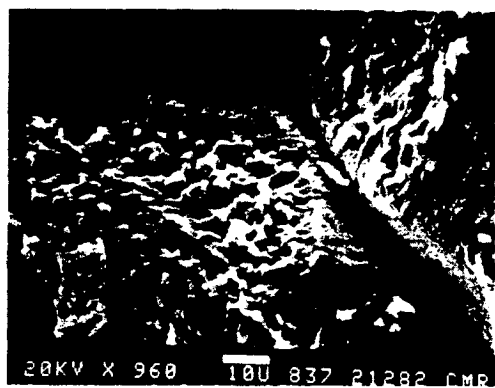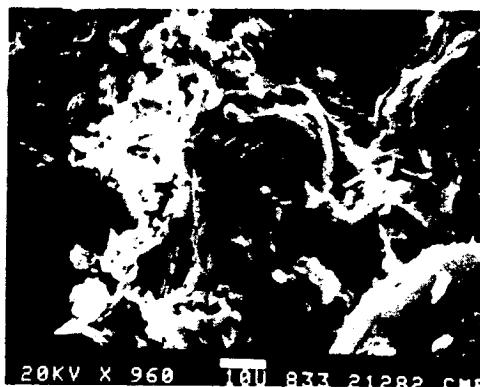
F

rocks (Dane, 1935, p. 93). Relatively large ($\sim$ 0.5 mm) lithic fragments of chert and other rock types are present, but are a minor constituent (< 5%). The small grains are dominantly quartzose, although chert and microcline are also observed. The cement is dominantly kaolinitic clays (figures 4-1 E,F). The clay is authigenic (figure 4-1 F). Calcite is also noted as a cement. Porosity of this rock is about 15%, and the dry density is about 2.4 g / cm^3 (Table 1).

DISCUSSION

Comparison of the SEM photographs of figure 4-1 reveal striking textural differences between the Moab and Slick Rock. Pores in the Slick Rock are clogged with kaolinite, while the Moab exhibits pristine pore throats. The total lack of cementation in the Moab, aside from pressure solution sutures, is noteworthy. The clay cement in the Slick Rock entwines and interlocks all of the quartz grains.

VELOCITY MEASUREMENTS

Ultrasonic compressional- and shear-wave velocities were measured in the laboratory for both the Moab and Slick Rock Members. Dynamic elastic moduli were calculated for both lithologies.

Several large blocks of relatively fresh Moab Member and Slick Rock Member were collected in the field. Cylindrical cores 2.5 cm in diameter were prepared parallel and perpendicular to bedding in both lithologies. The cores were trimmed and hand-lapped to give right-circular cylinders approximately 4 cm in length. The samples were jacketed and both shear and compressional velocities were measured in water saturated samples at ultrasonic frequencies (~ 1 MHz) by a pulse-transmission technique. Confining pressures and pore pressures were separately applied and controlled. We assume that the sandstones are linear isotropic elastic solids. Using standard formulations (Birch, 1966, p. 100), the dynamic elastic constants E (Young's modulus) and ν (Poisson's ratio) were computed using the velocity data and the saturated density. Table 1 contains the measured velocities and calculated elastic moduli for four representative cores under roughly equivalent confining pressure. The measurements are limited to relatively low confining pressures because the bicycle inner-tube sample jackets invariably failed at confining pressures of around 250 bars. This apparently occurs because the friable sandstone readily sheds loose sand grains and chips dislodge from the upper and lower edges of the cylinders. Pinprick holes then develop in the jacket over these small voids. Considerable difficulty was also encountered in determination of valid S-wave arrivals at these low confining pressures.

From the work of Cheng and Johnston (1981) it is known that at low confining pressures the dynamic elastic constants may differ by a factor of two

from the static elastic constants. Nevertheless, it is felt that the data of table 1 provide some quantitative basis for comparison of elastic properties between these two lithologies.

TABLE 1				
	Moab member		Slick Rock member	
	parallel	perpendicular	parallel	perpendicular
Density (dry) g/cm^3	2.10	2.11	2.26	2.22
Density (saturated)	2.28	2.30	2.40	2.38
Porosity (%)	18.4	19.4	14.2	16.1
Vp (Km/sec)	3.96	3.98	4.11	3.96
Vs (Km/sec)	2.18	-	2.23	-
E (Bars X 10^5)	2.48	-	3.09	-
ν	0.283	-	0.29	-
Pc (Bars)	200	150	300	200
Pp (Bars)	20	20	20	20

DISCUSSION

The experimentally-determined velocity data and computed elastic constants are given in table 1. Because of procedural difficulties inherent in working with friable sandstones at low confining pressures, this data must be viewed with a bit of caution.

The velocity data show no strong contrast between the Moab and Slick Rock for either P- or S-wave pulses. The dynamic Poisson's ratio is about the same for both rocks. The dynamic Young's modulus for the Slick Rock appears

to be about 20% higher than that of the Moab. This result is counterintuitive, for we expect the clay-rich Slick Rock to be more compliant, not stiffer, than the Moab.

THE ROLE OF ANISOTROPY

Nelson and Stearns (1977) investigated regional extensional fracture systems in various formations which crop out in the Lake Powell area of Utah and Arizona. They concluded that changes in strike of fracture systems from formation to formation are due to large-scale primary sedimentary structures within the rocks that make up each formation. These fractures have no obvious relation to local or regional structure. They argued that sedimentary structures can create mechanical anisotropies within a formation which control the orientation of subsequent regional fractures when subjected to regional tectonic forces. From empirical correlations they inferred that regional fractures tend to form perpendicular to the paleo-wind direction in eolian sediments.

The zoned joints and well-developed cross-bedding of the Moab Member allow a test of this hypothesis. The attitudes of more than 90 cross-beds were measured in an area of about 1 km^2 in Domain A. Orientations were also obtained on all J_1^A and J_2^A joint zones in this area. Figure 4-2 A is an equal-area stereonet plot, rotated to horizontal, showing poles to cross-bedding, the average cross-bedding orientation, the average pole to J_1^A and the average pole to J_2^A.

Figure 4-2 B compares the paleo-wind directions in the Moab, determined from cross-bedding, with the average strikes of J_1^A and J_2^A. Paleo-wind directions in the Moab show considerable variability. Winds blew from all
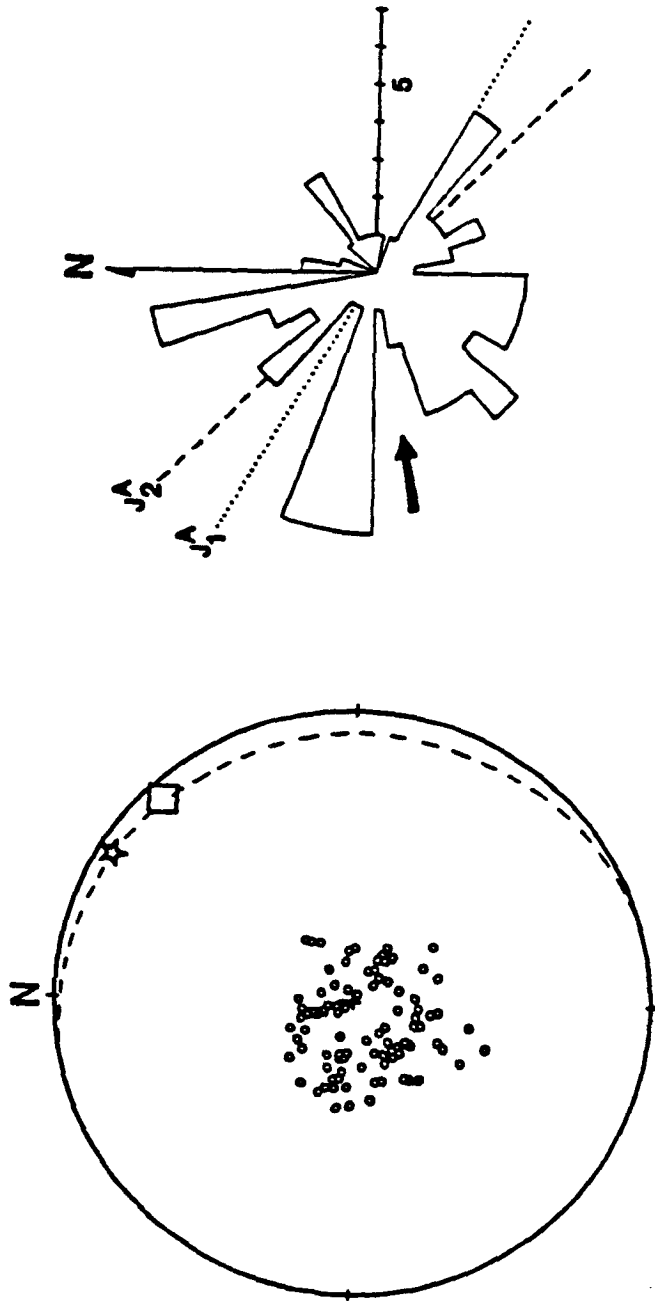
Figure 4-2.

(A) Equal area stereonet plot of poles to cross-bedding (open circles) and average orientation of cross-bedding (dashed line) for 92 measurements in a small part of *Domain A. Star* is average pole to J_1^A. Open box is average pole to J_2^A. All data has been rotated to horizontal.

(B) Wind rose derived from cross-bedding data of figure 4-2 A. Ten degree increments. Winds blow toward center. Heavy arrow is average wind direction. Dotted and dashed lines show average strike of J_1^A and J_2^A, respectively.

quarters, although there is a distinct minimum from the northeast quarter. The average wind direction, normal to the average strike of cross-bedding, is from S80W. This average corresponds to a relative minimum in the data. The large variability in the data give no reason to expect any strong preferred horizontal anisotropy to develop due to preferred orientation of cross-bedding.

The orientations of both J_1^A and J_2^A show no apparent correlation to the average cross-bedding fabric. Horizontal anisotropy due to preferred orientation of eolian cross-bedding appears to play no role in controlling joint orientations in this part of Domain A.

The area studied is considered typical of Domain A, an area of $\geq 8\ km^2$. The conclusions of Nelson and Stearns (1977) are based on studies over a region of about 13,000 km^2. Whether the joint sets of Domain A (J_1^A and J_2^A) qualify as "regional" fracture sets is arguable, since the area which constitutes a "region" is ambiguous. On the scale of the study area, $\sim 50\ km^2$, the joint sets of Domain A are clearly "regional" in extent.

CONCLUSIONS

Observations in the Moab Member provides no support for the hypothesis that development of horizontal strength anisotropy due to preferential orientation of eolian cross-bedding controls the orientation of regional fracture sets.

The Moab and Slick Rock Members show strongly differing styles of jointing. Zoned joints are non-existent in the Slick Rock and pervasive in the Moab. Field evidence in Domain B suggests that the Slick Rock is less susceptible to jointing that the Moab. Qualitative support for this suggestion is found in the textural contrasts between the Moab and Slick Rock. Large,

pristine pore throats and lack of cement characterize the Moab, while diagenetic clays clog pores and entwine grains in the Slick Rock. Fracture mechanics predicts three primary controls on crack growth: (1) loading; (2) crack size; and (3) a material property (fracture toughness or surface energy). There is little reason to suspect that the Slick Rock has undergone a significantly different loading history than the Moab. From a fracture mechanics viewpoint, crack growth in the Moab would be favored for two reasons. Interconnected pores in the Moab result in larger "flaws", which in themselves are favored for growth. Additionally, the diagenetic clays of the Slick Rock will tend to bond those grains together. A propagating crack in the Slick Rock must either break these clay bonds or shatter the quartz grains. Conversely, a propagating crack in the Moab need only separate grains along the pressure solution intergrowths.

Attempts to relate the jointing susceptibility of the Moab and Slick Rock to laboratory ultrasonic compressional- and shear-wave velocity data have so far been unsuccessful.

CHAPTER FIVE

THE STRESS FIELD ABOUT A JOINT ZONE

ABSTRACT

Because they grow perpendicular to a minimum principal stress (σ_3), zoned joints are paleostress markers. The younger joints of both Domains A and B show a systematic change in orientation as they approach older, throughgoing, zones. This change in orientation reflects a change in the stress field in which the younger joint set is growing. Analytic solutions for the stress field around a single joint zone subject to a combination of opening (Mode I) and anti-plane shear (Mode III) loadings are given. The sense of rotation and change in magnitude of principal stresses near a joint zone are functions of the orientation and ratio of magnitudes of the far-field stresses; and the coefficient of friction across the joint. Assuming that a later, non-parallel joint zone nucleates distant from, and grows toward the throughgoing joint zone, the stress field in which it is growing will be systematically rotated and changed by the presence of the throughgoing zone. The interaction effect between the older and younger joints is ignored in the analysis. The systematic change in orientation of the later joint zone reflects the change in principal stresses near the throughgoing zone, and can be used to place approximate limits on the ratio of the far-field horizontal stresses. The younger zoned joints of Domain A (J_2^A) probably grew in a stress field in which $-3 < \dfrac{\sigma_2^{\sim}}{\sigma_3^{\sim}} < -1/3$. The geometry of younger zoned joints of Domain B suggest that J_2^B grew in a stress field in which $-1/3 < \dfrac{\sigma_2^{\sim}}{\sigma_3^{\sim}} < 1$.

INTRODUCTION

Engelder and Geiser (1980) concluded from field studies on the Appalachian Plateau that regional systematic joints reflect the principal directions of the regional stress field which gave rise to the joints. Each set of joints is interpreted to represent a distinct episode of jointing. They concluded (Engelder and Geiser, 1980, p. 6333) that joints are extensional fractures

formed perpendicular to σ_3 and inferred that net tensile stresses were present during jointing. Superposition of multiple sets reflects a change in the orientation of regional stresses over time.

The observations on zoned joints in Arches National Park support these contentions. The field evidence in Arches clearly indicates that several generations of jointing have occurred. Rotation of the causative stress field is recorded by the change in mean strike direction of the various sets of zoned joints. An important characteristic of the zoned joints of Arches is that younger joint zones show a systematic change in their orientation near older, throughgoing zones. This systematic change occurs over large areas, or domains. The existence of a throughgoing set clearly exerts an influence on the form of later, non-parallel sets.

JOINTS AS PALEOSTRESS INDICATORS

Joints record an episode of brittle fracture in rock. Field evidence indicates that all of the zoned systematic joints in Arches originated as extensional fractures. As noted by Griggs and Handin (1960, p. 348), extension fractures form perpendicular to the direction of σ_3. Tensile fractures are a subset of extension fractures which form due to a tensile σ_3 (more correctly, when $\sigma_3 - P < 0$). There is a considerable body of theoretical and experimental evidence to support this geometric relation between the orientation of the extension fracture and the orientation of σ_3 (Griggs and Handin, 1960, p. 350-351; Odé, 1957; Hubbert and Willis, 1957; Kehle, 1964; Hoek and Bieniawski, 1965; Secor, 1965, 1969; Peng and Ortiz, 1973; Zoback and Pollard, 1978). The joints of Arches, then, provide a paleostress map of the elastic stress field at the time of jointing. The consistent change in orientation of younger joint

zones near older, throughgoing zones is interpreted as a local change in the stress field due to the presence of the throughgoing zone.

Solutions for the elastic stress field about an idealized single zone of joints are presented in the following pages. Assumptions about loading conditions allow a considerable simplification of the solutions. Maps are presented of the stress field about a single joint zone for a variety of loading conditions. These stress maps are interpreted in terms of the geometry that a younger joint set might develop if growing in this stress field. The interpretations involve rather restrictive assumptions. These assumptions are: (1) a tensile minimum principal stress (σ_3) is required for joint growth; (2) orientation of the tip of the growing joint is perpendicular to the local σ_3; and, (3) there is no interaction between the throughgoing joint and the growing joint. Comparisons are made with the systematic change in orientation observed in the younger zoned joints in Domains A, B and C (see chapter 2). No provision is made in this analysis for an internal fluid presure, P, within the crack. If such a fluid pressure were present, assumption (1) could more rigorously be stated as: joint growth requires that $(\sigma_3-P)<0$. The generalized solutions of appendix A do account for the effect of a uniform internal fluid pressure within the crack. Unfortunately, there is no evidence from which to accurately determine or estimate the magnitude or spatial variation of P during the jointing episodes in Arches, so this potentially important factor is ignored in the following analyses.

An elastic analysis indicates that the presence of a crack in an otherwise homogeneous, infinite isotropic body will locally perturb the stress field in the vicinity of the crack, leading to a local rotation and change in magnitude of the principal stresses. Although the criteria for the direction of growth of a later crack in such an inhomogeneous stress field is not certain, most theories

(summarized in Bergkvist and Guex, 1979) point toward the same end result: the younger crack will grow in a direction to align itself with the direction of the local principal stresses, i.e. the direction of crack growth will be such that it minimizes the resolved shear on the propagating crack tip. Using this criterion, we might expect a second crack growing in the perturbed stress field due to the through-going crack to follow the trace of the rotating principal stresses in the perturbed zone. Such a criterion ignores the interaction between cracks (Segall and Pollard, 1980) and the attraction effect which a free surface has on the growing crack (Pollard and Holzhausen, 1979). The complete problem, accounting for interactions between the two cracks, is not readily solvable by analytic means.

STRESS FIELD ABOUT A JOINT ZONE

Within a given domain, non-parallel generations of zoned joints display one of three characteristic interactions: (A) the younger joint zone curves into parallelism with the older joint zone; (B) the younger joint zone intersects the older zone at nearly a right angle; and, (C) younger zones cross older, healed zones with no deviation (figure 5-1). Some insight into the physical basis for this behavior may be gained from an elastic analysis of local stress perturbations about the throughgoing zone.

Chinnery (1963) used a dislocation analysis to examine the elastic stress changes that accompany strike-slip displacement for several geometries of faults. Rudnicki (1979) has described a procedure for determining the local rotation of principal stress axes caused by slip on an ellipsoidal inclusion in an infinite elastic body. The zoned nature of joints in the Moab Member allows a considerable simplification of the analysis. A joint zone may be considered mechanically equivalent to a single, infinitely long crack which has a

-150-
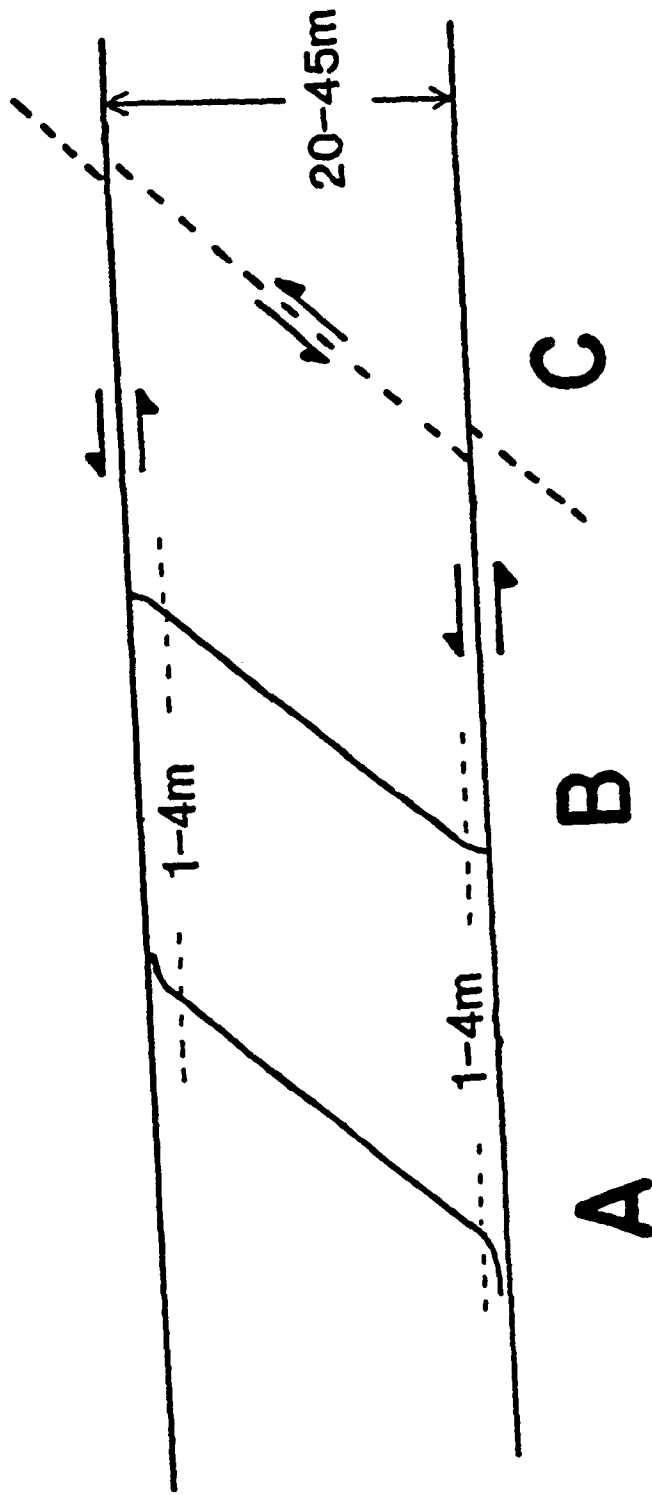
Figure 5-1.

Summary diagram of the three types of interactions noted between non-parallel sets of systematic, zoned joints in Arches National Park. In domains A and B, younger joints are bound by the older, through-going set. In domain A, the younger joints consistently curve into parallelism with the older set. In Domain B the younger joints consistently hook into set. In Domain B the younger joints at nearly a right angle. In Domain C, the younger, the older joints at nearly a right angle. In Domain C, the younger, through-going set cuts and offsets older zones (dashed lines) that have been the locus of cataclasis.

characteristic height of 2c (figure 5-2), and which is embedded in an infinite, isotropic, homogeneous elastic body. The crack is subjected to mixed Mode I (opening mode) and Mode III (antiplane shear) loading, as in figure 5-3.

The loading arises from far-field principal stresses σ_1^∞, σ_2^∞ and σ_3^∞. We use the sign convention that positive stresses are compressive and negative stresses are tensile. The field evidence requires that $\sigma_3^\infty - P < 0$ and that σ_3^∞ lie in the horizontal (Y-Z) plane. Because no estimates of the value of P are available, we assume that $P=0$, which requires that σ_3^∞ be tensile. We assume that σ_1^∞ is vertical (colinear with the X-axis) and compressive. σ_2^∞ lies in the Y-Z (horizontal) plane and may be either tensile or compressive. We will examine the changes in the stress field about the crack under various ratios of $\dfrac{\sigma_2^\infty}{\sigma_3^\infty}$.

Resolved stresses on the crack

When the far-field principal stresses are resolved into normal and shear components on the crack face, as in figure 5-4, we find the resolved far-field stresses to be:

$$\sigma_{yy}^\infty = \left[\frac{\sigma_2^\infty + \sigma_3^\infty}{2}\right] - \left[\frac{\sigma_2^\infty - \sigma_3^\infty}{2}\right]\cos[2(90-\varphi)] \qquad (5\text{-}1)$$

$$\sigma_{zz}^\infty = \left[\frac{\sigma_2^\infty + \sigma_3^\infty}{2}\right] + \left[\frac{\sigma_2^\infty - \sigma_3^\infty}{2}\right]\cos[2(90-\varphi)] \qquad (5\text{-}2)$$

$$\sigma_{yz}^\infty = \left[\frac{\sigma_2^\infty - \sigma_3^\infty}{2}\right]\sin[2(90-\varphi)] \qquad (5\text{-}3)$$

$$\sigma_{xx}^\infty = \sigma_1^\infty \qquad (5\text{-}4)$$

where φ is the angle between σ_2^∞ and the Z-axis.
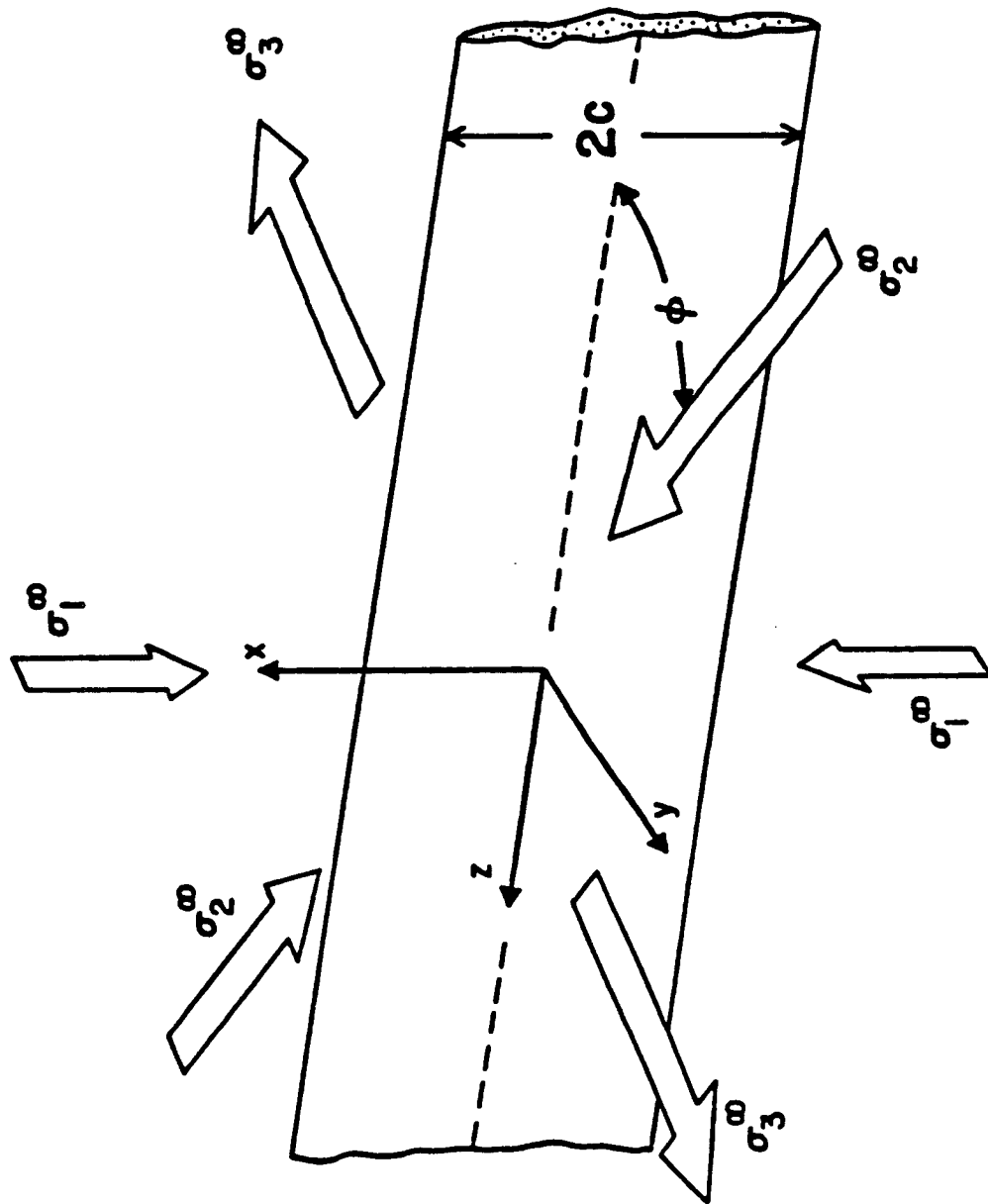
Figure 5-2.
Idealization of a joint zone as a single, infinitely long crack of height $2c$. The crack is subjected to far-field stresses in the horizontal plane (σ_3^{∞} and σ_2^{∞}). σ_1^{∞} is vertical and colinear with the X-axis.
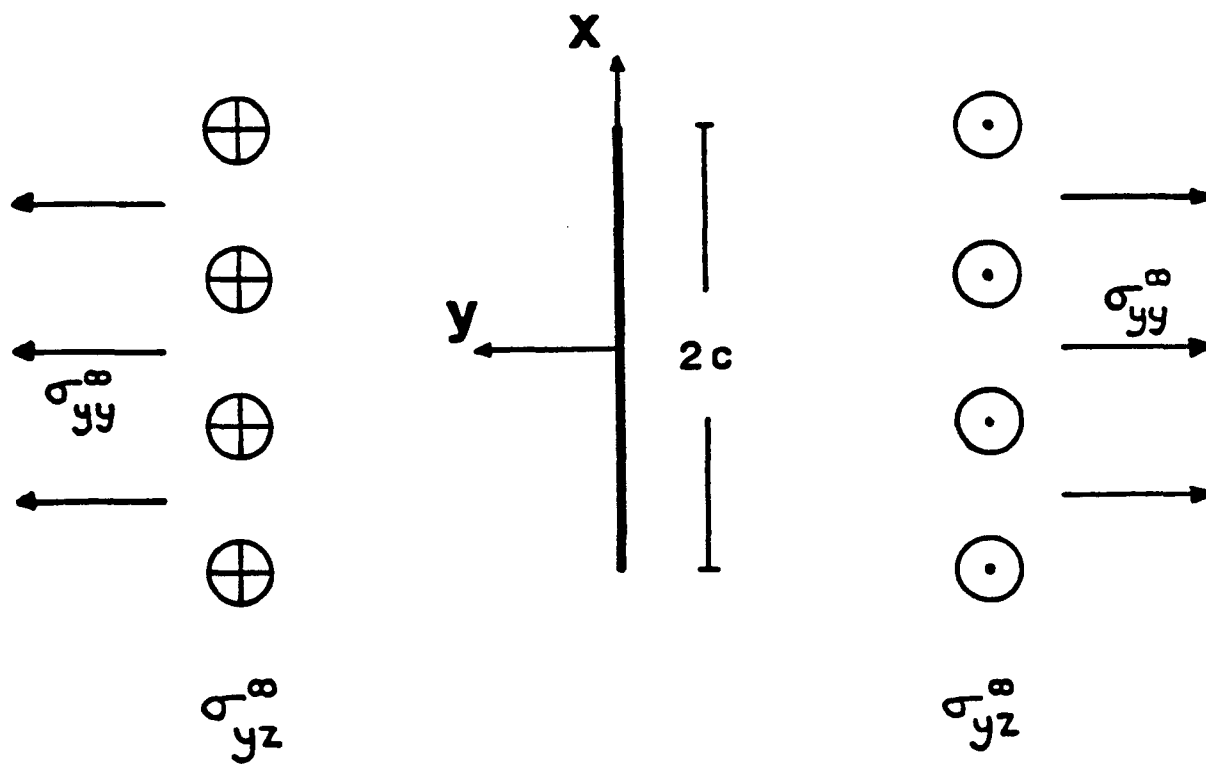
Figure 5-3.
A crack under combined antiplane (Mode III) and opening (Mode I) loading.
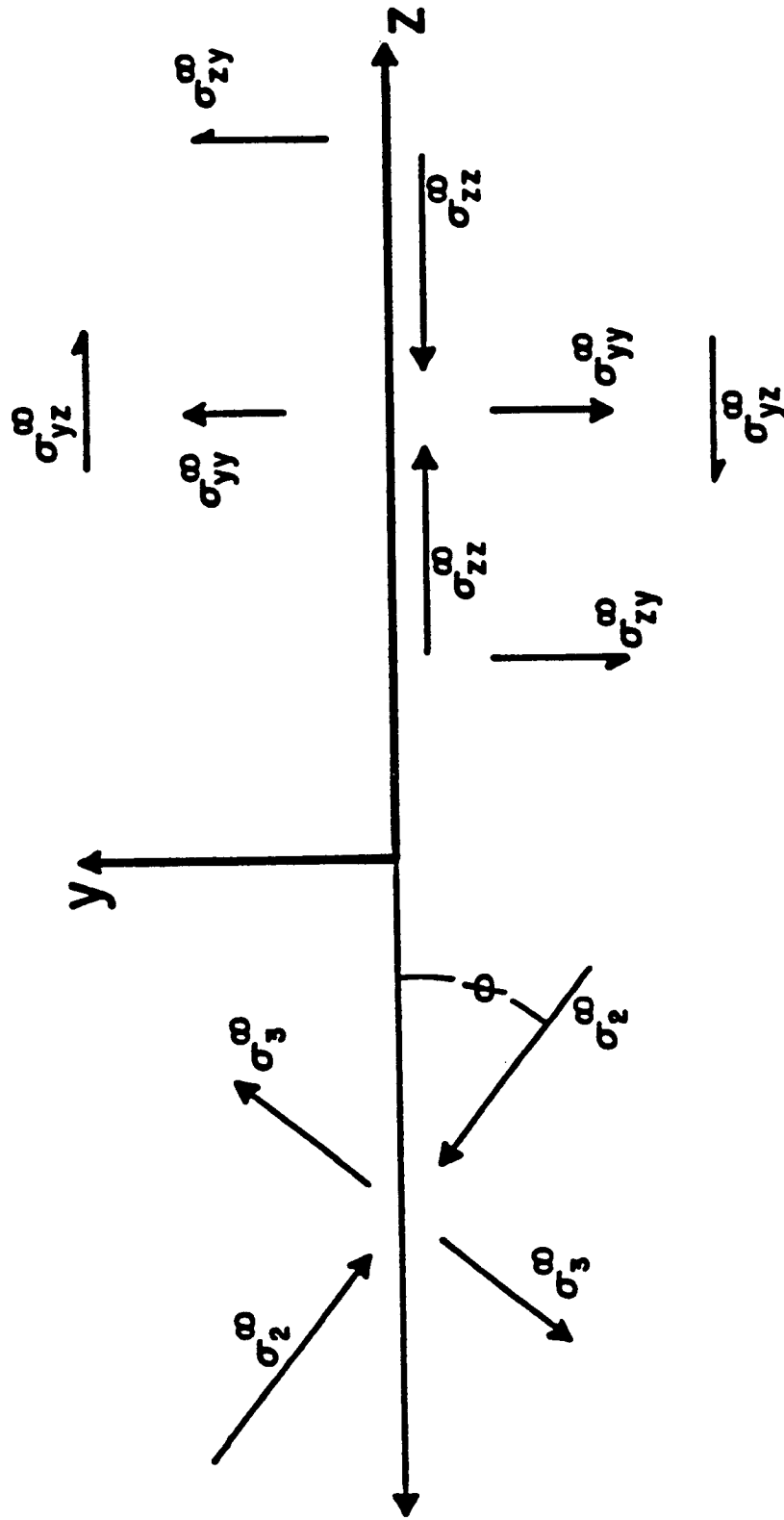
Figure 5-4.
Resolution of far-field principal stresses, σ_2^∞ and σ_3^∞ into normal and shear stresses on the crack gives σ_{yy}^∞, σ_{zz}^∞ and σ_{yz}^∞. We require that $\sigma_{zz}^\infty = \sigma_1^\infty$.

Solving for the stress field

This general loading is shown in figure 5-5A. Because of the presence of the crack (zoned joint), local variations in the stress field may occur. These variations will result in changes in the magnitude and orientation of the principal stresses. Solution of the problem must be independent of z, so the problem reduces to a superposition of two-dimensional problems in the X-Y plane and a uniform stress on the Z-axis (figure 5-5 B or C, D and E). Details of the solution for the perturbed stresses σ_{xx}, σ_{yy} and σ_{yz} are given in appendix A. The stress along the Z-axis, σ_{zz}, is the sum of a far-field uniform stress, $\bar{\sigma}_{zz}^{\infty}$, and an induced stress required to satisfy the plane strain geometry of our two-dimensional solutions, σ_{zz}^{I} (figure 5-5 B or C, and E).

$$\sigma_{zz} = \bar{\sigma}_{zz}^{\infty} + \sigma_{zz}^{I} \tag{5-5}$$

where $\sigma_{zz}^{I} = \nu(\sigma_{xx}+\sigma_{yy})$

and ν is Poisson's ratio. A typical value of ν for sandstones is about 0.1 (Birch, 1966, p.167). We will assume throughout that $\nu = 0.1$.

Far from the crack we require that

$$\sigma_{zz}^{\infty} = \bar{\sigma}_{zz}^{\infty} + \sigma_{zz}^{I}$$
$$= \bar{\sigma}_{zz}^{\infty} + \nu(\sigma_{xx}^{\infty}+\sigma_{yy}^{\infty})$$

so $$\bar{\sigma}_{zz}^{\infty} = \sigma_{zz}^{\infty} - \nu(\sigma_{xx}^{\infty}+\sigma_{yy}^{\infty}) \ . \tag{5-6}$$

If we limit our investigation to the plane x=0, then the only rotation of principal stresses will be about the X-axis. Once the stresses σ_{yy}, σ_{zz} and σ_{yz} are found at a point, the orientation and magnitude of the principal stresses σ_2 and σ_3 at that point can be found from a simple Mohr circle construction (figure 5-6). Ψ is defined as the angle between σ_2 and the Z-axis.

Figure 5-5

(A) Resolution of principal stresses σ_1^-, σ_2^- and σ_3^- into normal and shear components leads to this generalized loading on a crack which is infinitely long in the Z-direction and has a characteristic height ($=2c$) in the X-direction. One of the principal stresses (σ_{ms}^-) is colinear with the X-axis. If σ_{yy}^- is compressive, then the crack is closed and a σ_{ys} shearing stress of magnitude $K\sigma_{ys}\infty$ may exist on the crack surface. Solution of the perturbed stress field about the crack can be obtained by linear superposition of solutions to plane crack problems (B) and (D) and uniform stress states (C) and (E). Any arbitrary loading can be expressed as a combination of case (B) OR (C) plus (D) and (E).

(B) Opening mode (Mode I) crack under biaxial loading. This solution is only applicable if σ_{yy}^- is tensile, which requires the crack to be open. The normal and shear stresses on the crack surface, σ_{yy} ($y = 0$, $|x| < c$) and σ_{xy} ($y = 0$, $|x| < c$) are zero.

(C) If σ_{yy}^- is compressive, then the crack is closed and σ_{yy} is continuous across the crack plane. There is no Mode I perturbation of the stress field, and uniform normal (σ_{xx}^-, σ_{zz}^-) and shear stresses ($K\sigma_{xy}^-$) exist throughout the body. The plane strain geometry leads to an induced σ_{zz} stress of magnitude $\sigma_{zz}^I = \nu\left[\sigma_{xx}^- + \sigma_{yy}^-\right]$. For any given loading, either case (B) or (C) will be applicable, with each mutually exclusive of the other.

(D) Another solution component is that due to pure Mode III (antiplane shear) loading. This solution satisfies the case of a far-field shear stress of magnitude $(1-K)\sigma_{yz}^-$ applied to a crack whose surfaces are stress-free. If $\sigma_{yy}\infty$ is tensile, then $K=0$.

(E) A uniform stress in the Z direction, $\bar\sigma_{zz}^-$, may be superimposed on the body without altering any of the other solutions.
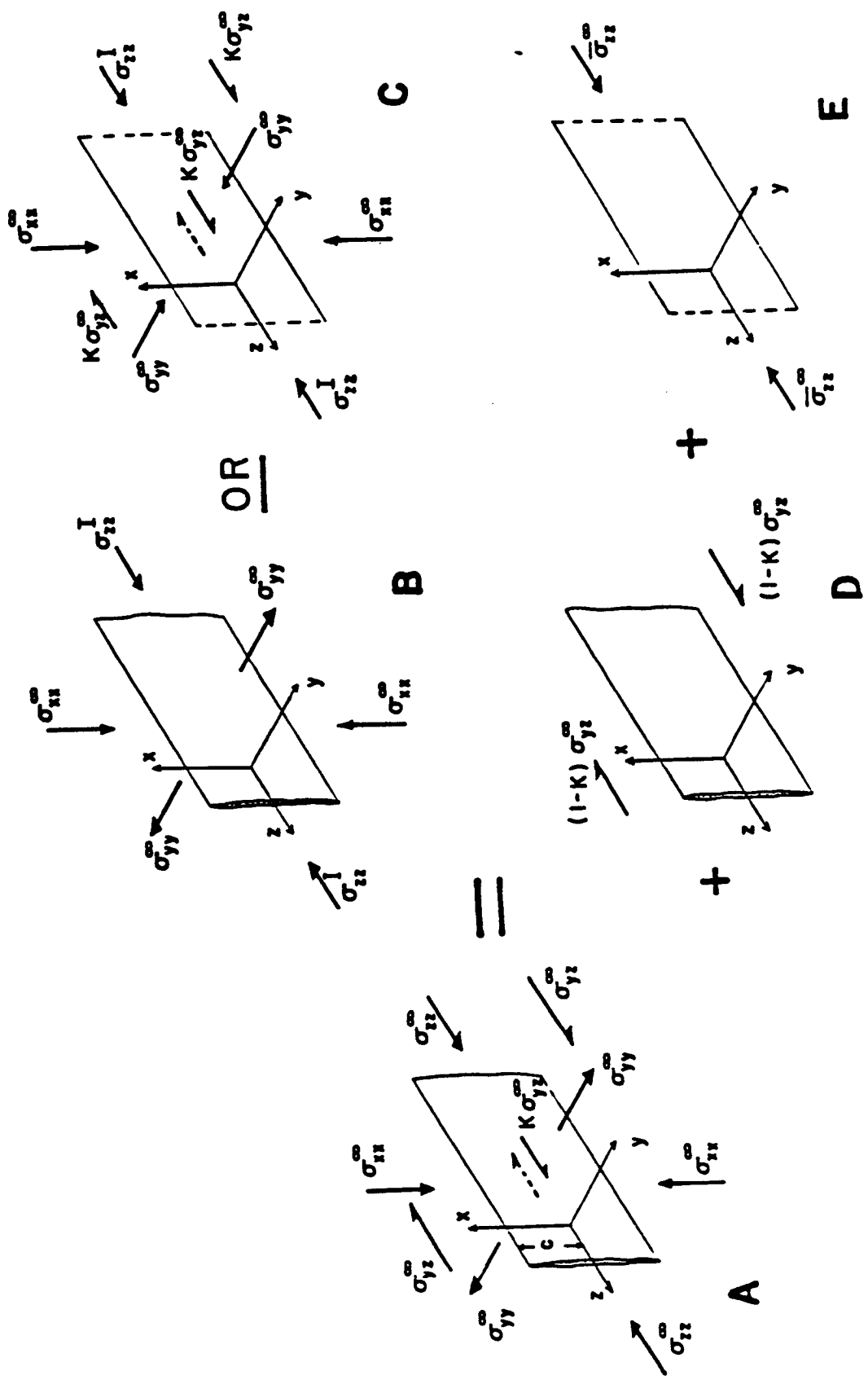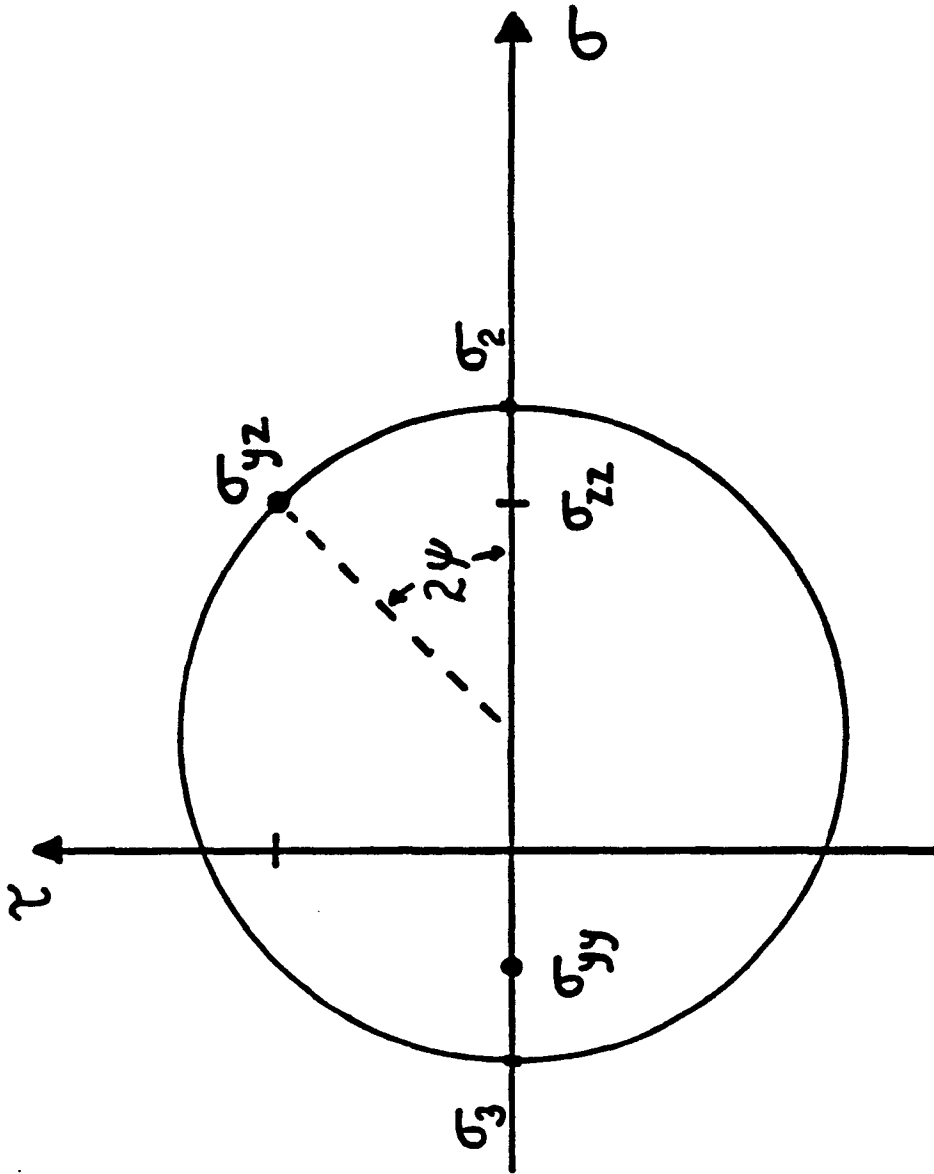
Figure 5-6.

Mohr circle construction for finding the magnitude (σ_2, σ_3) and orientation (ψ) of the principal stresses after we have solved for σ_{yy}, σ_{zz} and σ_{yz}.

$$\Psi = \frac{1}{2}\tan^{-1}\left[\frac{2\sigma_{yz}}{(\sigma_{zz} - \sigma_{yy})}\right] \quad (5\text{-}7)$$

$$\sigma_2 = \left[\frac{\sigma_{zz} + \sigma_{yy}}{2}\right] + \frac{1}{\cos 2\Psi}\left[\frac{\sigma_{zz} - \sigma_{yy}}{2}\right] \quad (5\text{-}8)$$

$$\sigma_3 = \left[\frac{\sigma_{zz} + \sigma_{yy}}{2}\right]\left[1 - \frac{1}{\cos 2\Psi}\right] \quad (5\text{-}9)$$

We limit our investigation to the plane $x = 0$ because of the great simplification in the analysis which results. Off of the $x = 0$ plane, σ_{xy} and σ_{xz} shear stresses will exist which will tend to rotate the principal stresses about the Z- and Y-axes, respectively. These shearing stresses will increase near the crack tip ($y = 0$, $x = \pm c$). Appendix B is an investigation of the range of validity of our simple solution when compared to the full solution.

BOUNDARY CONDITIONS

There are two general situations we wish to investigate: (1) when the through-going zone is an open crack, and (2) when the crack is closed and there may be frictional sliding on the crack.

1. Open crack $(\sigma_{yy}^\infty < 0)$

If the resolved far-field stress perpendicular to the crack face (σ_{yy}^∞) is tensile, then the crack is open, and the crack face is traction-free. The boundary conditions which must be satisfied are

$$at \quad y = 0; \quad |x| < c \qquad \sigma_{yy} = \sigma_{yz} = 0 \quad (5\text{-}10)$$

$$at \quad \sqrt{x^2 + y^2} \to \infty \qquad \left.\begin{aligned} \sigma_{yy} &= \sigma_{yy}^\infty \\ \sigma_{zz} &= \sigma_{zz}^\infty \\ \sigma_{yz} &= \sigma_{yz}^\infty \end{aligned}\right\} \quad (5\text{-}11)$$

-160-

This situation corresponds to a superposition of the problems illustrated in figure 5-5, parts B, D and E. The solution is given by superposition of the plane crack Mode I and Mode III solutions (equations A-9, A-10, and A-19 in appendix A). On the plane $x = 0$, the non-zero stresses are

$$\sigma_{yy}(x=0) = \sigma_{yy}^{\infty}\left[\frac{|y^3|}{(y^2 + c^2)^{3/2}}\right] \tag{5-12}$$

$$\sigma_{zz}(x=0) = \sigma_{yy}^{\infty}\left[\frac{|y|(y^2 + 2c^2)}{(y^2 + c^2)^{3/2}} - 1\right] + \sigma_{zz}^{\infty} \tag{5-13}$$

$$\sigma_{yz}(x=0) = \sigma_{yz}^{\infty}\left[\frac{y}{\sqrt{y^2 + c^2}}\right] \tag{5-14}$$

$$\sigma_{xx}(x=0) = \bar{\sigma}_{xx}^{\infty} + \nu(\sigma_{zz} + \sigma_{yy}). \tag{5-15}$$

Substituting in equations (5-8), (5-12) and (5-13), equation (5-15) becomes:

$$\sigma_{xx}(x=0) = \bar{\sigma}_{xx}^{\infty} + \nu\left[\sigma_{yy}^{\infty}\left[\frac{2|y^3 + yc^2|}{(y^2 + c^2)^{3/2}} - 2\right]\right]. \tag{5-16}$$

From equations (5-12) - (5-16) and (5-7) - (5-9) the orientation and magnitude of the principal stress σ_2 and σ_3 can be determined on the plane $x=0$. σ_1 will be colinear with the X-axis and have the magnitude of σ_{xx} as given by equation (5-13). It is worth emphasizing that on the plane $x = 0$, σ_2, σ_3 and Ψ are independent of σ_1^{∞}.

2. Closed crack ($\sigma_{yy}^{\infty} > 0$)

If the resolved far-field stress perpendicular to the crack face, σ_{yy}^{∞}, is compressive, then the crack is closed and there can be no Mode I perturbation of the stress field. It is still possible for the crack to be shear stress free. Such a situation might arise if the crack were perfectly lubricated. In general,

the shear stress on the crack face will have some intermediate value between zero and σ_{yz}^{∞}. This situation corresponds to a superposition of the problems shown in figure 5-5, parts C, D and E.

The boundary conditions for this problem are:

$$\left.\begin{aligned} \sigma_{yy} &= \sigma_{yy}^{\infty} \\ \sigma_{zz} &= \sigma_{zz}^{\infty} \end{aligned}\right\}$$
(5-17)

$$\text{for } y=0, \ |x|<c \qquad \sigma_{yz} = K\sigma_{yz}^{\infty} \quad (0 \le K \le 1)$$
(5-18)

$$\text{for } \sqrt{x^2 + y^2} \to \infty; \qquad \sigma_{yz} = \sigma_{yz}^{\infty}$$
(5-19)

K is the shear stress ratio given by

$$K = \frac{\sigma_{yz}(y=0)}{\sigma_{yz}^{\infty}}.$$

$K = 0$ corresponds to a perfectly lubricated crack while $K = 1$ corresponds to a locked crack. If a Byerlee-type sliding friction relation is used, then on the crack face ($y=0$, $|x|<c$):

$$\sigma_{yz} = C^{*}\sigma_{yy}^{\infty} = K\sigma_{yz}^{\infty}$$

$$\text{and} \quad K = C^{*}\frac{\sigma_{yy}^{\infty}}{\sigma_{yz}^{\infty}}$$
(5-20)

where C^{*} is the coefficient of sliding friction.

Solution of the boundary value problem is obtained by the superposition of two solutions corresponding to figure 5-5, parts C and D.

$$\sigma_{yz} = \sigma_{yz}^{C} + \sigma_{yz}^{D}$$
(5-21)

where

$$\sigma_{yz}^{C} = K\sigma_{yz}^{\infty} \quad (0 \le K \le 1)$$
(5-22)

-162-

is the uniform shear stress in an uncracked infinite body (figure 5-5 C), and

$$\sigma_{yz}^{D} = (1-K)\sigma_{yz}^{\infty} \frac{y}{\sqrt{y^2 + c^2}} \qquad (5\text{-}23)$$

is the shear stress at the point (x=0,y,z) due to the existence of a frictionless, infinitely long crack of height 2c subjected to a far-field anti-plane shear (mode III loading) of magnitude $(1-K)\sigma_{yz}^{\infty}$. The full Mode III solution is given in appendix A, equation A-17. This problem is illustrated in figure 5-5 D.

Equation (5-21) becomes

$$\sigma_{yz}(x=0) = \sigma_{yz}^{\infty} \left[K\left(1 - \frac{y}{\sqrt{y^2 + c^2}}\right) + \frac{y}{\sqrt{y^2 + c^2}} \right]$$

$$= \sigma_{yz}^{\infty} \left[K + \left(1-K\right)\frac{y}{\sqrt{y^2 + c^2}} \right]. \qquad (5\text{-}24)$$

It may easily be verified that equation (5-23) satisfies the boundary conditions of (5-18) and (5-19). To complete the solution, we note that:

$$\left. \begin{array}{l} \sigma_{xx} = \sigma_{xx}^{\infty} = \sigma_1^{\infty} \\[2mm] \sigma_{yy} = \sigma_{yy}^{\infty} \\[2mm] \sigma_{zz} = \overline{\sigma}_{zz}^{\infty} + \nu\left(\sigma_{xx}^{\infty} + \sigma_{yy}^{\infty}\right) = \sigma_{zz}^{\infty} \\[2mm] \sigma_{xy} = 0. \end{array} \right\} \qquad (5\text{-}25)$$

We may now solve for the principal stresses σ_2 and σ_3 on the plane x=0 and determine their orientation by using the results of (5-24) and (5-25) in equations (5-7) - (5-9). On x=0, σ_1 will be vertical, with $\sigma_1 = \sigma_1^{\infty}$.

As with the open crack, it is worth noting that the orientation and magnitude of σ_2 and σ_3 is independent of σ_1^{∞} on the plane x=0.

EXAMPLES

Figures 5-7, 5-8, 5-9, 5-11 and 5-13 are maps of the elastic stress field about a joint under a variety of combinations of far-field stresses and degree of healing of the joint. All examples assume no internal fluid pressure in the joint ($P = 0$). All maps are of the plane x=0, the near-horizontal plane perpendicular to and bisecting the joint. In all the examples, the far-field principal stresses, σ_2^∞ and σ_3^∞, lie in the Y-Z plane, and σ_2^∞ makes an angle of 30° with the joint face (the Z-axis). The positive X-axis (approximately vertical) is normal to the page. The trace of the joint falls on the Z-axis. On the plane x=0, the solution is independent of the z coordinate. For generality, the Y-axis has been non-dimensionalized. For comparative purposes, the joint half-height $\left(= c\right)$ in the Moab Member is 13.5 meters. Stresses are in arbitrary units.

If we accept the hypothesis that the local crack propagation direction is perpendicular to the local minimum principal stress, then it is tempting to use the perturbed elastic stress field to make a predictive plot of the trace of a joint which grows in the perturbed stress field. We will attempt this, after first noting the following important qualifications.

When a second crack is introduced into the body, the problem becomes enormously more complicated. As discussed earlier, the role of crack interaction between two three-dimensional cracks, one of which is non-planar and whose detailed geometry is not well known, is a poorly understood problem. On the stress maps, successive points have been purposely offset to remind us that these solutions are strictly valid only for the case of a *single*, throughgoing joint. If we could somehow introduce a second crack in the body, yet require that this later crack not alter the stress field which arises solely from the throughgoing crack, then an examination of the stress field could

provide valuable information about the geometry of this later crack. The degree to which this assumption violates reality is unknown, yet adoption of the assumption may allow the use of this simple analysis as a first order approximation to the much more complex multiple-crack problem.

I. CLOSED CRACK

For $\sigma_3^{\infty} = -1$ (unit tension), σ_1^{∞} vertical and an angle between σ_2^{∞} and the Z-axis of 30°, the crack will be closed if $\sigma_{yy}^{\infty} > 0$. For the geometry specified, the condition that $\sigma_{yy}^{\infty} > 0$ requires that $\sigma_2^{\infty} > 3$. In examples I.A - I.C, σ_2^{∞} has been assigned an arbitrary value of 5. Variations in the shear stress ratio on the crack, (K), lead to variations in the stress field about the crack. Solution for the stresses follows from equations (5-5) and (5-17) - (5-24).

I.A LOCKED JOINT

A locked joint or crack is one that is totally healed due to some prior chemical or mechanical processes. Such a crack has the same mechanical properties as unjointed rock. A locked crack is mechanically invisible and results in the trivial case illustrated in figure 5-7. The boundary conditions for this case are given by equations (5-17) - (5-19), with $K = 1$. The solution follows from equation (5-24).

As shown in figure 5-7, there is no perturbation of either the orientation or magnitude of the principal stresses. If a second joint set were forming normal to σ_3, we would expect this second joint to propagate without deviation across the locked joint. This is in accord with the observations in Domain C, where open joints cross older joints (now totally healed cataclastic bands) with no deviation.
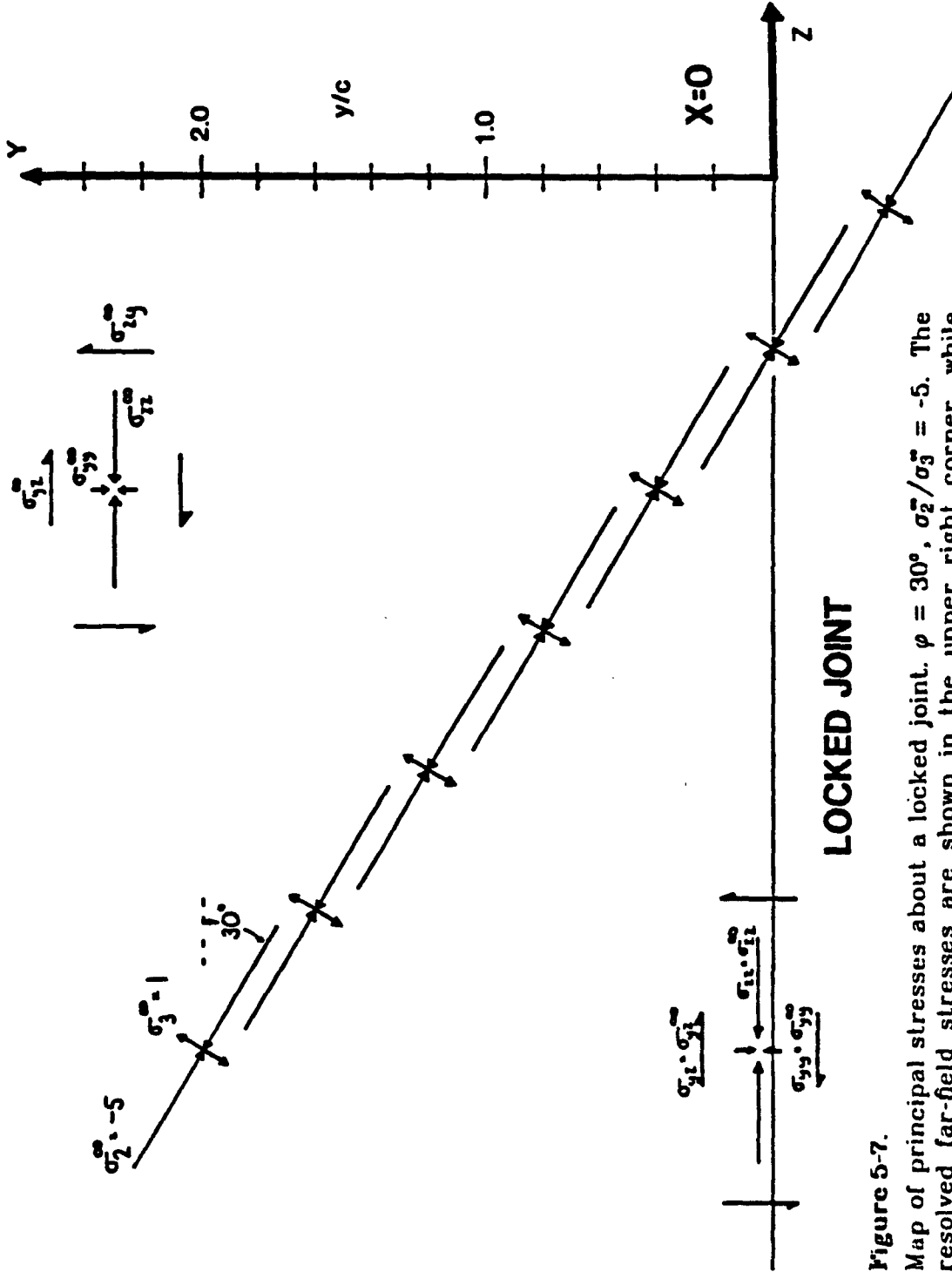
Figure 5-7.

Map of principal stresses about a locked joint. $\varphi = 30°$, $\sigma_2^\infty/\sigma_3^\infty = -5$. The resolved far-field stresses are shown in the upper right corner, while resolved stresses on the healed joint are shown in the lower left. Note that there is no change in either the orientation or magnitude of the principal stresses.

I.B FRICTIONAL SLIDING

If the resolved normal stress on the joint, σ_{W}^{-}, is compressive, then the joint is closed. If the joint is not completely locked, it is possible that some frictional sliding relationship will control the shear stresses on the joint face. Byerlee (1977) found that rock type has little or no effect on friction, and that for normal stresses up to 2 Kbar the shear stress required to cause sliding is given approximately by:

$$\tau = 0.85\, \sigma_n$$

Byerlee noted that at low stresses there is a wide variation in rock friction, and attributed this to variation in surface roughness.

Zoned joints in the Moab Member are near-planar features that display negligible surface relief. For this reason a slightly lower coefficient of friction has been assumed. Figure 5-8 is the stress map resulting from use of the frictional relation

$$\sigma_{yx} = 0.6\, \sigma_{W}^{-} \qquad (at\ y = 0;\ |x| < c)$$

as the boundary condition on the joint face. The full boundary conditions are given by equations (5-17) - (5-19), with $K = 0.12$ for the far-field stress state illustrated. The solution is obtained from equation (5-24) with the magnitude and orientation of the perturbed principal stresses determined from equations (5-7) - (5-9).

The perturbed principal stresses undergo a counter-clockwise rotation in orientation. Additionally, at $\frac{y}{c} \approx 0.5$, the minimum principal stress, σ_3, undergoes a sign change, switching from a tensile stress for $\frac{y}{c} > 0.5$ to a compressive stress for $\frac{y}{c} < 0.5$. From $\frac{y}{c} = \infty$ to $\frac{y}{c} = 0.5$, the principal stresses
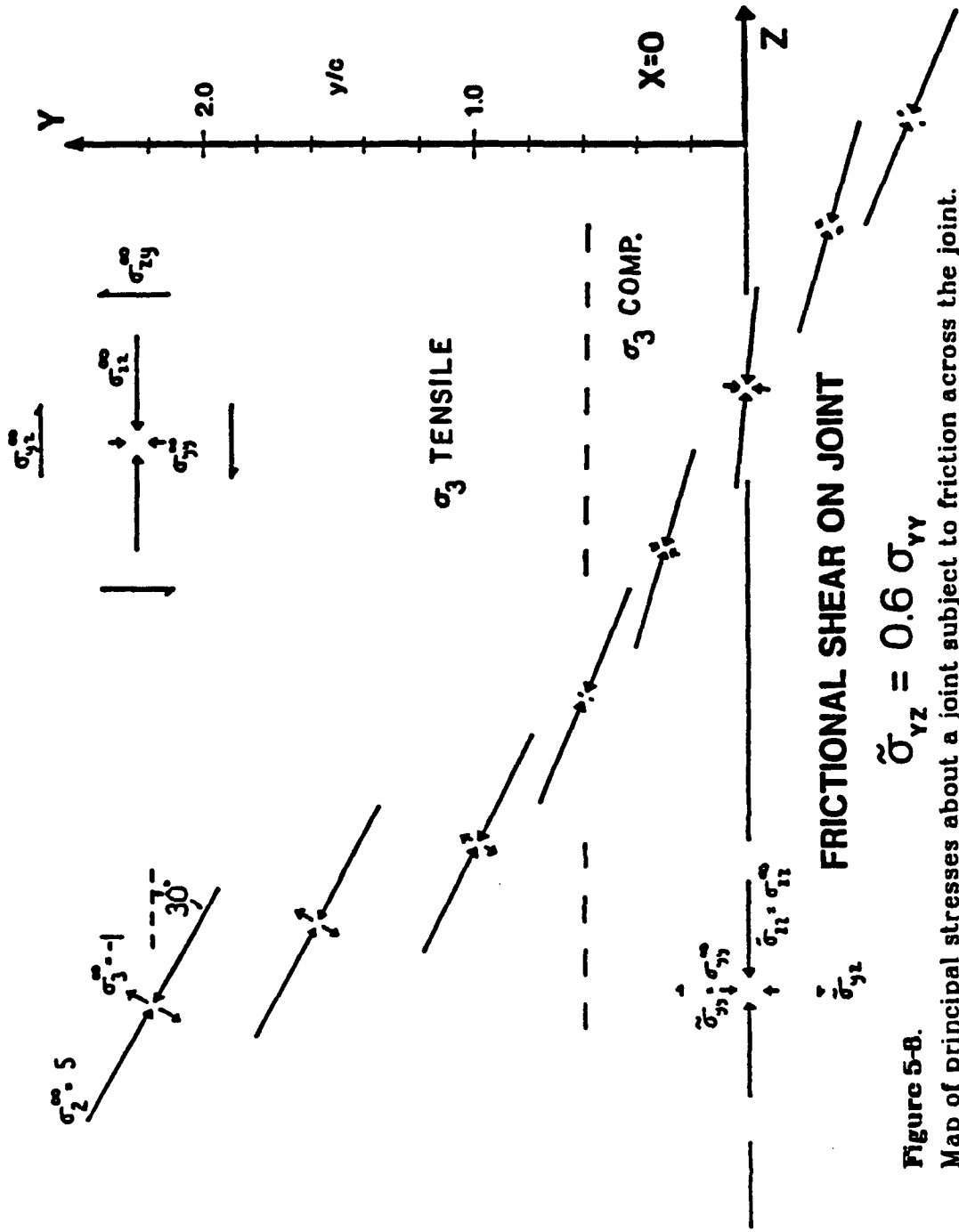
Figure 5-8.

Map of principal stresses about a joint subject to friction across the joint. Far-field stresses are $\sigma_2^\infty/\sigma_3^\infty = -5$, $\varphi = 30°$. Resolved far-field stresses are shown in the upper right. Boundary conditions on the crack are shown in the lower left. A Byerlee-type friction law is used to specify shear stress on the joint (σ_{yz}). Note that σ_3 changes sign at $\frac{y}{c} \approx 0.6$. See text for details.

-168-

undergo a counter-clockwise rotation of 8 degrees.

I.C FRICTIONLESS JOINT

If we use the same far-field stress as in the previous two examples, but let the joint be totally lubricated, we obtain the stress map shown in figure 5-9. The boundary conditions for this problem are given by equations (5-17) - (5-19), with $K = 0$. The solution follows that of the previous two examples.

From figure 5-9, we see that a counterclockwise rotation of the principal stresses occurs as we approach the throughgoing joint. As in the frictional sliding case, the minimum principal stress, σ_3, undergoes a sign change from tensile to compressive at $\frac{y}{c} \approx 0.6$.

PROPAGATION OF A YOUNGER JOINT

A question of considerable practical interest is whether we can predict the trace of a joint which nucleates far from the throughgoing joint of figures 5-8 or 5-9 and propagates toward the preexisting, throughgoing joint. How might the local perturbation of the stress field, due to the presence of the throughgoing joint, affect the orientation and propagation of the growing joint?

A basic tenet of linear elastic fracture mechanics is that the magnitude of stresses near a crack tip are proportional to the stress intensity factors (K_i, where $i =$ I, II, III denotes, respectively, the opening, sliding and tearing modes of crack displacement) (Broek, 1978, p. 8-17). For a three dimensional (elliptical) crack, K_i is a function of position on the crack front, the crack geometry and the loading conditions (Broek, 1978, p. 80-86). Growth of an individual crack is expected to occur when K_i somewhere on the crack front reaches a critical value which is a material property: the *fracture toughness*
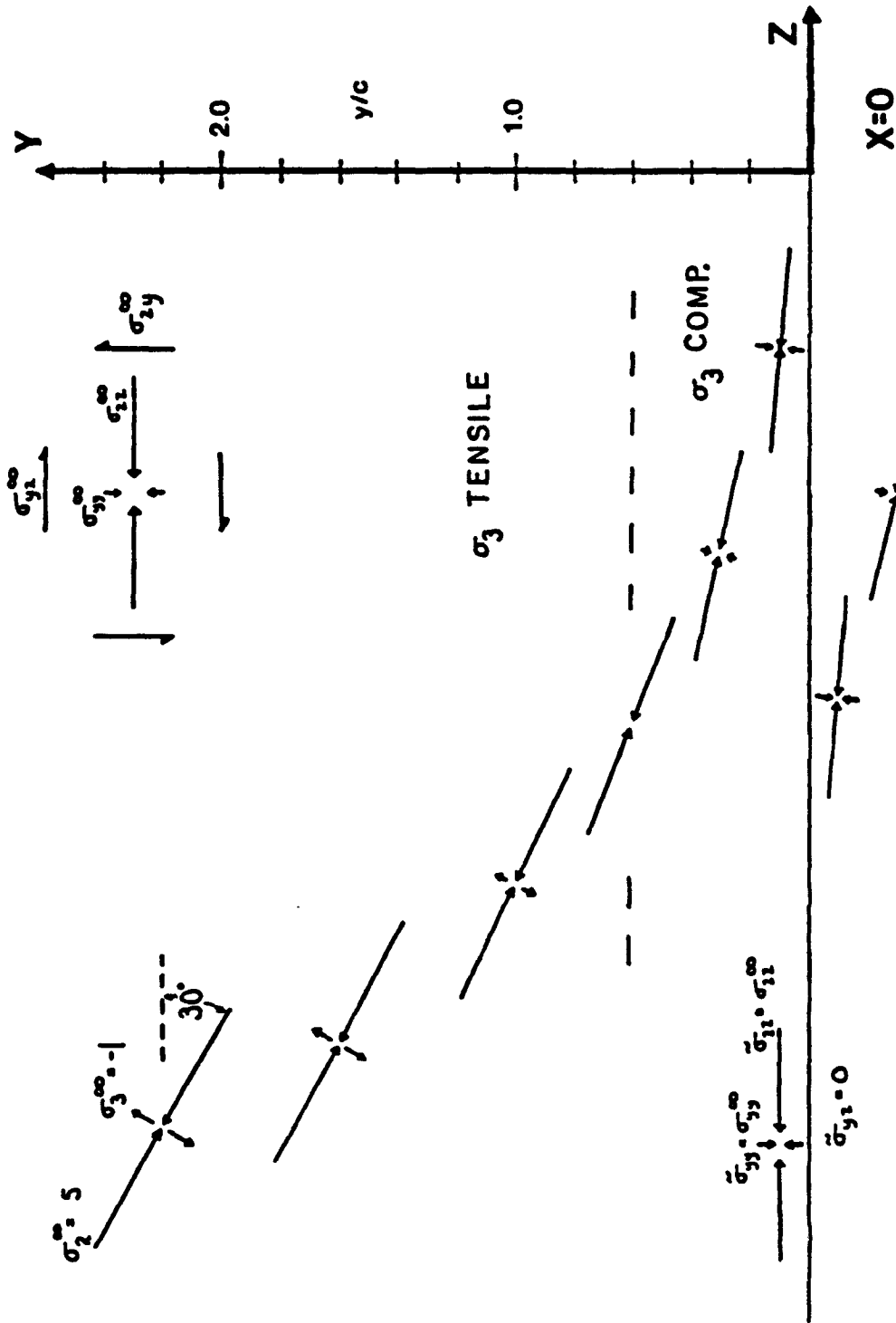
FRICTIONLESS JOINT

Figure 5-9.

Map of principal stresses about a frictionless joint under far-field stresses of $\sigma_2^\infty / \sigma_3^\infty = -5$; $\varphi = 30°$. Resolved far-field stresses are shown in the upper right. The joint ($y/c = 0$) is shear-stress free (for $y=0$; $|x|<c$, $\sigma_{yz} = 0$). Note change in sign of σ_3 at $\frac{y}{c} \approx 0.6$.

(K_1^C). As discussed in chapter two, there is abundant field evidence in Arches to support the contention that the zoned joints in the Moab Member originally propagated as extensional, or mode I (opening mode) fractures. This in turn indicates that critical parameters needed to predict crack behavior include an evaluation of K_I along the crack front, and a measurement of the fracture toughness, Kf, of the Moab Member.

Although extensive compilations of basic solutions of stress intensity factors exist for various simple crack geometries and loading conditions (e.g. Paris and Sih, 1964, appendix II), a general solution which considers multiple (interacting) non-planar three dimensional cracks of arbitrary shape subjected to generalized loading conditions is probably not analytically feasible. Numerical solutions for particular configurations may be tractable, but their applicability would be clouded by the uncertainty of the geometry of the crack front. Even the excellent exposures in Arches give little information regarding the exact geometry of crack fronts.

The failure criteria of linear elastic fracture mechanics (fracture propagation when $K_I = Kf^C$) is simple, elegant and apparently physically sound. However, direct application of this simple propagation criterion to the problem of interest invokes enormous complications.

Intuitively, we might expect the tip of the growing crack to cease propagating when it passes from a region of tensile stress normal to the crack front into a region of compressive stress normal to the crack front. In the Moab Member, assuming the loading conditions of either figures 5-8 or 5-9, this sign change in σ_3 would occur at a distance of about 7 meters from the throughgoing joint zone. The shortcoming of intuition was convincingly demonstrated by Lachenbruch (1961; 1962), who showed that a planar crack

growing perpendicular to a varying stress field can propagate a considerable distance into a zone of compressive normal stress. This is possible due to the "lever effect" whereby normal tensile stresses near the center of the crack contribute significantly to the overall stress intensity (K_I) at the crack tip, allowing high K_I values even though the crack tip proper is subject to a normal compressive stress. Thus, although the propagating crack of figures 5-8 and 5-9 will propagate some distance into the zone of compressive σ_3, it is not currently possible to predict exactly how far it should grow into this compressive zone because of our inability to specify a K_I value for the crack front. Nevertheless, growth of the second crack (J_2) will be retarded within the compressive zone.

For $\sigma_3^{\infty} = -1$ and $\varphi = 30^\circ$, as σ_2^{∞} increases, the magnitude of the retarding compressive stress within the compressive zone will increase, and the size of the compressive zone itself will increase. Thus, for $\sigma_2^{\infty} \gg |\sigma_3^{\infty}|$, we might expect the propagating joint (J_2 of figure 5-10) to grow only a small distance into the compressive zone. This is clearly in disagreement with the Arches observations that in Domain A the later generation joints parallel the throughgoing set some tens of centimeters distant from the throughgoing set (J_1).

For the boundary conditions illustrated in figures 5-8 and 5-9, the situation is less clearcut. Although the younger joint, J_2, will grow some distance into the compressive zone, it seems doubtful that the crack will be able to extend itself by a length of more than 1.5 c, which would be required to duplicate the sigmoidal geometry observed in Domain A.
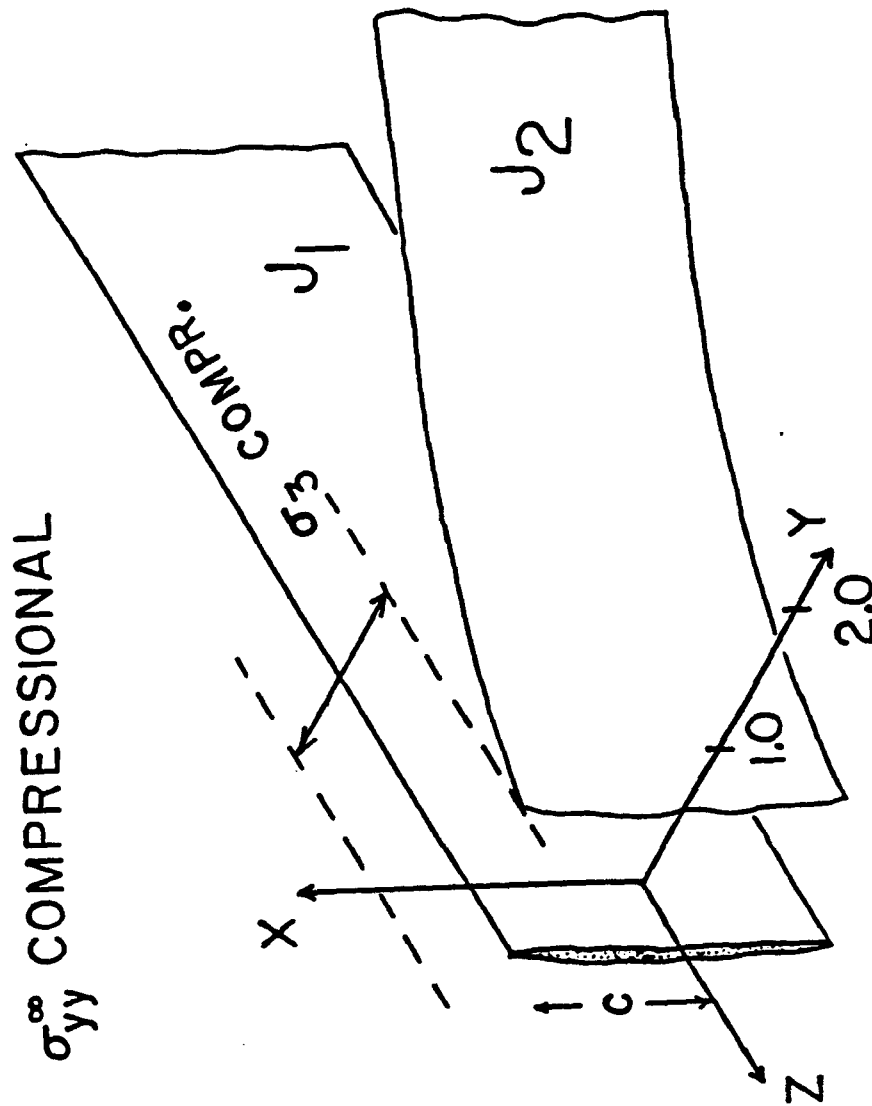
Figure 5-10.

Inferred resultant geometry of a younger joint zone (J_2) growing toward a through-going zone (J_1) for the case of σ_{yy}^∞ compressive. A zone will exist around J_1 in which σ_3 becomes compressive. Growth of J_2 will be retarded as it encounters this zone due to the absence of tensile stresses at the crack tip. For a Byerlee-type friction law on J_1, σ_3 switches from tensile to compressive at $\frac{\mu}{c} \approx 0.6$. The maximum change in orientation of J_2 at the compressive zone boundary will be about 8° from its far-field orientation.

-173-

II. OPEN CRACK

If the resolved normal stress on the joint, σ_{yy}^∞, is tensile, then the joint is open and is a free surface. For $\sigma_3^\infty = -1$, σ_1^∞ vertical and an angle of 30° between σ_2^∞ and the Z-axis, σ_{yy}^∞ will be tensile for the range $-1 < \sigma_2^\infty < 3$. The boundary conditions for this situation are specified in equations (5-10) and (5-11). An additional distinction can be made based on the magnitude of σ_{zz}^∞. For the specified geometry, σ_{zz}^∞ will be compressive if $\sigma_2^\infty > 1/3$. Over the range $-1 < \sigma_2^\infty < 1/3$, σ_{zz}^∞ will be tensile. Solution for the local stresses is by equations (5-12) - (5-15). The principal stresses and their orientations are found from equations (5-7) - (5-9). On the joint surface, we require that the principal stresses be perpendicular and parallel to the surface. This requires a rotation of the principal stresses, which can be accomplished by either a clockwise or counter-clockwise rotation. The direction of rotation of the principal stresses is controlled by the magnitude of σ_{zz}^∞.

II.A σ_{zz}^∞ is compressive

If the resolved stress parallel to the joint, σ_{zz}^∞, is compressive, then the rotation will be counter-clockwise, as shown in figure 5-11. A pertinent feature of this solution is that the minimum principal stress, σ_3, remains tensile for all $y > 0$.

Ignoring crack interaction, we might expect that a joint originating a distance from the throughgoing zone and propagating toward it would systematically curve in response to the rotation of the minimum principal stress, as in figure 5-12. In addition, for all $y > 0$ there is a tensile σ_3 available to provide a driving force for the crack. In this manner, it might be possible for a younger joint to grow arbitrarily close to a throughgoing zone, with the

JOINT IS FREE SURFACE
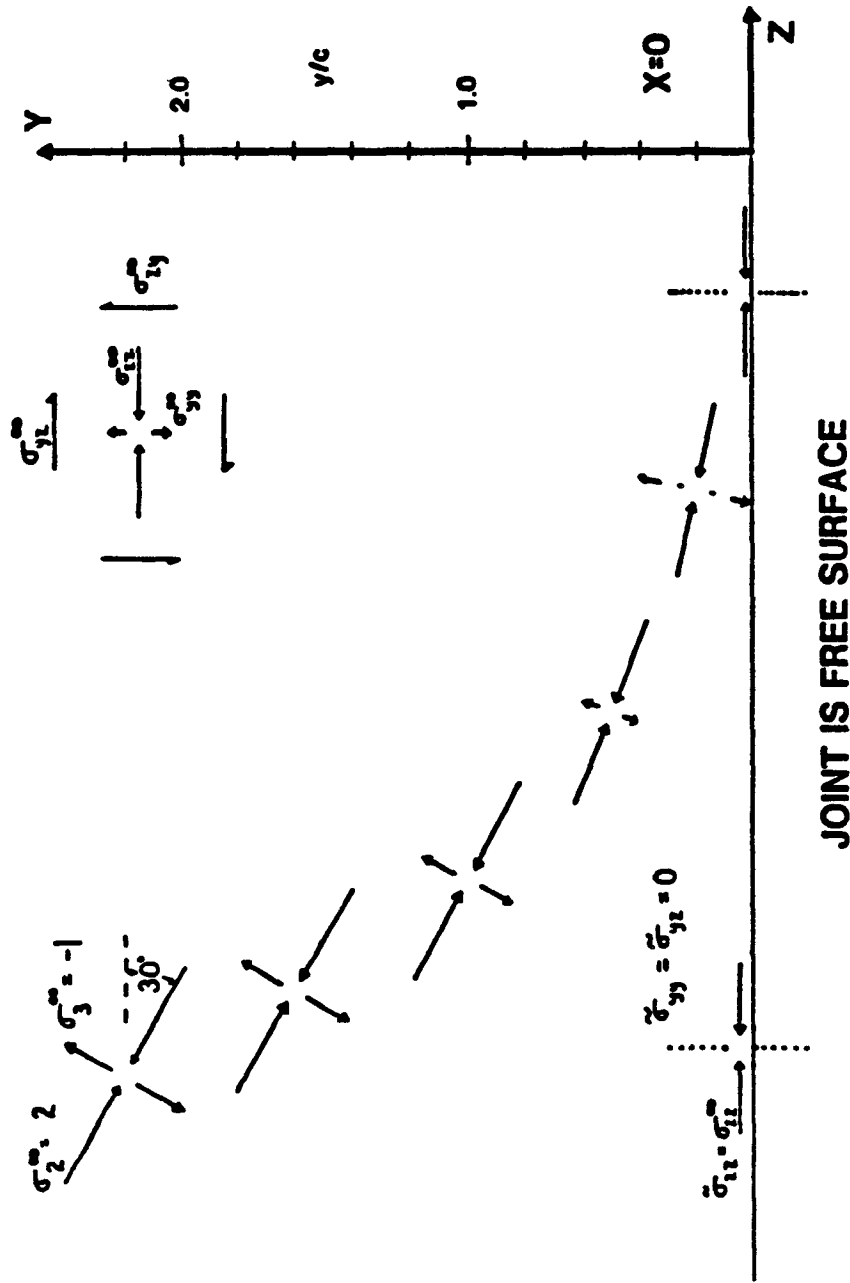
Figure 5-11.

Map of principal stresses about a joint when the resolved far-field stress normal to the joint σ_{yy}^{∞} is tensile. The joint is subject to the far-field stresses $\sigma_2^{\infty}/\sigma_3^{\infty} = -2$; with $\varphi = 30°$. Since the joint is open, $\sigma_{yy} = \sigma_{ys} = 0$ on the joint surface. Note that σ_3 remains tensile for all $\frac{y}{c} > 0$. As $\frac{y}{c} \rightarrow 0$, the principal stresses rotate such that they become parallel and perpendicular to the free surface.

σ_{yy}^{∞} TENSILE

Figure 5-12.

Inferred resultant geometry of a younger joint zone (J_2) growing toward a through-going zone (J_1) when the resolved far-field stress normal to J_1 (σ_{yy}^{∞}) is tensile. J_1 will be a free surface. J_2 may grow arbitrarily close to, and subparallel with, J_1. Compare with figure 2-9.

younger joint systematically changing its orientation until it parallels the throughgoing zone. Note that the sigmoidal form could be achieved without the younger joint undergoing a shear strain anywhere along its length. Thus, a curved fracture trace need not be an indicator of a shearing mode of crack growth, as suggested by Beach (1980).

The stress map of figure 5-11 and the hypothetical joint trace of figure 5-12 bear a striking resemblance to the geometries observed on the younger joint zones in Domain A (compare with figure 2-9). This suggests that the systematic geometries noted on J_2^A are indicative of growth of this joint set in a regional stress field in which $-3 < \dfrac{\sigma_2^\infty}{\sigma_3^\infty} < -1/3$. This estimate is strictly valid only for those J_2^A which, far from J_1^A, show a dihedral angle of 30° with J_1^A.

II.B σ_{yy}^∞ and σ_{zz}^∞ are both tensile

If the joint is open, but σ_{zz}^∞ is tensile, then the situation illustrated in figure 5-13 is applicable. A clockwise rotation of the perturbed principal stresses will occur. The rotation is most pronounced closest to the joint. σ_3 is everywhere tensile.

Again ignoring crack interaction, we might expect a joint originating far away and growing toward the throughgoing zone to curve abruptly *into* the older zone (figure 5-14). The sudden change in curvature would occur at $\dfrac{y}{c} \approx 0.2$. For the Moab Member, the characteristic distance at which the curvature would be expected to abruptly change is about 2.7 meters. This is in excellent agreement with the observations in Domain B (compare with figures 2-12, 2-13).

The similarities between the geometries of J_2^B joints and the hypothetical
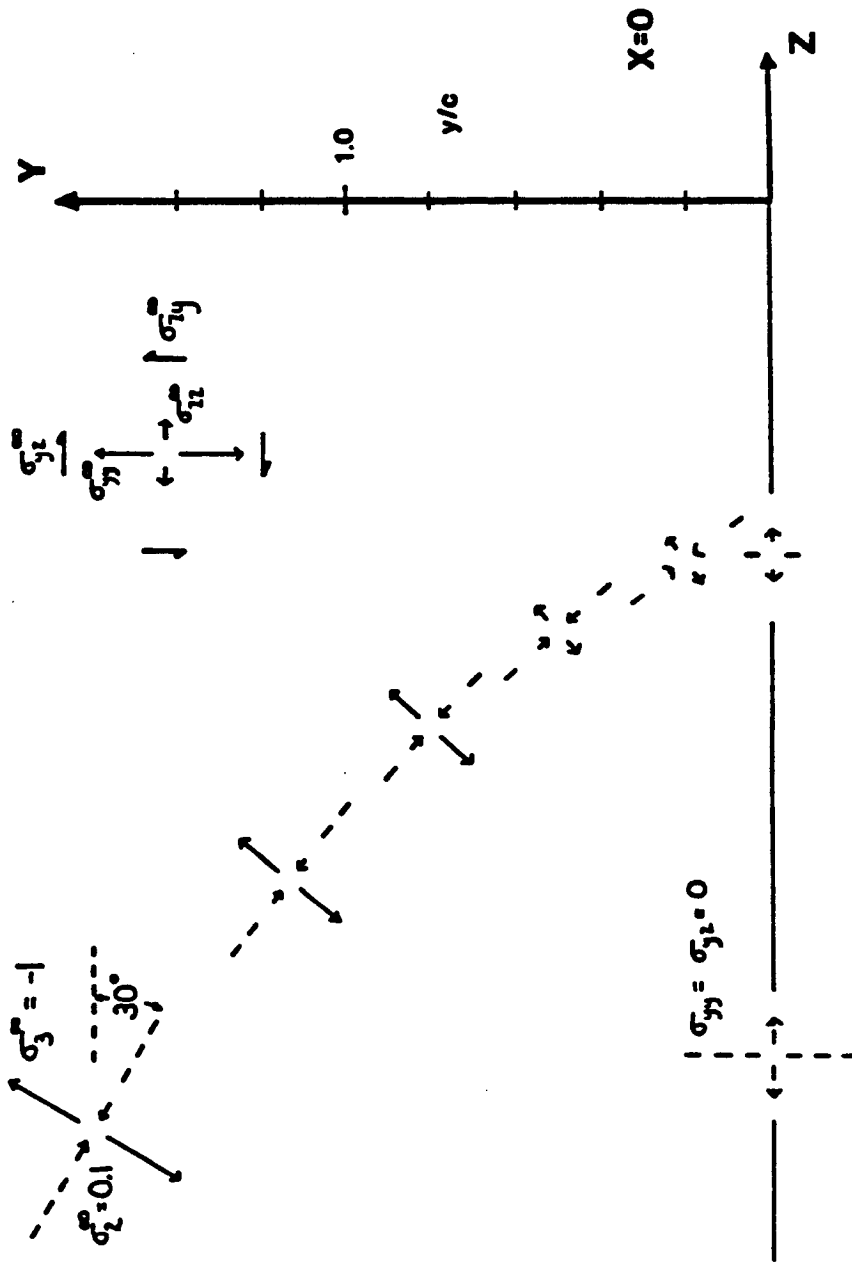
JOINT IS FREE SURFACE

Figure 5-13.

Map of principal stresses about a joint zone under the far-field loading $\sigma_2^{\infty}/\sigma_3^{\infty} = -0.3$; for $\varphi = 30°$. Since the resolved far-field stress normal to the zone (σ_{yy}^{∞}) is tensile, the joint will be an open crack, hence a free surface. Additionally, σ_{zz}^{∞} is tensile, causing a clockwise rotation of the principal stresses as $y \to 0$. σ_3 will be tensile everywhere. Note the abrupt change in orientation of the principal stresses at $\frac{y}{c} \approx 0.2$.
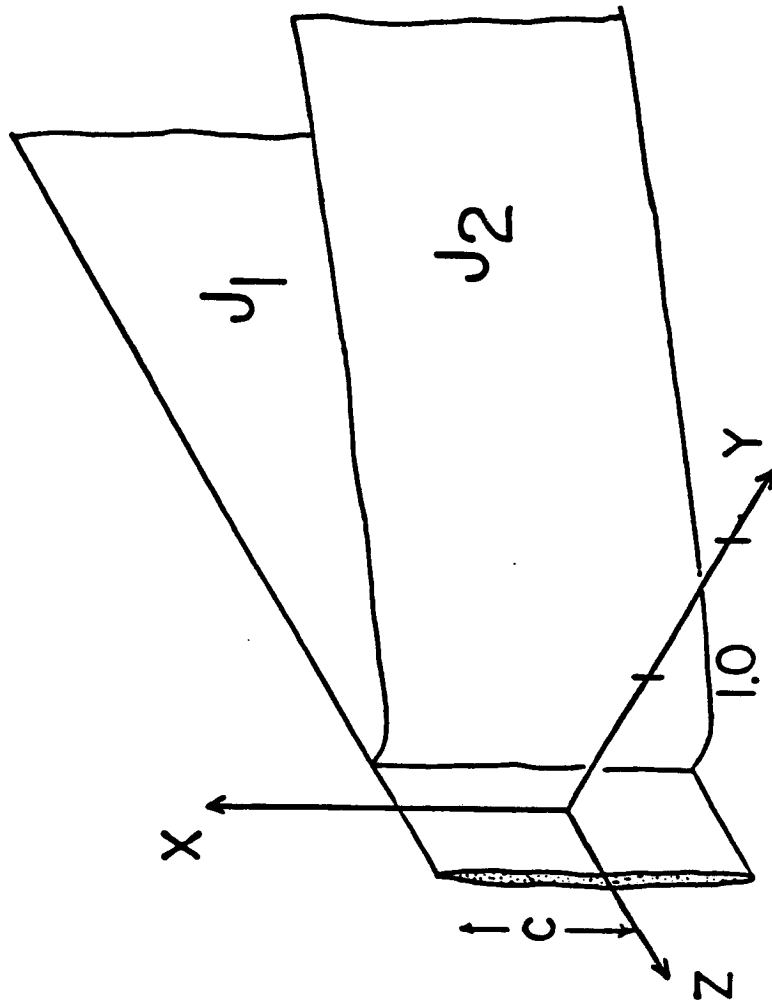
Figure 5-14.

Inferred resultant geometry of a younger joint zone (J_2) growing toward a through-going zone (J_1) when the resolved far-field stresses σ_{yy}^{∞} and σ_{zz}^{∞} are both tensile. If the propagation path of J_2 is controlled by the stress field about J_1, it will abruptly curve *into* J_1, at a characteristic distance of $\frac{y}{c} \approx 0.2$.

joint trace of figure 5-14 suggest that J_2^β grew in a regional stress field in which

$-1/3 < \dfrac{\sigma_2^-}{\sigma_3^-} < 1$. This assumes that J_2^β makes a far-field dihedral angle of 30°

with J_1^β.

CONCLUSIONS

Several generations of zoned joints are developed in the Moab member of the Entrada Sandstone in Arches National Park, Utah. The sets of zoned joints are paleostress indicators. Although a joint zone originates in response to a tensile driving stress ($\sigma_3 - P < 0$), later rotation of the principal stresses leads to a resolved shear on the plane of the crack. Younger joints growing in the rotated stress field may display a systematic change in their orientation near an older, throughgoing zone. The interactive geometries observed are due to local rotation of principal stresses near a pre-existing, throughgoing joint zone. Characteristic interactions between different generations of zoned joints may be used to infer the ratio of the far-field horizontal principal stresses during an episode of joint growth. Different domains characterize areas in which the ratio of far-field principal horizontal stresses is essentially constant. These areas range in size from 1 km^2 to more than 8 km^2.

TABLE OF SYMBOLS

J_i^k —————————————————— the ith set of zoned joints in domain k

c, c_o, c_1 —————————————————— crack half-length (or half-height)

X,Y,Z —————————————————— axes of cartesian coordinate system

x, y, z —————————————————— cartesian coordinates

Φ —————————————————— angle between X-axis and σ_1 (equation 3-5)

φ —————————————————— angle between σ_2^- and Z-axis (figures 5-2, 5-4)

Ψ —————————————————— angle between σ_2 and Z-axis (figure 5-6)

$r_m, \theta_m; \ r_1, \theta_1; \ r_2, \theta_2$ ——————————— polar coordinates from crack midpoint and tips (see figure A-1)

r, θ —————————————————— polar coordinates near crack tip (figure 3-2)

P —————————————————— uniform internal fluid pressure within crack

P_c —————————————————— confining pressure

P_p —————————————————— pore pressure

$\sigma_1^-, \sigma_2^-, \sigma_3^-$ —————————————————— far-field principal stresses

$\sigma_{xx}^-, \sigma_{yy}^-, \sigma_{zz}^-, \sigma_{yz}^-$ —————————————————— resolved far-field stresses on plane of crack

$\sigma_1, \sigma_2, \sigma_3$ —————————————————— local principal stresses

$\sigma_{xx}, \sigma_{yy}, \sigma_{zz}, \sigma_{xy}, \sigma_{xz}, \sigma_{yz}$ ——————————— stresses resolved to cartesian coordinate system

$\sigma_3^{\cdot}$ —————————————————— driving stress for Mode I crack deformation, $= \sigma_3 - P$

$\bar{\sigma}_{zz}^-$ —————————————————— far-field uniform stress in Z-direction

σ_{zz}^I —————————————————— induced stress in Z-direction to satisfy plane strain

K_i —————————————————— stress intensity in ith mode of deformation

K_i^C —————————————————— fracture toughness in ith mode of deformation

$C^{\cdot}$ —————————————————— coefficient of sliding friction

K —————————————————— shear stress ratio

ν ————————————————————— Poisson's ratio

E ————————————————————— Young's modulus

γ ————————————————————— free surface energy per unit area

L_i ————————————————————percentage difference between exact
and approximate stress solutions

APPENDIX A

The approximation of a single zone of joints as a simple, infinitely long crack with a characteristic height allows a relatively straight-forward analytic solution of the elastic stress fields about the crack. Because of the simple geometry and assumptions made about the loading, we can obtain a solution to the three-dimensional problem as a linear superposition of the solutions to two separate, well-known two-dimensional problems from linear elastic fracture mechanics: the plane (Mode I loading) and antiplane (Mode III loading) problems. The treatment follows the standard methodology, differing only in that the entire solution is utilized, not just the crack tip approximation.

The solutions are based on the complex potential method of Westergaard (1939), which is treated lucidly in Appendix I of Paris and Sih (1965). Limitations of Westergaard's solutions are discussed by Sih (1966), Eftis and Liebowitz (1972) and Eftis, et al (1977).

We assume infinitesimal linear elasticity in an infinite, isotropic homogeneous body. Body forces are not considered. Crack geometry and coordinate system are shown in figure A-1. One of the far-field principal stresses, σ_1^∞ or σ_2^∞ is colinear with the X-axis. Based on field evidence, we assume throughout that σ_1^∞ is vertical and colinear with the X-axis.

Mode I problem

When the far-field normal stress on the crack face (σ_{yy}^∞) is tensile, as in figure 5-5B, the Mode I (opening mode) solution of linear elastic fracture mechanics is applicable. If a uniform internal pressure within the crack, P, is considered, then the Mode I solution is applicable if $(\sigma_{yy}^\infty - P) < 0$. For the

plane, two-dimensional crack in the X-Y plane subjected to biaxial loading, we must satisfy the equilibrium equations:

$$\left.\begin{array}{l} \dfrac{\partial \sigma_{xx}}{\partial x} + \dfrac{\partial \sigma_{xy}}{\partial y} = 0 \\[2mm] \dfrac{\partial \sigma_{xy}}{\partial x} + \dfrac{\partial \sigma_{yy}}{\partial y} = 0 \\[2mm] \sigma_{xy} = \sigma_{yx}. \end{array}\right\}$$ A1

while the strain-displacement relations and Hooke's law lead to the compatibility equation

$$\left[\dfrac{\partial^2}{\partial x^2} + \dfrac{\partial^2}{\partial y^2}\right]\left(\sigma_{xx} + \sigma_{yy}\right) = 0.$$ A2

If a uniform internal pressure within the crack, P, is considered, then the boundary conditions to be satisfied are:

$$\text{for } y = 0, \quad |x| < c: \quad \left\{\begin{array}{l} \sigma_{yy} = P \\[2mm] \sigma_{xy} = 0 \end{array}\right.$$

$$\text{for } \sqrt{x^2 + y^2} \to \infty; \quad \left\{\begin{array}{l} \sigma_{yy} = \sigma_{yy}^{\infty} \\[2mm] \sigma_{xx} = \sigma_{xx}^{\infty}. \end{array}\right.$$ A3

It is convenient to use the coordinate system defined in figure A-1. The general solution to the plane, uniform biaxial loading problem of figure 5-5B can be derived using the methodology of Paris and Sih (1964, Appendix I). The full solutions are:

$$\sigma_{xx} = \left(\sigma_{yy}^{\infty} - P\right)\left[\dfrac{r_m}{\sqrt{r_1 r_2}}\cos\left(\theta_m - \dfrac{\theta_1 + \theta_2}{2}\right) - \dfrac{|y|\,c^2}{\left[r_1 r_2\right]^{3/2}}\sin\left(\dfrac{3}{2}\left(\theta_1 + \theta_2\right)\right)\right]$$

$$+ \sigma_{xx}^{\infty} - \left(\sigma_{yy}^{\infty} - P\right).$$ A4
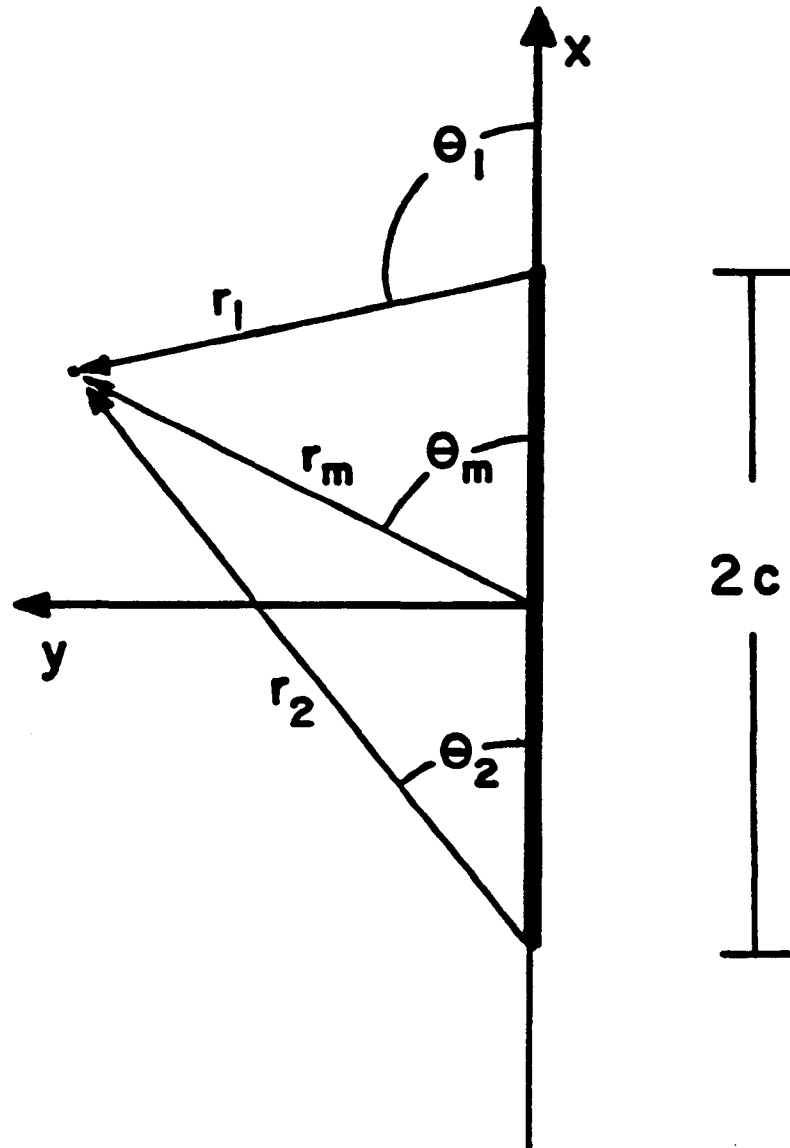
-184-

Figure A-1.

Coordinate system used for the full solution of the elastic stress field about a plane flat elliptical crack.

$$\sigma_{yy} = \left(\sigma_{yy}^{\infty} - P\right)\left[\frac{r_m}{\sqrt{r_1 r_2}}\cos\left(\theta_m - \frac{\theta_1 + \theta_2}{2}\right) + \frac{|y|c^2}{\left[r_1 r_2\right]^{3/2}}\sin\left[\frac{3}{2}\left(\theta_1 + \theta_2\right)\right]\right] + P \quad . \qquad A5$$

$$\sigma_{xy} = \left(\sigma_{yy}^{\infty} - P\right)\left[\frac{yc^2}{\left[r_1 r_2\right]^{3/2}}\cos\left[\frac{3}{2}\left(\theta_1 + \theta_2\right)\right]\right]. \qquad A6$$

$$\sigma_{zz}^{I} = \nu\left(\sigma_{xx} + \sigma_{yy}\right). \qquad A7$$

In general, σ_{xy} shearing stresses will increase near the crack tips, leading to a local rotation of principal stresses about the Z-axis. If we limit our investigation to the plane x=0, then:

$$\left.\begin{array}{l}\theta_m = \dfrac{\pi}{2} \\[2mm] \theta_1 + \theta_2 = \pi \\[2mm] r_m = y \\[2mm] r_1 = r_2 = \sqrt{y^2 + c^2}, \end{array}\right\} \qquad A8$$

and equations A4 - A6 become:

$$\sigma_{xx}\left(x=0\right) = \left[\left(\sigma_{yy}^{\infty} - P\right)\frac{|y|}{\sqrt{y^2 + c^2}}\left[1 + \frac{c^2}{y^2 + c^2}\right]\right] + \sigma_{xx}^{\infty} - \left(\sigma_{yy}^{\infty} - P\right), \qquad A9$$

$$\sigma_{yy}\left(x=0\right) = \left[\left(\sigma_{yy}^{\infty} - P\right)\frac{|y|}{\sqrt{y^2 + c^2}}\left[1 - \frac{c^2}{y^2 + c^2}\right]\right] + P \quad , \qquad A10$$

$$\sigma_{xy}\left(x=0\right) = 0 \quad . \qquad A11$$

For $\sigma_{xy} = 0$, there will be no principal stress rotations about the Z-axis due to the Mode I part of the solution.

Mode III problem

The problem shown in figure 5-5 D corresponds to the antiplane strain (Mode III loading) problem of linear elastic fracture mechanics. In this problem, an infinitely long crack with characteristic height 2c is subjected to a far-field antiplane pure shear of magnitude $\left[1 - K\right]\sigma_{yz}^{\infty}$, where K is defined by equation (5-20). We require that the crack face be traction-free. If u, v, w are displacements in the X, Y and Z directions, respectively, then the Mode III problem is specified by :

$$u = 0; \quad v = 0; \quad w = w\left[x, y\right] . \qquad \text{A12}$$

Since this is a case of pure shear,

$$\sigma_{xx}^{D} = \sigma_{yy}^{D} = \sigma_{zz}^{D} = \sigma_{xy}^{D} = 0 , \qquad \text{A13}$$

where the superscript D refers to figure 5-5 D.

The equilibrium equations become

$$\frac{\partial \sigma_{xz}^{D}}{\partial x} + \frac{\partial \sigma_{yz}^{D}}{\partial y} = 0, \qquad \text{A14}$$

while the strain-displacement relations and Hooke's law give

$$\left. \begin{array}{l} \varepsilon_{xz}^{D} = \dfrac{\partial w}{\partial x} = \dfrac{\sigma_{xz}^{D}}{G} \\[4mm] \varepsilon_{yz}^{D} = \dfrac{\partial w}{\partial y} = \dfrac{\sigma_{yz}^{D}}{G} \end{array} \right\} \qquad \text{A15}$$

where G is the shear modulus.

The boundary conditions for the Mode III problem are:

$$\left. \begin{array}{l} at \ y = 0, \ |x| < c: \quad \sigma_{yz}^{D} = \sigma_{xz}^{D} = 0 , \\[3mm] at \ \sqrt{x^2 + y^2} \to \infty: \quad \sigma_{yz}^{D} = \left[1 - K\right]\sigma_{yz}^{\infty} . \end{array} \right\} \qquad \text{A16}$$

Using the coordinate system defined in figure A-1, the solution is given by Eshelby (1968, equation 20) as:

$$\sigma_{yz}^D = \left(1 - K\right)\sigma_{yz}^\infty \frac{r}{\sqrt{r_1 r_2}} \cos\left[\theta - \frac{\theta_1 + \theta_2}{2}\right].$$

A17

$$\sigma_{zz}^D = \left(1 - K\right)\sigma_{yz}^\infty \frac{r}{\sqrt{r_1 r_2}} \sin\left[\theta - \frac{\theta_1 + \theta_2}{2}\right].$$

A18

On the plane $x = 0$, using the relations of A8, we find that

$$\sigma_{yz}^D \left(x = 0\right) = \left(1 - K\right)\sigma_{yz}^\infty \frac{y}{\sqrt{y^2 + c^2}}.$$

A19

$$\sigma_{zz}^D \left(x = 0\right) = 0.$$

A20

Non-zero σ_{yz} and σ_{zz} shearing stresses will cause rotation of the principal stresses about the X- and Y-axes, respectively. On the plane $x = 0$, the only non-zero shear stress is σ_{yz}. This will lead to a rotation of the principal stress axes about the X-axis.

APPENDIX B

Although the principal stress solutions obtained by the use of equations (5-7) - (5-9) and either (5-12) - (5-16) or (5-17) and (5-24) are exact on the plane $x=0$, we may inquire about the usefulness of this simple solution for characterizing the stress state elsewhere in the body. Away from the plane $x=0$, non-zero σ_{xy} and σ_{xz} shearing stresses will cause rotations of the principal stress axes about the Z- and Y-axes, respectively. Additionally, σ_{xx} will no longer be independent of σ_{zz}^{-}.

Except for the singularity at the crack tips ($x = \pm c$, $y=0$), the six independent components of the full stress tensor (σ_{xx}, σ_{xy}, σ_{xz}, σ_{yy}, σ_{yz} and σ_{zz}) at any point (x,y) in the body can be determined using the full solutions given in Appendix (A). The magnitude and orientation of the principal stresses (σ_1, σ_2, σ_3) at (x,y) can be found using common techniques (see, for instance, Malvern, 1969, p. 85-92). We can then compare the magnitude and orientation of the principal stresses at (x,y), found from use of the full solutions, against the principal stresses at $(x=0, y)$.

The question of how good an approximation must be to be good enough is one without an easy answer. To introduce some measure of objectivity, we define

$$L_i = \left| \frac{\sigma_i \left[x,y\right] - \sigma_i \left[x=0,y\right]}{\sigma_i \left[x=0,y\right]} \right| \qquad \text{for } i = 1,2,3. \qquad \text{B1}$$

L_i is merely the percentage difference between the magnitudes of $\sigma_i(x,y)$ and $\sigma_i(x=0,y)$, with respect to $\sigma_i(x=0,y)$. We may now map regions around the crack in which all L_i are less than or equal to some specified maximum allowable percentage difference, L_{max}. The plots of figures B-1 and B-2 define

the regions in which the principal stresses $\sigma_i(x,y)$ and $\sigma_i(x=0,y)$ satisfy the condition that

$$L_i \leq L_{max} \quad \text{for } i = 1,2,3. \qquad \text{B2}$$

For a given L_{max}, expressed as a percentage, the region below the curve satisfies equation (B2). Because the stress field is symmetric about the X-axis, only half the crack is shown on each plot. The crack extends out perpendicular to the page and its trace on the X-Y plane corresponds to the heavy line on the X-axis. Length scales are normalized by the crack half-length, c.

Unlike the solution on $x=0$, the general solution is not independent of the vertical stress (σ_1^∞). The effects of varying σ_1^∞ are shown by the left and right sides of figures B-1 and B-2. Because of the symmetry of the problem, each set of curves is symmetric about both the X- and Y-axes.

Another possible criterion for comparison is the orientation of the plane perpendicular to $\sigma_3(x,y)$. On the plane ($x = 0$), σ_3 will be horizontal, and any fracture which forms will here be a vertical fracture with some strike direction. At the point (x,y), σ_3 will have experienced some rotation in space. Since the components of the stress tensor and the values of the principal stresses are known, the direction cosines of σ_3 may be found (see Jaeger and Cook, 1979, p. 19-20). The strike and dip of the plane perpendicular to σ_3 at (x,y) can be determined and compared with the strike of the vertical plane at $(x=0, y)$. In figures B-1 and B-2 the light and dark stipled regions indicate areas in which either the strike or dip of the plane normal to σ_3 at (x,y) differs by more than five and ten degrees, respectively, from the strike and dip of the plane normal to σ_3 at $(x=0, y)$.
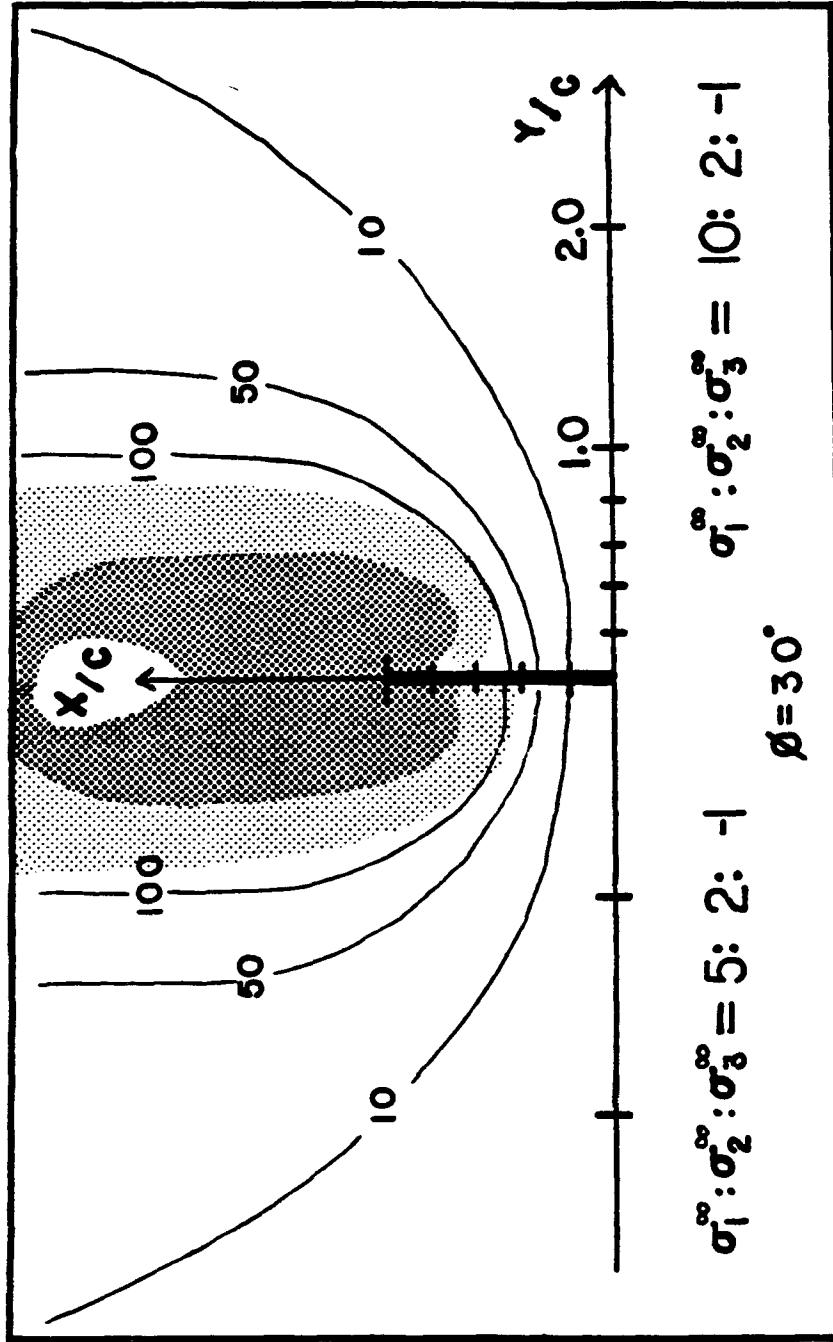
Figure B-1.
Comparison of the stress solution on ($x = 0$) to the full, three-dimensional solution in a plane perpendicular to the joint zone for the open joint of figure 5-11. Only the top half of the joint zone is shown. Curves are lines of constant L_4 (see text). In light and dark stipled regions, either the strike or dip of the plane normal to σ_3 at the point (x,y) differs by more than five and ten degrees, respectively, from the strike and dip of the plane normal to σ_3 at ($x = 0, y$). Left side of the figure shows results for $\sigma_1^\infty = 5$, while results on the right side are for $\sigma_1^\infty = 10$.

Example 1.

Figure B-1 compares the stress solution on $x = 0$ to the full solution for the open crack problem illustrated in figure 5-11. Excluding the crack tips, at the point (x,y), the six independent components of the stress tensor $(\sigma_{xx}, \sigma_{xy}, \sigma_{xz}, \sigma_{yy}, \sigma_{yz}$ and $\sigma_{zz})$ are found from equations (A4), (A6), (A18), (A5), (A17) and (5-5), respectively.

The solution on $x = 0$ (figure 5-11) indicates that the principal stresses will rotate, with σ_3 becoming parallel to the Y-axis as $y -> 0$, and σ_3 tensile for all $|y| > 0$. Figure B-1 shows that σ_3 will be tensile for at least the range $|\frac{x}{c}| < 0.5$ for all y. Due to the singularity at the crack tip, σ_3 will in fact reach higher and higher tensile values near the crack tips.

A rotation of the principal stresses is required by the boundary condition that $\sigma_3 = 0$ at $y = 0$, $|\frac{x}{c}| < 1$. For the region $|\frac{x}{c}| < 0.4$, the strike and dip of the plane normal to $\sigma_3(x,y)$ is within five degrees of that given by the solution on $x = 0$. An increase in σ_1^- increases the range of $|\frac{x}{c}|$ over which this is true.

It appears that the relatively simple solution on $x = 0$ effectively characterizes the behaviour of the principal stresses for at least the region $|\frac{x}{c}| \leq 0.5$ for all values of $|\frac{y}{c}|$. For $|\frac{y}{c}| > 1$, the solution on $x = 0$ appears to be a reasonable approximation for all values of x.

Example 2.

In figure B-2 the solution on $x = 0$ is compared with the full solution at (x,y) for the frictional sliding example shown in figure 5-8. At the point (x,y)
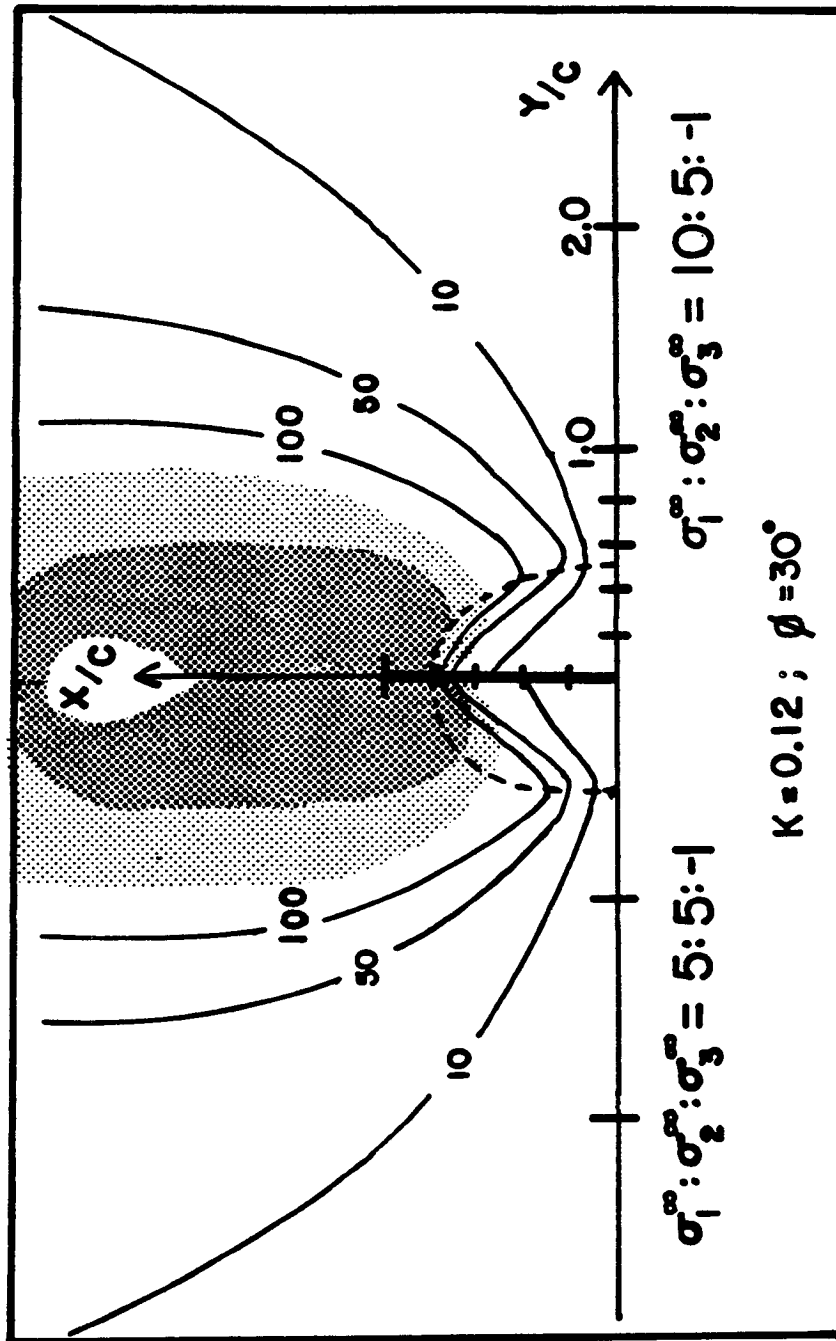
-192-

Figure B-2.
Comparison of the stress solution on ($z = 0$) to the full three-dimensional solution in a plane perpendicular to the joint zone for the friction-law joint of figure 5-8. Only the upper half of the joint is shown. $\sigma_1^* = 5$ on the left side and $\sigma_1^* = 10$ on the right side. Curves are lines of constant L_4 (see text). Stipling pattern and meaning is same as in figure B-1.

the six independent components of the stress tensor (σ_{xx}, σ_{xy}, σ_{xz}, σ_{yy}, σ_{yz} and σ_{zz}) are found from equations (5-17), (5-25), (A18), (5-25), (A17) and (5-25), respectively. The dashed line is the boundary of the compressive zone. This zone is elliptical in shape and includes the region of the crack $|\frac{x}{c}| < 0.8$. The poor match between $\sigma_i(x,y)$ and σ_i ($x=0$, y) near $|\frac{y}{c}| = 0.5$ is due to the extremely small values of σ_3 ($x=0,y$) and σ_3 (x,y) as they change signs at the boundary of the compressive zone. Closer to the crack, σ_i ($x=0,y$) appears to be a reasonable approximation to σ_i (x,y) for $|\frac{x}{c}| \leq 0.7$. For $|\frac{y}{c}| > 1$ the solution on $x = 0$ seems to be a reasonable approximation for all values of x.

The strike and dip of the plane normal to σ_3 (x,y) will be within five degrees of that predicted by σ_3 ($x=0,y$) for $|\frac{x}{c}| \leq 0.5$. As σ_1^- increases, the range over which this is true will increase.

In general, throughout the range $|\frac{x}{c}| \leq 0.7$, the behaviour of the principal stress at (x,y) follows the pattern seen on the plane $x = 0$. The relatively simple solution on $x = 0$ effectively characterizes the nature, if not the exact details, of the change in magnitude and rotation of the principal stresses over about 70 percent of the total crack height.

REFERENCES CITED

Anderson, E.M., 1951, *The Dynamics of Faulting;* Oliver and Boyd, Ltd., Edinburgh.

Anderson, E. R., 1978, Propagation and interaction of pressurized cracks in photoelastic gelatin; M.S. Thesis, Stanford University, 40 p.

Aydin, A., 1977, Faulting in sandstone; PhD dissertation, Stanford University, 246 p.

Aydin, A. and Z. Reches, 1982, Number and orientation of fault sets in the field and in experiments; Geology, V. 10, p. 107-112.

Baars, D. L., 1979, The Colorado Plateau aulocogen - key to continental scale basement rifting; Proc. 2nd Internat. Conf. on Basement Tectonics; Basement Tectonics Committee, Inc., Denver, Colo., p. 157-164.

_____, 1966, Pre-Pennsylvanian paleotectonics - key to basin evolution and petroleum occurrences in Paradox Basin, Utah and Colorado; Bull. Am. Assoc. Petrol. Geol., V. 50, p. 2082-2111.

Beach, A, 1980, Numerical models of hydraulic fracturing and the interpretation of syntectonic veins; J. Struct. Geol., V. 2, p. 425-438.

Bergkvist, H. and L. Guex, 1979, Curved crack propagation; Int. J. Fracture, V. 15, p. 429-441.

Birch, F., 1966, Compressibility; elastic constants; *in:* S. P. Clark, ed., *Handbook of Physical Constants;* Geol. Soc. Am. Memoir 97, p. 97-173.

Bodell, J. M. and D. S. Chapman, 1982, Heat flow in the north-central Colorado Plateau; J. Geophy. Res., V. 87, p. 2869-2884.

Bombolakis, E. G., 1973, Brittle crack growth under uniaxial compression; *in:* G. C. Sih, ed., *Brittle Crack Growth;* Noordhoff, p. 103-112.

Brace, W. F., 1960, An extension of the Griffith theory of fracture to rocks; J. Geophy. Res., V. 65, p. 3477-3480.

Broek, D., 1978, *Elementary Engineering Fracture Mechanics* ; Sijthoff and Noordhoff, The Netherlands, 437p.

Burger, H. R. and M. N. Hamill, 1976, Petrofabric stress analysis of the Dry Creek Ridge anticline, Montana; Geol. Soc. Am. Bull., V. 87, p. 555-566.

Byerlee, J., 1977, Friction of rocks; *in:* J. F. Evernden, ed. *Proc. Conf. II: Experimental studies of rock friction with application to earthquake prediction;* U. S. Geol. Surv., p. 55-79.

Carter, W. D., 1957, Disconformity between Lower and Upper Cretaceous in western Colorado and eastern Utah; Geol. Soc. Am. Bull., V. 68, p. 307-314.

Cater, F. W., 1970, Geology of the Salt Anticline region in southwestern Colorado; U. S. Geol. Surv. Prof. Paper 637, 80p.

Cheng, C. H. and D. H. Johnston, 1981, Dynamic and static moduli; Geophy. Res. Ltrs., V. 8, p. 39-42.

Chinnery, M. A., 1963, The stress changes that accompany strike-slip faulting; Bull. Seis. Soc. Am., V. 53, p. 921-932.

Craig, L. C., 1959, Measured sections of Morrison and adjacent formations; U. S. Geol. Surv. Open-file report.

Dane, C. H., 1935, Geology of the Salt Valley Anticline and adjacent areas, Grand County, Utah; U. S. Geol. Surv. Bull. 863, 184p.

Delaney, P. T. and D. D. Pollard, 1981, Deformation of host rocks and flow of magma during growth of minette dikes and breccia-bearing intrusions near Ship Rock, New Mexico; U. S. Geol. Surv. Prof. Paper 1202.

Durney, D. W. and J. G. Ramsey, 1973, Incremental strains measured by syntectonic crystal growths; *in* : DeJong, K. and R. Scholten, eds., *Gravity and Tectonics* , Wiley Interscience, New York, p. 67-96.

Dyer, R., 1979, A 3-D elastic bending-plate model for joint formation (abst.), EOS, V. 60, p. 944,

Eftis J. and H. Liebowitz, 1972, On the modified Westergaard equations for certain plane crack problems; Int. J. Fracture Mech., V. 8, p. 383-392.

Eftis, J., N. Subramonian and H. Liebowitz, 1977, Crack border stress and displacement equations revisited; Engr. Fracture Mech., V. 9, p. 189-210.

Elston, D. P., E. M. Shoemaker and E. R. Landis, 1962, Uncompahgre Front and Salt Anticline region of Paradox Basin, Colorado and Utah; Am. Assn. Petrol. Geol. Bull., V. 46, p. 1857-1878.

Engelder, T. and P. Geiser, 1980, On the use of regional joint sets as trajectories of paleostress fields during the development of the Appalachian Plateau, New York; J. Geophys. Res., V. 85, p. 6319-6341.

Erdogan, F. and G. C. Sih, 1963, On the crack extension in plates under plane loading and transverse shear; J. Basic Engr., Trans. ASME, V. 85, p. 519-527.

Eshelby, J. D., 1968, Stress analysis; *in* : *Fracture Toughness*, ISI Publication 121, The Iron and Steel Institute, London, p. 13-48.

Fisher, D. J., C. E. Erdmann and J. B. Reeside, Jr., 1960, Cretaceous and Tertiary formations of the Book Cliffs: Carbon, Emery and Grand Counties, Utah, and Garfield and Mesa Counties, Colorado; U. S. Geol. Surv. Prof. Paper 332, 80p.

Gard, L. M. Jr., 1976, Geology of the north end of the Salt Valley Anticline, Grand County, Utah; U. S. Geol. Surv. Open-file Report 76-303, 35p.

Gilluly, J. and J. B. Reeside, Jr., 1928, Sedimentary rocks of the San Rafael Swell and some adjacent areas in eastern Utah; U. S. Geol. Surv. Prof. Paper 150, p. 61-110.

Griffith, A. A., 1924, Theory of rupture; Proc. First Int. Cong. Appl. Mech., p. 55-63.

_____, 1921, The phenomena of rupture and flow in solids; Phil. Trans. Roy. Soc., London, Ser. A, V. 221, p. 163-198.

Griggs, D. and J. Handin, 1960, Observations on fracture and a hypothesis of earthquakes; *in* : Rock Deformation (A Symposium); Geol. Soc. Am. Memoir 79, ed. by D. Griggs and J. Handin, p. 347-364.

Hanley, J. H., 1976, Paleosynecology of nonmarine Mollusca from the Green River and Wasatch Formations (Eocene), southwestern Wyoming and northwestern Colorado; *in:* R. W. Scott and R. R. West, eds., *Structure and Classification of Paleocommunities;* Dowden, Hutchinson and Ross, Inc., p. 235-261.

Harris, J. F., G. L. Taylor and J. L. Walper, 1960, Relation of deformational fractures in sedimentary rocks to regional and local structures; Am. Assn. Petrol. Geol. Bull., V. 44, p. 1853-1873.

Hite, R. J., 1977, Subsurface geology of a potential waste emplacement site, Salt Valley anticline, Grand County, Utah; U. S. Geol. Surv. Open-file Report 77-761.

Hobbs, D. W., 1967, The formation of tension joints in sedimentary rocks: an explanation; Geol. Mag., V. 104, p. 550-556.

Hodgson, R. A., 1965, Genetic and geometric relations between structures in basement and overlying sedimentary rocks, with examples from Colorado Plateau and Wyoming; Am. Assoc. Petrol. Geol. Bull., V. 49, p. 935-949.

_____, 1961a, Regional study of jointing in Comb Ridge - Navajo Mountain area, Arizona and Utah; Am. Assn. Petrol. Geol. Bull., V. 45, p. 1-38.

_____, 1961b, Classification of structures on joint surfaces; Am. Jour. Sci., V. 259, p. 493-502.

Hoek, E. and Z. T. Bieniawski, 1965, Brittle fracture propagation in rock under compression; Int. J. Frac. Mech., V. 1, p. 137-155.

Hubbert, M. K. and D. G. Willis 1957, Mechanics of hydraulic fracturing; Trans. Am. Inst. Min. Metal. and Petrol. Engrs.; V. 210, p. 153-166.

Hunt, C. B., 1958, Structural and igneous geology of the La Sal Mountains, Utah; U. S. Geol. Prof. Paper 294-I.

Huntoon, P. W. and H. R. Richter, 1979, Breccia pipes in the vicinity of Lockhart Basin, Canyonlands area, Utah; in: Permianland; Four Corners Geol. Soc. Guidebook, 9th Field Conf., p. 47-53.

Jacobs, M. B. and P. F. Kerr, 1965, Hydrothermal alteration along the Lisbon Valley fault zone, San Juan County, Utah; Geol. Soc. Am. Bull., V. 76, p. 423-440.

Jaeger, J. C., and N. G. W. Cook, 1979, Fundamentals of Rock Mechanics; 3rd ed., Halsted Press, 593 p.

Joesting, H. R. and J. E. Case, 1962, Regional geophysical studies in Salt Valley - Cisco area, Utah and Colorado; Am. Assoc. Petrol. Geol. Bull., V. 46, p. 1879-1889.

Kehle, R. O., 1964, The determination of tectonic stresses through analysis of hydraulic well fracturing; J. Geophy. Res., V. 69, p. 259-273.

Kelley, V. C. and N. J. Clinton, 1960, *Fracture Systems and Tectonic Elements of the Colorado Plateau;* Univ. of New Mexico Pub. in Geology, No. 6, 104p.

Kirkland, P. L., 1963, Permian stratigraphy and stratigraphic paleontology of a part of the Colorado Plateau; Four Corners Geol. Soc., 4th Ann. Field Conf., p. 80-100.

Lachenbruch, A. H., 1962, Mechanics of thermal contraction cracks and ice-wedge polygons in permafrost; Geol. Soc. Am. Sp. Paper 70, 69 p.

_____,1961, Depth and spacing of tension cracks; J. Geophy. Res., V. 66, p. 4273-4292.

Ladeira, F. L. and N. J. Price, 1981 Relationship between fracture spacing and bed thickness; J. Struct. Geol., V. 3, p. 179-183.

Lawn, B. R. and T. R. Wilshaw, 1975, *Fracture of Brittle Solids;* Cambridge University Press, 204 p.

Lohman, S. W., 1975, The geologic story of Arches National Park; U. S. Geol. Surv. Bull. 1393, 113p.

Malvern, L. E., 1969, *Introduction to the Mechanics of a Continuous Medium;* Prentice-Hall, Inc., 713p.

Mavko, G. M. and A. Nur, 1978, The effect of nonelliptical cracks on the compressibility of rocks; J. Geophys. Res., V. 83, p. 4459-4468.

McClintock, F. A. and J. B. Walsh, 1962, Friction on Griffith cracks in rocks under pressure; Proc. 4th U. S. Nat. Cong. Appl. Mech., p. 1015-1021.

McKnight, E. T., 1940, Geology of area between Green and Colorado Rivers, Grand and San Juan Counties, Utah; U. S. Geol. Surv. Bull. 908, 147p.

Miller, W. D., 1959, The general geology of Moab Valley, Moab [Grand County], Utah; M. S. Thesis, Texas Tech Univ., 121p.

Muehlberger, W. R., 1961, Conjugate joint sets of small dihedral angle; J. Geology, V. 69, p. 211-219.

Nelson, R. A. and D. W. Stearns, 1977, Interformational control of regional fracture orientations; *in:* H. K. Veal, ed., *Exploration Frontiers of the Central and Southern Rockies;* Rocky Mtn. Assoc. Geol, p. 95-101.

Nickelsen, R. P., 1979, Sequence of structural stages of the Alleghany orogeny, at the Bear Valley strip mine, Shamokin, Pennsylvania; Am. J. Sci., V. 279, p. 225-271.

_____, 1976, Early jointing and cumulative fracture patterns; Proc. 1st Int. Conf. on the New Basement Tectonics, Utah Geol. Assoc. Pub #5, p. 193-199.

Nur, A., 1981, The tensile origin of fracture lineaments; Proc. 3rd Int. Conf. on the New Basement Tectonics, Stockholm, p. 155-167.

Odé, H., 1957, Mechanical analysis of the dike pattern of the Spanish Peaks area, Colorado; Geol. Soc. Am. Bull., V. 68, p. 567-576.

Ohlen, H. R. and L. B. McIntyre, 1965, Stratigraphy and tectonic features of Paradox Basin, Four Corners area; Am. Assoc. Petrol. Geol. Bull., V. 49, p. 2020-2040.

O'Sullivan, R. B., 1981, Stratigraphic sections of Middle Jurassic Entrada Sandstone and related rocks from Salt Valley to Dewey Bridge in East-Central Utah; U. S. Geol. Surv. Oil and Gas Investigations Chart OC-113.

Paris, P. C. and G. C. Sih, 1965, Stress analysis of cracks; *in* : *Fracture Toughness and Testing* ; ASTM Special Technical Publication No. 381; Soc. for Testing and Materials, Phila., Pa., p. 30-81.

Parker, J. M. III, 1942, Regional systematic jointing in slightly deformed sedimentary rocks; Geol. Soc. Am. Bull., V. 53, p. 381-408.

Peng, S. S. and C. A. Ortiz, 1973, Crack propagation and fracture of rock specimens loaded in compression; *in:* G. C. Sih, ed., *Dynamic Crack Propagation;* Noordhoff, 1973, p. 113-129.

Pfiffner, O. A. and J. G. Ramsay, 1982, Constraints on geological strain rates: arguments from finite strain states of naturally deformed rocks; J. Geophy. Res., V. 87, No. B1, p. 311-321.

Pipiringos, G. N. and R. B. O'Sullivan, 1978, Principal unconformities in Triassic and Jurassic rocks of western interior United States - a preliminary report; U. S. Geol. Surv. Prof. Paper 1035-A.

Pollard, D. D. and G. Holzhausen, 1979, On the mechanical interaction between a fluid-filled fracture and the earth's surface; Tectonophysics, V. 53, p. 27-57.

Price, N. J., 1966, *Fault and Joint Development in Brittle and Semi-Brittle Rock* ; Pergamon Press, Oxford, 176p.

Ramsay, J. G., 1967, *Folding and Fracturing of Rocks;* McGraw-Hill, New York.

Ramsay, J. G. and R. H. Graham, 1970, Strain variation in shear belts; Can. J. Earth Sci., V. 7, p. 786-813.

Reches, Z., 1976, Analysis of joints in two monoclines in Israel; Geol. Soc. Am. Bull., V. 87, p. 1654-1662.

Roering, C., 1968, The geometrical significance of natural en echelon crack-arrays; Tectonophysics, V. 5, p. 107-123.

Rudnicki, J. W., 1979, Rotation of principal stress axes caused by faulting; Geophys. Res. Ltrs., V. 6, p. 135-138.

Secor, D. T., 1969, Mechanism of natural extension fracturing at depth in the earth's crust; Geol. Surv. Canada Paper 68-52, p. 3-47.

_____, 1965, Role of fluid pressure in jointing; Am J. Sci., V. 263, p. 633-646.

Segall, P., 1981, The development of joints and faults in granitic rocks; PhD dissertation, Stanford Univ., 233 p.

Segall, P. and D. D. Pollard, 1980, Mechanics of discontinuous faults; J. Geophys. Res., Vol. 85, No. B8, p. 4337-4350.

Shainin, V. E., 1950, Conjugate sets of en echelon tension fractures in the Athens Limestone at Riverton, Virginia; Bull. Geol. Soc. Am., V. 61, p. 509-517.

Shoemaker, E. M. and W. L. Newman, 1959, Moenkopi Formation (Triassic? and Triassic) in Salt Anticline region, Colorado and Utah; Bull. Am. Assoc. Petrol. Geol., V. 43, p. 1853-1851.

Sih, G. C., 1966, On the Westergaard method of crack analysis; Int. J. Fracture Mech., V. 2, p. 628-631.

Simmons, G. C., 1957, Contact of Burro Canyon Formation with Dakota Sandstone, Slick Rock district, Colorado, and correlation of Burro Canyon Formation; Bull. Am. Assn. Petrol. Geol., V. 41, p. 2519-2529.

Sowers, G. M., 1973, Theory of spacing of extension fracture; *in:* H. Pincus, ed., *Geological Factors in Rapid Excavation;* Engineering Geology Case History Number 9; Geol. Soc. Am., p. 27-52.

Spencer-Jones, D., 1963, Joint patterns and their relationships to regional trends; J. Geol. Soc. Australia; V. 10, p. 279-298.

Stearns, D. W., 1968, Certain aspects of fracture in naturally deformed rocks; *in:* R. E. Riecker, ed., *Rock Mechanics Seminar, Vol. I;* pub. by Air Force Cambridge Labs., available from Nat. Tech. Information Service, 5285 Port Royal Road, Springfield, Va., 22161, Publication No. AD-669 375.

Stearns, D. W. and M. Friedman, 1972, Reservoirs in fractured rocks; *in:* R. E. King, ed., *Stratigraphic Oil and Gas Fields;* Am. Assoc. Petrol. Geol. Memoir 16, p. 82-106.

Stewart, J. H., 1961, Stratigraphy and origin of the Chinle Formation (Upper Triassic) of the Colorado Plateau; PhD. dissertation, Stanford University.

Stewart, J. H., G. A. Williams, H. F. Albee and O. B. Raup, 1959, Stratigraphy of Triassic and associated formations in part of the Colorado Plateau; U. S. Geol. Surv. Bull. 1046-Q.

Stokes, W. L., 1952, Lower Cretaceous in Colorado Plateau; Bull. Am. Assn. Petrol. Geol., V. 36, p. 1766-1776.

Ziony, J. I., 1966, Analysis of systematic jointing in part of the Monument Upwarp, Southeastern Utah; PhD. dissertation, U. C. L. A., 112 p.

Zoback, M. D. and D. D. Pollard, 1978, Hydraulic fracture propagation and the interpretation of pressure-time records for in-situ stress determinations; 19th U. S. Symposium on Rock Mechanics, p. 14-22.